# RomUkrSeis: seismic model of the crust and upper mantle across the Eastern Carpathians – from the Apuseni Mountains to the Ukrainian Shield

Vitaly Starostenko[1], Tomasz Janik[2], Victor Mocanu[3], Randell Stephenson[4], Tamara Yegorova[1], Tatiana Amashukeli[1], Wojciech Czuba[2], Piotr Środa[2], Anna Murovskaya[1], Katerina Kolomiyets[1], Dmytro Lysynchuk[1], Jan Okoń[2], Alina Dragut[3], Victor Omelchenko[1], Olga Legostaieva[1], Dmytro Gryn[1], James Mechie[5], Anatoly Tolkunov[6]

[1] *Institute of Geophysics, National Academy of Sciences of Ukraine, Kiev, Ukraine*
[2] *Institute of Geophysics, Polish Academy of Sciences, Warsaw, Poland*
[3] *University of Bucharest, Romania*
[4] *School of Geosciences, University of Aberdeen, Scotland*
[5] *Deutsches GeoForschungsZentrum – GFZ, Section "Geophysical Deep Sounding", Telegrafenberg, 14473 Potsdam, Germany*
[6] *Ukrgeofizika, Kiev, Ukraine*

Paper for submission to *Tectonophysics*

**ABSTRACT**

RomUkrSeis is a controlled source wide-angle reflection and refraction (WARR) profile acquired in August 2014. It is 675 km long, running roughly SW-NE from the Apuseni Mountains in Romania and the Transylvanian Basin, crossing the arc of the Eastern Carpathian orogen and terminating in the East European Craton (EEC) in SW Ukraine. Well-constrained 2-D ray-tracing P- and partly S-wave velocity models have been constructed along the profile from 348 single-component seismic recorders and eleven shot points. The Eastern Carpathian arc formed in the Cenozoic and have obscured the pre-existing Teisseyre-Tornquist Zone (TTZ), which is a transition zone between the Precambrian EEC and continental terranes accreted to it from the southwest in the Palaeozoic. The TTZ is characterised by low-velocity through its entire crust (6.0-6.3 km/s) and a considerable width (~140 km). It is interpreted as EEC crust stretched during rifting and continental margin formation in the Neoproterozoic and early Palaeozoic. The crust of the TTZ has a "trough in trough" structure wherein an upper body of ~40 km width comprising Outer Carpathian ($V_p$ 4.9 km/s) and Late Palaeozoic-Mesozoic ($V_p$ 5.4 km/s) units to 15 km depth lies above a wider, deeper one of inferred Neoproterozoic-early Palaeozoic strata. The crust of the Transylvanian Basin and Apuseni Mountains is relatively thin (~32 km). A high-velocity body at 4-12 km depth in this area is interpreted as a rootless fragment of an ophiolite complex exposed at the surface in this area. The lower crust beneath the Transylvanian Basin displays higher velocities than adjacent segments. Moho topography is strongly differentiated along the profile, varying from 32 to 50 km. The Moho shape, especially in the area between the Inner and Outer Carpathians, suggests a NE dip and, hence, thrusting of the Tisza-Dacia lowermost crustal and upper mantle units under the TTZ domain which, in turn, could be thrust under the cratonic (EEC) block.

**Keywords:** Apuseni Mountains, Transylvanian Basin, TTZ, Eastern Carpathians, East European Craton, lithospheric structure, WARR profile

## 1. Introduction

This paper presents the results of the RomUkrSeis WARR seismic profile acquired in Romania and Ukraine, in the region from the Apuseni Mountains in the SW, across the Transylvanian Basin and Carpathian Mountains, to the East European platform in the NE (Fig. 1). As such, RomUkrSeis provides an integrated image of a segment of continental crust and upper mantle affected and modified by lithosphere-scale processes from the Archaean until almost the present-day: a sequence including Precambrian cratonisation; continental break-up; Palaeozoic orogenesis and continental accretion leading to Pangaea supercontinent formation followed by large-scale destabilisation until the Mesozoic and ending with subduction, back-arc basin formation and orogenesis in the Cenozoic.

RomUkrSeis uniquely complements a series of WARR-type profiles acquired in Ukraine (including coverage in the neighbouring countries of Poland, Belarus, Hungary and Romania)

during the last two decades. The Donbas foldbelt and eastern Black Sea basin were covered by the DOBREfraction'99 (DOBREfraction'99 Working Group, 2003) and DOBRE-2 (Starostenko et al., 2017) profiles. The Carpathian arc in western Ukraine and Hungary was covered by PANCAKE (DOBRE-3; Starostenko et al., 2013a; Verpakhovska et al., 2018). The area from the Pre-Dobrogea Trough across the southern part of the Ukrainian Shield was investigated during the DOBRE-4 experiment (Starostenko et al., 2013b). The Odessa Shelf of the Black Sea and the Crimea peninsula were covered by the most southern profile, the EW-trending DOBRE-5 profile (Starostenko et al., 2015). The Pripyat-Dnieper-Donets Basin was studied during the EUROBRIDGE'97 (Thybo et al., 2003) and the GEORIFT 2013 (Starostenko et al., 2018) projects.

The RomUkrSeis profile crosses a highly complex crustal transition zone that separates the Baltica proto-continent, comprising the Archaean-Palaeoproterozoic lithosphere of the East European Craton (EEC), and lithospheric domains accreted to it during later, Phanerozoic tectonic episodes (the Palaeozoic Caledonian and Variscan orogenies overprinted by the Mesozoic-Cenozoic Alpine-Carpathian orogeny). This transition zone between Baltica and the subsequently accreted terranes is known as the Teisseyre-Tornquist Zone (TTZ; e.g. Pharaoh, 1999; Pharaoh et al., 2006; Narkiewicz et al., 2015; Grad, 2019) and is located on the inset map of Figure 2 including its presumed trace beneath the overprinting Alpine-Carpathian geology crossed by RomUkrSeis.

The objective of RomUkrSeis was to investigate the architecture of the sedimentary cover and the structure of the crystalline crust and uppermost mantle of the south-western margin of the EEC (including the adjacent south-western part of the Ukrainian Shield), Carpathian orogen and its foredeep, and the Transylvanian Basin and Apuseni Mountains. The results are to help clarify the spatial extent of the component tectonic units, the evolution and the nature of the boundaries between them and to supply new data for understanding resource potential in this area. A particular interest was crystalline basement affinity and Moho depth along the profile, in particular in the vicinity of the TTZ.

The results, based on state-of-the-art techniques of controlled-source WARR seismic data acquisition and interpretation, add new constraints to the existing geophysical data set of the area and have contributed to a better understanding of the crustal architecture in the lithosphere transition between Ukraine and Romania that is obscured by the overlying accretionary prism of the Outer Carpathians and the Carpathian foredeep.

## 2. Geology crossed by the RomUkrSeis profile

The RomUkrSeis profile crosses the following tectonic units from the south-west to the north-east (Fig. 2): the Apuseni Mountains, Transylvanian Basin, Inner Carpathians, Outer Carpathians and the southwestern part of the East European Craton (EEC), adjacent to the southwestern Ukrainian Shield. These Archaean to Cenozoic domains have different tectonic origins and geodynamic histories and the geology of each is briefly described in the following

paragraphs.

The tectonic evolution of the region of Apuseni Mountains-Transylvanian Basin-Carpathian Orogen as a whole is understood to be one of Cenozoic subduction and continental collision between the European plate and the composite ALCAPA-Tisza-Dacia terrane (Fig. 2) within the Alpine-Tethys orogenic belt (Săndulescu, 1988; Csontos and Vörös, 2004). The ALCAPA-Tisza-Dacia terrane is, in turn, understood to comprise separate continental blocks and oceanic and sub-oceanic domains formed during the Permo-Triassic to Late Jurassic break-up of Pangaea. An intrinsic part of the process of Pangaea break-up was the opening of the Neotethys oceanic domain as well as back-arc basin formation within the Alpine-Tethys belt associated with the contemporaneous subduction and closure of the older Paleotethys oceanic domain. As part of these processes the Tisza terrane was amalgamated with the Dacia terrane in the Late Jurassic-Cretaceous and, in turn, the Tisza-Dacia composite terrane with the ALCAPA terrane in the Cenozoic (Fodor et al., 1999; Csontos and Vörös, 2004; Golonka et al., 2006; Schmid et al., 2008).

The Apuseni Mountains formed during the convergence and suturing of the Tisza and Dacia terranes and the eventual closure of the Neotethys or back-arc oceanic domain that separated them (e.g. Săndulescu, 1975; Csontos et al., 1992 Schmid et al., 2008). The suture between Tisza and Dacia has been mapped south into the Balkan Peninsula and is associated with significant volumes of ophiolitic rocks of Triassic age presumed to be derived from the consumed (sub-)oceanic crust during basin closure (e.g. Schmid et al., 2008). This is particularly evident in the southern Apuseni Mountains in the vicinity of the RomUkrSeis profile. The northern Apuseni Mountains consist of crystalline Precambrian or Palaeozoic basement units with overlying deformed sedimentary units. Rock types in the former include schists and amphibolites intruded by granites. The age of the metamorphism and intrusion is Palaeozoic. The overlying sedimentary succession includes Triassic, Jurassic and pre-Senonian Cretaceous units.

Deformation associated with the amalgamation of Tisza-Dacia with ALCAPA is distributed within the crustal-scale Mid-Hungarian Fault Zone (MHFZ; Fig. 2) where seismic reflection profiling reveals that the northern ALCAPA unit overrode the southern Tisza-Dacia unit (Csontos and Nagymarosym, 1998; Csontos and Vörös, 2004) The southern boundary of the MHFZ is known as the Mid-Hungarian Line, which is inferred to continue eastwards as the Dragos Voda Fault as far as the RomUkrSeis profile (DVF; Fig. 2).

The Transylvanian Basin is a syn-tectonic entity lying within the arc of the Carpathian Mountains and east of the Apuseni Mountains. The present morphology and structure of the region is the result of the Carpathian, Cretaceous to Miocene, convergence and collision, with the basin fill displaying varying degrees of associated mild folding and doming (e.g. Krézsek and Filipescu, 2005; Krézsek and Bally, 2006; Tiliţă et al., 2013). Up to 8 km of post-Cenomanian sedimentary strata (e.g. Ciulavu et al., 2000) overlie Middle Cretaceous basement nappes (of the Inner Carpathians) that form the hinterland of the Carpathian Mountains “backstop” against the East European Craton (e.g. Fig. 2). The basement nappes

consist of crystalline and sedimentary rocks of Triassic to Early Miocene age. The sedimentary pile of the basin is mainly Miocene and younger. The Transylvanian Basin has been affected by Neogene deformation along faults displaying complex kinematic relationships (e.g. Linzer et al., 1998; Ciulavu et al., 2000), some of which are associated with low-level seismicity at present (Bala et al., 2017).

The Ukrainian-Romanian Carpathians are part of the Eastern Carpathians, which is the segment of the Alpine arcuate fold-and-thrust belt of the Carpathians thought to have formed in response to subduction and continental collision between the European plate and the composite ALCAPA-Tisza-Dacia terrane at the southwestern margin of the EEC (Săndulescu, 1988; Csontos and Vörös, 2004). The foreland of the Romanian Eastern Carpathians overlies parts of the Scythian and Moesian platforms (i.e., atop Precambrian crystalline crust) as well as the Mesozoic North Dobrogea orogen and the marginal part of the EEC directly. The Romanian Eastern Carpathians are the natural southward prolongation of the Ukrainian Eastern Carpathians and have almost the same structure and lithology.

The Eastern Carpathians developed above the south-western margin of the EEC and, accordingly, the TTZ. The orogen is traditionally divided into two major units: the Inner and the Outer Carpathians (Uhlig, 1907). The Inner Eastern Carpathians (sometimes referred to as "Dacides") were formed in the middle Cretaceous at the early stages of collision and involve deformation and displacement of Precambrian and/or Palaeozoic crystalline basement and its Mesozoic (pre-Cenomanian) sedimentary cover (Săndulescu, 1984; 1988). The Outer Eastern Carpathian thrust-and-fold belt (sometimes referred to as "Moldavides") is a stack of eastward-verging nappes that were thrust over the margin of the EEC during the final stages of tectonic shortening in the Eocene-Pliocene (Gągała et al., 2012). This accretionary wedge now overrides the TTZ and the relatively undeformed EEC margin. Except for the most external, and youngest, molasse units, the nappes of the Outer Carpathians consist of flysch complexes of Cretaceous to Early Miocene age and are up to 8 km thick (Plašienka et al., 1997; Gągała et al., 2012; Nakapelyukh et al., 2018; Zayats, 2013).

The Ukrainian part of the RomUkrSeis profile runs across the Carpathian foredeep, including the Volyn-Podolsk monocline (VPM), and onto the southwestern part of the Ukrainian Shield (Fig. 2), so confined to what is known as the predominantly Archaean-aged Sarmatian segment of the EEC (Gorbatschev and Bogdanova, 1993). According to borehole and seismic data, the disposition of crystalline basement changes from some 2600 m below sea level at the Carpathian thrust front to about 250 m above sea level in the Ukrainian Shield. Basement-involving normal faults offsetting Neoproterozoic and Palaeozoic strata but covered by unfaulted Carpathian foredeep strata are recognised on seismic profiling in this area (Zayats, 2013).

The part of the EEC crust and lithosphere that underlies the VPM is thought to have been affected by tectonic and magmatic (re)activation as a result of extension and rifting during the Neoproterozoic break-up of the Rodinia supercontinent (e.g. Powell et al., 1993; Sliaupa et al., 2006; Kravchenko, 2007; Pease et al., 2008; Usenko, 2010; Gordienko et al., 2011) and

separation of the proto-continents Baltica and Amazonia (now forming the core of northern South America). This was the event that formed the southwestern continental margin of Baltica, with the facing oceanic domain later closed during Palaeozoic accretionary orogens. The formation of the Baltican margin was accompanied by notable magmatism (Volyn Series within the VPM), which in part lies near the trace of the RomUkrSeis profile.

The part of the Ukrainian Shield traversed by RomUkrSeis is known as the Podolian Domain (Fig. 2), which consists of Archaean-Palaeoproterozoic granulites and granitoids (e.g. Shcherbak et al., 2005; 2008; Shumlyansky et al., 2015). A number of regional shear zones/fault zones, the main ones striking NW-SE and as wide as 8-15 km (Gintov, 2004) have been mapped in the area. A thin layer (0-50 m) of unconsolidated Cenozoic sediments covers the crystalline basement.

## 3. Potential field and heat flow data in the vicinity of the RomUkrSeis profile

The main tectonic units crossed by the RomUkrSeis profile correspond in varying degrees with the potential field (gravity and magnetic) patterns along the RomUkrSeis profile (Fig. 3). The main feature of the regional Bouguer gravity field (taken from EG-99 data base; Wybraniec et al., 1998) is the strongly negative anomaly (less than -120 mGal) associated with the Carpathian belt and its foredeep. This is caused by the thick flysch complexes of the Eastern Carpathian nappes and presumably deeper sources within and at the base of the crust, which will be elucidated by the seismic results presented below. Another dominant feature is that the gravity field is characterised by a contrast between negative values in the southwestern part of the profile (-20 to -40 mGal) over the Transylvanian Basin with positive values (0 to +10 mGal) in the northeastern part over the older Volynsk-Podolsk Monocline and southwestern part of the Ukrainian Shield (Podolian Domain). This change in gravity on either side of the Carpathian belt can be largely explained by contrasting depths to the crystalline basement, which is exposed in the Ukrainian Shield, but is at a depth of some 6-8 km below sedimentary strata in the Transylvanian Basin. The effects of the sedimentary layer are also evident in the magnetic field (for which the EMAG2 data were used; www.ngdc.noaa.gov/geomag/emag2.html), which is subdued west of the Carpathians and much more vivid to the east. The anomalous gravity field of the Apuseni Mountains is subdued compared to the Carpathian belt, with amplitudes in the ranging -20 to +20 mGal from the western end of the profile through to SP15303 or so where they reduce to less than -40 mGal (with a central “high” of more than -20 mGal) over the Transylvanian Basin (Fig. 3). The anomalous magnetic field above the Apuseni Mountains and the Transylvanian Basin, where they are intersected by RomUkrSeis, is quiet and generally close to 0 nT (Fig. 3).

Figure 3 also shows surface heat flow in the vicinity of the RomUkrSeis profile (from Hurtig et al., 1991). The high heat flow (up to 80 $mW/m^2$) observed between SP15304 and SP15305 in the Inner Carpathians is associated with young tectonics and thermal activity expressed as numerous magmatic intrusions of Neogene age (e.g. Seghedi et al., 2004; Kutas, 2015). Elsewhere there is low heat flow (30-50 $mW/m^2$) in the Volyn-Podolsk Monocline and

Ukrainian Shield, as would be expected for a cratonic region and there is a region of reduced heat flow in the Transylvanian Basin (less than 30 $mW/m^2$), which could in part indicate a sedimentary blanketing effect (e.g. Gordienko and Zavgorodnyaya, 1995; Majorowicz and Wybraniec, 2011).

## 4. Field experiment and seismic data

RomUkrSeis data were acquired in August 2014. The field programme was carried out by an international consortium involving institutions and personnel from Romania, Ukraine, Poland and Scotland. Recording instruments included 230 "DSS Cubes" provided by the Geophysical Instrument Pool of the Deutsches GeoForschungsZentrum (GFZ), Potsdam, and by the Institute of Geophysics of the Polish Academy of Sciences (deployed in Romania) and 118 RefTek "Texans" from the institutes of Geophysics of the Ukrainian and Polish academies of sciences (deployed in Ukraine). The RomUkrSeis profile runs from Bethausen village, Timisoara county, Romania (45.8151°N; 21.9049°E) to Yosypivka village, Vinnitsa region, Ukraine (49.5950°N; 28.8606°E), a total length of 675 km, with 403 km in Romania and 272 km in Ukraine (Fig. 1). The distance between recorders along the profile was 1.75-2 km in Romania and 2-2.25 km in Ukraine. There were 11 shot points used during the field data acquisition (Table 1), 7 shots in Romania and 4 in Ukraine. The distance between the shot points was 20-65 km and their locations can be seen in Figures 1 and 2.

The quality of the recorded data depends mainly on local ground conditions and the shot-recorder offset distance. Seismograms of length 105 seconds starting at 5 s before each shot time (Table 1) were extracted for analysis after field acquisition and initial data processing. The extracted traces were collated into shot gathers. The resulting P-wave shot gathers are presented in Figures (4a,b) using a reduction velocity of 8 km/s. For presentation purposes all traces were subjected to a Butterworth 2-15 Hz bandpass filter, followed by amplitude normalization. S-wave arrivals of good quality were recorded on the cratonic part of the profile, for shots SP15306-SP15311. Weaker S-wave arrivals were recorded for SP15301-SP15305. Examples are shown in Figure 4c.

The seismic data are of high quality and allow good correlation of first arrivals of the following phases: $P_{sed}$ – P-waves refracted from boundaries within the sedimentary supracrustal succession; $P_g$, $S_g$ – P and S refractions from boundaries in the upper and middle crystalline crust; $P_{ov}$, $S_{ov}$ – P and S overcritical crustal phases; $P_cP$ – P reflections from mid-crustal discontinuities, $P_MP$, $S_MS$ – P and S reflections from the Moho; $P_n$, $S_n$ – P and S refractions from Moho boundary; $P_2P$ and $P_{mantle}$ – P-wave phases from the upper mantle. Additional information regarding the accuracy of the travel-time picks and modelling is presented in section 5.6, below.

### *4.1 P-phases*

The $P_{sed}$ phase is observed as first arrivals in the vicinity of shot points up to offsets of only 2-

3 km in the westernmost shot points SP15301 and SP15302 (Fig. 4a). Further to the east, in the SP15303-SP15307 shot gathers, this phase can be traced near shot points at offsets of up to 10 km. The apparent velocities are 3.6-5.0 km/s. The most spectacular differences between the apparent velocities for small offsets of the NE and SW travel-time branches are seen in sections for SP15303 and SP15305 (Fig. 4a). $P_{sed}$ is practically not observed in the area of the East European Craton (EEC), starting from SP15309 towards the eastern end of the profile (Fig. 4b).

The $P_g$ phase from the crystalline basement (upper crust) can be correlated at offsets up to 230 km from the shot point on the craton in the eastern part of the profile. $P_g$ in the western part of the profile typically displays apparent velocities that differ in opposite directions from the shot point (e.g., for SP15303, $P_g$ velocities to the SW and NE are ~6.4 km/s and ~5.5 km/s, respectively). This is mostly because the refracting interface dips to the northeast and the $P_g$ phase may also be affected by lateral variations in the composition of the underlying layer. Higher velocities are observed among the first three shot points SP15301-SP15303 (Fig. 4a). The $P_g$ phase travel-time curves have a discontinuous character and show steps and gaps in the correlation (marked with blue ellipses in Figs. 4a,b), which could indicate the presence of low velocity layers in the upper/middle crust. Conversely, some correlated $P_g$ fragments exhibit remarkably higher apparent velocity than elsewhere, most likely due to localised high velocity bodies (red ellipses in Figs. 4a,b). In the SP15301 shot gather, the $P_g$ phase is correlated at offsets 0-100 km. At larger distances its amplitude decreases and is much smaller than very strong Moho reflections in later arrivals. A similar situation is observed on the reverse branch of SP15302, but with a more pronounced increase in apparent velocity from 5.5 to 6.0 km/s. In the eastern part of the SP15302 shot gather, $P_g$ is observed as a first arrival at distances from 0 to 130 km (Fig. 4a).

The $P_g$ phase refracted in the upper and middle crust is observed in both directions from shot points SP15303, SP15304 and SP15305 at offsets up to 200 km. Its apparent velocity increases from 5.9 to 6.2 km/s with distance. Concurrently, there are discontinuities in the correlated travel-time curves of the $P_g$ phase as, for example, in the easterly direction of the SP15303 record at distances of 30 and 130 km, and SP15304 at an offset of 110 km, which may indicate the presence of low velocity zones. The western branches look more continuous, but a slight decrease in the amplitude of $P_g$ is visible on the SP15303 record at a distance of 80 km and at offsets of 100-110 km on SP15304 and SP15305 (Fig. 4a).

The SP15306 and SP15307 record sections contain clear $P_g$ arrivals in both directions from the respective shot points at offsets of 10-180 km, with an apparent velocity of 5.7-5.9 km/s to the west (Fig. 4 b). The eastern branches of the $P_g$ phase, well correlated to 180 km offset, are characterised by an apparent velocity 6.0-6.2 km/s. $P_g$ in both directions on SP15308, SP15309, SP15310 and SP15311 is visible at offsets up to 180-230 km, with apparent velocities of 6.0-6.2 km/s. At larger distances (200-400 km offsets) this phase merges with a overcritical reflection, which is very confidently correlated in the secondary arrivals with apparent velocity in the range of 6.2-6.7 km/s on the SP15304-SP15311 shot gathers (Figs. 4a,b). These phases are very important for the velocity modelling because they provide

information from the deeper crustal layers, especially in the lower crust, helping to estimate maximum lower crustal velocity.

Intracrustal reflections, $P_cP$, are found on several seismic sections with different intensities and degrees of correlation.

The Moho reflections ($P_MP$) were correlated beyond distances of ~70 km on most of the record sections. Particularly clear $P_MP$ phases are observed in the record sections of SP15301 and SP15305-SP15311 at 70-170 km offset (Figs. 4a,b). $P_n$ phases refracted immediately beneath the Moho discontinuity are observed at large offsets (>170 km). The best quality $P_n$ phases are seen on the SP15301, SP15303, SP15304, SP15306, SP15307 and SP15310-SP15311 shot records. Phases interpreted as reflections from upper mantle discontinuities ($P_{mantle}$) are detected in record sections SP15301, SP15303, SP15304, SP15306, SP15307, SP15310 and SP15311 at offsets of 200-400 km (Fig. 4a,b).

### *4.2 S-phases*

Examples of S-wave record sections are presented in Figure 4c with a reduction velocity of 8.0 km/s and a band pass filter of 1-18 Hz. Some S-phases are also identified on Figures 4a,b. S-waves were mainly observed in the northeastern part of the profile (SP15306-SP15311) and, due to the poor signal-to-noise ratio, only a limited number of travel-times were picked. Although the main reflected and some refracted S-wave phases are identifiable and can be picked with some uncertainty, construction of a complete S-wave velocity model was not possible. Instead, the best quality branches of the S-wave travel-times were used to estimate the $V_p/V_s$ ratio in the crystalline crust and upper mantle in the northeastern part of the profile.

## 5. Seismic modelling

### *5.1 Ray-tracing modelling strategy*

The acquired seismic data and obtained travel-time picks (Fig. 4a,b) served as a basis for forward modelling the crustal and upper mantle structure beneath the RomUkrSeis transect. Modelling was done by trial-and-error using the 2-D ray-tracing SEIS83 package (Červený and Pšenčík, 1983) with the graphical user interfaces MODEL (Komminaho, 1998) and ZPLOT (Zelt, 1994). SEIS83 is based on a high frequency approximation of the wave equation for computation of ray paths, travel-times and synthetic seismograms. The model consists of layers that are separated by velocity discontinuities (Fig. 5) with the velocities determined by bicubic spline interpolation between arbitrarily located velocity nodes. The P-wave model seen in Figure 5 displays only those crustal discontinuities that could be determined from clear P-phases. Figure 6 provides examples of modelling of P-phases for selected shot points.

The initial P-wave velocity model was prepared using existing geological and geophysical

information about the structure of the uppermost crust in Romania and Ukraine, including the geological cross-sections of Stefanescu et al. (1988), which were based on early shallow reflection seismic profiling, augmented by some newer seismic investigations (e.g. Krézsek and Bally 2006) as well as velocity data from several boreholes along the profile (with projected locations on Figure 5 but as far away as ~60 km for wells 5 and 6 in Romania).

One of the difficulties encountered during modelling is related to the complicated Moho geometry seen in the resulting model (large and abrupt Moho depth variations; Fig. 5). In the ray theory (geometrical optics) based approach that was used, such structures produce 'shadow zones', areas where model travel-times cannot be calculated and cannot be checked against observed travel-times. Accordingly, full waveform synthetic seismograms using a finite-difference approach were also computed (using TESSERAL; Kostyukevich et al., 2000). The results of the TESSERAL modelling are presented in the top panels of Figure 6.

For modelling the S-phases the P-wave velocity model was converted into an initial S-wave model using a $V_p/V_s$ ratio of 1.73 for the whole domain after which velocity modelling was performed iteratively, with fixed layer boundary geometry from the initial P-wave model, until the least misfit of S-phase travel-times was reached. The final S-wave velocity model is shown in the bottom panel of Figure 5. Figure 7 provides an overview of the S-wave modelling as does Figure 6 for the P-wave modelling. Accordingly, it was possible to determine crustal $V_p/V_s$ ratios in some parts of the RomUkrSeis profile (Fig. 5; bottom panel).

### *5.2 Crustal model*

The thickness of the sedimentary layer along the profile (Fig. 5) ranges from a few tens of metres (Apuseni Mountains, km ~130; Carpathians, km ~310; and EEC) to ~6 km (Transylvanian Basin), with P-wave velocities varying between 2.3 and 4.9 km/s. A ~40 km wide, higher velocity body ($V_p$ ~5.4 km/s) lies within the sedimentary layer, near the surface at km 50-90; it has a maximum thickness of ~2 km. Bodies with velocities as high as ~5.9 km/s occur at the surface along the profile, at km ~125 and km ~307.

The most striking element of the crustal model is a ~15 km deep and 40 km wide sedimentary(?) wedge with P-wave velocities of 3.0-5.4 km/s inferred below the Carpathian belt (km ~320-360). This wedge-like feature is bounded on both sides by steeply dipping boundaries. Only a few reflections from these steep velocity interfaces were observed in the dataset (as would be expected for wide-angle measurements such as those acquired along the RomUkrSeis profile). The modelled shape of the sedimentary(?) wedge was "imaged" mainly on the basis of refracted waves. The shape of this body as seen in Figure 5 represents the smallest volume of low-velocity material that allows for a satisfactory fit to the travel-time data. A similar fit can be obtained with a broader low-velocity wedge incorporating part of the area of what is shown as Body 4, immediately to its southwest. Both (and all intermediate) solutions are possible. In any case, this profound structure separates two distinct crustal regions along the profile.

To the southwest, the crust underlying the Apuseni Mountains, Transylvanian Basin and Eastern Carpathians is characterised by velocities of 6.0-6.4 km/s southwest of km 115 and somewhat higher velocities in the lower part of the crust (>6.5 km/s) from there to the Carpathian belt. This part of the crust also displays velocity inversions in its upper part: a body at km 0-95 and depth 3-10 km with $V_p$ ~6.35 km/s overlying material with $V_p$ 6.20 km/s and a body at km 95-200 and depth 1-6.5 km with $V_p$ 6.07-6.20 km/s overlying material with $V_p$ ~5.95 km/s.

On the other, northeast, side of the Carpathian structure, the crust is not dissimilar to that of the southwesternmost segment at distances of ~340-440 km: $V_p$ of 6.2-6.4 km/s, though with an absence of any velocity inversion in the upper crystalline crust. Beyond ~km 440 km a 20 km thick lower crustal body with $V_p$ ~6.45-6.6 km/s is inferred. Velocities in the lower crust are based on the overcritically reflected $P_MP$ phases ($P_{ov}$) on several record sections (e.g. SP15301, SP15304 and SP15307). The upper part of the crust for the whole northeastern part of the model consists of two layers that display homogeneous velocities of $V_p$ 6.0-6.15 km/s and $V_p$ 6.2-6.35 km/s, respectively.

### *5.3 Moho boundary and upper mantle*

The Moho boundary along the RomUkrSeis profile (Fig. 5) shows profound depth variability. In the southwestern part of the profile, beneath the Apuseni Mountains and part of the Transylvanian Basin, the depth to the Moho gradually increases from 31 km (km 40) to 38 km (km ~220) after which it shallows quite abruptly to 31 km (km 240). This significant depth change was modelled based on two branches of $P_MP$ (cf. SP15301 and SP15304, km 0-300; Figs. 6 a,c). Going further to the northeast, under the Carpathians, the Moho reaches a depth of ~51 km (km 340), after which, over a distance of just ~10 km, it rises to ~37 km (km 350), creating a narrow wedge of crustal material to its southwest. It remains at this depth to about km 430. The unusual structure of the modelled Moho in this region is justified by the SP15303 and SP15304 data, where, in their northeastern parts, two $P_n$ branches with different apparent velocities ($V_{app}$) are observed, one at ~8 s reduced time (km 310-450, $V_{app} \leq 8$ km/s), and a second one at a similar reduced time but with a higher apparent velocity (km 400-470, $V_{app} > 8$ km/s) (Figs. 6b,c). Double-branched $P_n$ travel-time curves like this one are caused by the complex Moho topography in this area leading to very different ray paths for two groups of rays refracted at the Moho. To the northeast of km 430 the Moho shallows to about 34 km (km 450) and then gradually deepens to ~40 km at km 600.

The immediately sub-Moho velocities are quite uniform along the whole profile. Slightly lower velocities are observed at the ends of the profile ($V_p$ ~8.15 km/s) than in its central part (up to 8.21 km/s). There are two zones in the model where boundaries in the upper mantle are inferred. These are beneath the eastern Transylvanian Basin-Carpathians (km 255-315 at a depth less than 50 km) and within the East European Craton (EEC; km 480-575 at a depth less than 50 km), both primarily based upon the $P_2P$ upper mantle reflected phase seen in many of the sections presented in Figure 6. Below these reflectors, velocities of $V_p$ 8.35 km/s and $V_p$ 8.3 km/s were adopted in the model, based on the $P_{mantle}$ refracted phases seen, for

example but not exclusively, in sections SP15307 and SP15311 (Figs. 6e,g). There is also a suggestion of a sub-Moho mantle refractor dipping eastward in the range km 430-450 from around the same point as the southwestern extremity of higher lower crustal velocities beneath the EEC.

### *5.4 S-wave velocity model and $V_p/V_s$ ratios*

In the S-wave modelling, the geometry of discontinuities was assumed to be the same as in the P-wave velocity model (Fig. 5). $S_g$, $S_MS$ and $S_n$ phases were observed and only those with good amplitude were used for modelling (see Figs. 4c and 7).

The S-wave velocity model can be seen in the lower panel of Figure 5. Results were obtained for a shallow segment of the P-velocity model at the southwestern end of the profile and for the whole of the crust for the part of the P-velocity model northeast of the Carpathian belt (i.e., EEC crust). In the former, which is constrained by S-phases of low quality, there is an uncertain suggestion of $V_s$ ~3.80 km/s and $V_p/V_s$ 1.67(?) for the $V_p$ 6.35 km/s body forming a velocity inversion with its underlying, lower-velocity body. In the EEC there is an inferred S-velocity of ~3.7-3.6 km/s to a depth of ~7 km (km 350-650) over which the $V_p/V_s$ ratio increases from 1.64 to 1.71. Below this layer, at distance km 360-480, $V_s$ is ~3.77 km/s with $V_p/V_s$ 1.64 to ~30 km depth; beyond km 480 $V_s$ decreases to ~3.60 km/s but $V_p/V_s$ increases to ~1.72. For the lower crustal layer (km 420-600) $V_s$ ~3.81 km/s and $V_p/V_s$ 1.70 were derived from the modelling. Finally, $V_s$ ~4.61 km/s ($V_p/V_s$ 1.76) is estimated for the sub-Moho mantle (~km 460).

### *5.5 Full waveform synthetic sections*

Synthetic sections were calculated using a full waveform modelling program TESSERAL (Kostyukevich et al., 2000), which uses a fast and accurate finite-difference computational scheme. The model is built of ordinary polygons, layer-like polygons, top and bottom type horizons and multiple segment lines representing faults. Individual layers of the final ray-tracing velocity models (Fig. 5) were converted to polygons of uniform P- and S-velocities. These were then edited and smoothed. Surface topography was also taken into account. Due to the large volume of input data, the computations were parallelised using a grid of computers (e.g. Kolomiyets and Kharchenko 2008).

Several source wavelets were tested; the Puzyrev wavelet with 8 Hz frequency provided the best similarity to the observed wave field, at least at near offsets. Good agreement of synthetic sections with observed data was achieved, which also tends to confirm the validity of the velocity models, as discussed at greater length below. Comparison of the full waveform synthetic sections with seismic record sections as well as the ray-trace diagrams for SP15301, SP15303, SP15304, SP15306, SP15307, SP15310 and SP15311 are presented in Figure 6.

### *5.6 Resolution analysis*

505 Shot locations and origin times were measured with high precision GPS receivers. Timing
506 was verified by checking differences of first arrivals on reciprocal travel-time branches.
507 Nevertheless, velocity and boundary depth uncertainties in the final velocity models result
508 from non-uniqueness of the solution and potential phase misidentification. Other sources of
509 error include the misfit between observed and calculated travel-times, as well as the
510 ambiguity of subjectively picked travel-times. The sampling interval of the data is 0.01 s. The
511 actual picking uncertainty is presumably much greater. Assuming a 5-10 Hz dominant signal
512 frequency (i.e., pulse length 0.1-0.2 s), the accuracy of locating the precise onset of the slope
513 increase at a phase arrival can be realistically estimated as not less than ~0.05 s for manual
514 picking using visual phase identification. For secondary arrivals and where there is reduced
515 signal to noise ratio, this uncertainty would be higher. In the case of S-waves, where
516 observed, uncertainties are also higher. S-phase arrivals occur within the P-wave coda and
517 their onsets are more diffuse and difficult to identify. It is also possible that they derive from a
518 P-to-S conversion at some near-surface discontinuity, with slightly different travel-time and
519 ray path than the direct S-wave generated at the source.
520
521 The overall high quality of the RomUkrSeis data (signal-to-noise ratio and ray coverage)
522 permitted constructing a model that provided a good fit of computed to observed travel-times
523 for refracted as well as reflected seismic phases. Only one initial model was used – as
524 described previously in the text – with upper-crustal/sedimentary structure based on
525 independent geological and geophysical (mainly exploration seismic reflection profiling)
526 information and with deeper layer boundaries initially defined as horizontal (i.e., 1-D velocity
527 distribution). Subsequently, during the modelling process, this initial model was perturbed in
528 order to obtain the fit between observed and computed phase arrivals. A wide spectrum of
529 models was tested. For example, at first no (or little) Moho topography was assumed and only
530 at the point when no satisfactory fit could be obtained this way (i.e., by only changing the
531 crustal velocity field) was Moho topography introduced, starting with the least possible
532 change and proceeding incrementally from there. Several concurrent variants of structure
533 were constructed and tested in problematic segments of the model (for example, the shape of
534 the southwestern part of the (meta)sedimentary wedge beneath the Carpathians).
535 Considerations articulated in previous work using datasets similar to that of RomUkrSeis
536 show that uncertainties in the final RomUkrSeis model are not worse than ±0.1 km/s for
537 crustal P-velocities and ±2 km for Moho depth in well resolved parts of the model (e.g. Grad
538 et al., 2006a,b; Środa et al., 2006; Grad et al., 2008; Janik et al., 2009a).
539
540 A comparison of computed and observed travel-times for all the P-velocity model phases
541 along the RomUkrSeis profile, travel-time residuals and ray coverage are shown in Figure 8.
542 The root mean square of travel-time residuals (RMS) is acceptable, being ~0.08 s for crustal
543 phases (waves refracted and reflected in the crust) and ~0.10 s for Moho reflections as well as
544 upper mantle refracted phases. The RMS value for purely refracted phases in the crust is 0.08
545 s while for reflections it is 0.09 s. The overall RMS value for 3794 picks is 0.09 s. RMS
546 values for all the phases are similar. Accuracy is slightly better for refracted crustal phases
547 than for reflected and upper mantle waves. The seismic velocity is well determined, in
548 particular the crustal structure, obtained mainly from refracted P-waves. Where S-waves are

observable along the RomUkrSeis profile, they are quite well recorded (Figs. 4c and 7) and thus it is estimated that the uncertainties in crustal S-velocities are not worse than ±0.1 km/s, which is about twice the error percentage of the crustal P-velocities.

## 6. Interpretation and discussion of the RomUkrSeis velocity model

The velocity structure of the crust and uppermost mantle on the RomUkrSeis profile reveals three main domains, which also correspond to the character of the gravity, magnetic and heat flow anomalies along the profile (Fig. 5). These domains from simplest to most complex are 1) the East European Craton (EEC) and its margin, comprising the south-western part of the Ukrainian Shield and the Volyn-Podolsk Monocline; 2) the southern Apuseni Mountains and the Transylvanian Basin, both thought to have formed on the crust of the Tisza-Dacia composite terrane; and 3) the Eastern Carpathians, emplaced above the Teisseyre-Tornquist Zone (TTZ) and representing the junction zone between domains 1) and 2). A tectonic interpretation of the derived velocity structure is presented in Figure 9 and its main features are described and discussed in the following sections for these three tectonic domains in turn, including how the RomUkrSeis results compare to the results of earlier WARR images acquired nearby for each. This is then followed by an integrated overview of crustal and upper mantle structure along the profile as a whole and its implications for large-scale tectonic processes affecting the RomUkrSeis lithosphere through time (section 7).

### *6.1 The eastern domain: East European Craton (km 430-675)*

This domain of the RomUkrSeis profile (the southwestern Ukrainian Shield, where crystalline basement is exposed beyond about km 550, plus the Volyn-Podolsk Monocline, where a thin layer of younger sediments overlies crystalline basement) comprises the northeastern ~35% part of the profile as a whole, about 255 km in length in total.

#### *6.1.1 Sedimentary cover*

The thin sedimentary layer ($V_p$<5 km/s; green colours in Figs. 5, 9 and 10) represents Palaeozoic platform sediments or proximal shelf sediments of the newly developing continental margin of Baltica in the Early Palaeozoic (e.g. Nikishin et al., 1996; Sliaupa et al., 2006). They overlie highly indurated late Neoproterozoic (Cryogenian-Edicarian; *viz.* late Riphean-Vendian) sediments, probably conformably overlying crystalline basement based on what is observed elsewhere along the margin and in the interpreted seismic reflection section of Zayats (2013) reproduced in Figure 10. The late Neoproterozoic and earliest Palaeozoic sedimentary succession is resolved as the layer that reaches a depth of about 5 km at the southwestern limit of this segment of the RomUkrSeis velocity model ($V_p$ 6.0-6.15 km/s to a depth of ~7 km at ~km 350). The velocities and $V_p/V_s$ ratio inferred for this layer are consistent with quartz-rich metasedimentary rocks (e.g. Yegorova et al., 2004; Hollbrook et al., 1992; Christensen, 1996) although, in the velocity model, this layer merges to the northeast with the uppermost crystalline basement of the exposed Ukrainian Shield; cf. Figs. 5

593 and 9).
594
595 *6.1.2 Crystalline crust*
596
597 The crystalline basement of this segment of RomUkrSeis is the tectonically oldest on the
598 profile, terminating in the Podolian Domain of the EEC, which is one of its principal
599 Archaean units (Chekunov, 1989; Bogdanova et al., 2006) although strongly reworked in the
600 Palaeoproterozoic (Claesson et al., 2006). The prevailing rock types are Archaean- and
601 Palaeoproterozoic-aged granulites (Claesson et al., 2006). The upper-middle crustal layer in
602 the model has $V_p$ 6.15-6.35 km/s, Vs 3.60-3.65 km/s and, accordingly, $V_p/V_s$ 1.67-1.72 (Fig.
603 5). The lower crust of this domain displays velocities $V_p$ 6.45-6.6 km/s, Vs 3.82 km/s (and
604 $V_p/V_s$ 1.70). The upper boundary of the lower crust is marked by a clear seismic boundary
605 shallowing from a depth of 25 km at km 570 to 15-16 km at km 460-500 before deepening
606 again to the southwest. The 6.45-6.57 km/s lower crustal layer appears to be truncated at
607 about km 430-440 (the nominal limit of the "EEC domain" in the velocity model), with lower
608 crustal velocities immediately to the southwest being in the range 6.30-6.40 down to the
609 Moho at ~38 km depth (Fig. 5). The availability of both P- and S-wave velocities in the crust
610 and upper mantle of the EEC domain of the RomUkrSeis profile allows some inferences to be
611 made regarding crustal lithological composition. Upper and middle crustal velocities are
612 typical of felsic rocks such as granites and granitic gneisses, whereas the velocities in the
613 lower crust suggest the prevalence of felsic granulites and, to a lesser extent, intermediate
614 granulites or amphibolites (Hollbrook et al., 1992; Rudnick and Fountain, 1995; Christensen,
615 1996).
616
617 *6.1.3 Moho and upper mantle*
618
619 The topography of the Moho is sub-parallel to the antiformal geometry of the upper boundary
620 of the 6.45-6.57 km/s lower crustal layer. The Moho shallows from 40 km at the northeastern
621 end of the profile to 34 km at km 450-470 km and it deepens again to the southwest. In the
622 distance range km 430-440, essentially the southwestern boundary of the EEC domain of
623 RomUkrSeis, the Moho signature in the seismic data is highly complex. The presence of a
624 short seismic discontinuity segment in the uppermost mantle in this range of the model is
625 highly uncertain. It was necessitated by the technical limitations of the ray-tracing code, rather
626 than being obtained by modelling of clearly observed seismic phases. Ray-trace modelling of
627 $P_n$ in this area was problematic because the Moho step at km ~430 results in a "shadow zone"
628 for shot points located southwest of it, which are the key constraining shot points. This
629 discontinuity segment was introduced in order to refract the propagating $P_n$ rays upwards to
630 generate computed travel-times that could be used for modelling. Indeed, the full-waveform
631 simulation demonstrates that this discontinuity fragment is not necessary to observe the $P_n$
632 phase (SP15310 and SP15311; cf. Figs. 6f,g).
633
634 Upper mantle velocities are $V_p$ 8.1-8.2 km/s, $V_s$ 4.61 km/s and, accordingly, $V_p/V_s$ 1.76. A
635 reflector is observed in the upper mantle beneath this segment of RomUkrSeis, shown at a
636 depth of ~47 km in Figures 5 and 9 but the data do not permit determining whether it

637 represents a velocity increase or a velocity decrease. Figure 5 shows $V_p$ 8.3(?) km/s but it
638 could just as well be $V_p$ less than 8.15-8.2 km/s. The upper mantle velocities are consistent
639 with ultramafic rocks, specifically peridotite (Rudnick and Fountain, 1995; Christensen,
640 1996) as is typical and has been observed elsewhere in the southeastern EEC (e.g. Janik et al.,
641 2009b).
642
643 *6.1.4 Comparison with nearby WARR profiles on the EEC*
644
645 The velocity structure of the Podolian Domain observed by RomUkrSeis and other WARR
646 profiles, notably profile EB'97 (Thybo et al., 2003; Kozlovskaya et al., 2004; Yegorova et al.,
647 2004; Bogdanova et al., 2006), which intersects the northwestern end of the RomUkrSeis
648 profile at SP15311, and DOBRE-4 (Starostenko et al., 2013), south of Moldova (see Fig. 1 for
649 location of the profiles) are comparable. There is similarity as regards the seismic boundary
650 around 25 km depth and the distinct lack of a high-velocity lower crust (i.e., $V_p$ is no greater
651 than 6.9 km/s directly above the Moho). There are some differences in crustal structure,
652 however. The velocities in the upper part (to 25 km depth) part are higher (6.15-6.45 km/s) in
653 the EB'97 profile than on the RomUkrSeis profile (6.10-6.35 km/s). Further, the velocities in
654 the lower crust of EB'97 are ~0.25 km/s higher than RomUkrSeis and the depth to the Moho
655 is ~5 km greater on EB'97 profile than on RomUkrSeis. These two profiles intersect one
656 another towards the northeastern end of RomUkrSeis (nearby SP15311; cf. Fig. 1) and,
657 although they intersect at the surface, the seismic rays controlling their respective velocity
658 models at Moho depths are some 40 km from each other. Accordingly, the differences in their
659 respective velocity models at lower crustal and Moho depths could be the result of
660 intrinsically poorer data coverage and greater uncertainties near the ends of the respective
661 profiles or the possibility of crustal anisotropy (given the obliqueness of the intersecting
662 profiles), not to mention even slightly different modelling approaches. It is noted that, nearby,
663 there is evidence from Deep Seismic Sounding transect VIII (Grad and Tripolsky, 1995; see
664 Fig. 1 for location) about 100 km south of the intersection of EB'97 and RomUkrSeis of quite
665 abrupt changes in Moho depth within the Podolian Domain of the Ukrainian Shield, from ~54
666 km to ~40 km over ~80 km distance on the westernmost part of VIII. There are also abrupt
667 changes in Moho depth below the DOBRE-4 profile (see Fig. 1), a ~10 km change of Moho
668 depth over a ~40 km distance beneath the South Ukraine Precambrian Platform (Starostenko
669 et al., 2013).
670
671 The lack of a lower crustal layer with $V_p$ >6.9 km/s is a previously observed feature of the
672 velocity structure of the Podolian Domain of the Ukrainian Shield, revealed on both the
673 RomUkrSeis and the EB'97 profiles as well as in the EEC crust below platform cover on
674 DOBRE-4. It contrasts with generally higher velocities ($V_p$ 6.75-7.1 km/s) attributed to the
675 lower crust in neighbouring parts of the EEC (e.g. Pavlenkova, 1996; Grad et al., 2006b; Janik
676 et al., 2009b, 2011). Many of these neighbouring studies image crust of the Fennoscandian
677 segment of the EEC (Gorbatschev and Bogdanova, 1993), in particular its Svecofennian
678 Domain, which comprises lithosphere accreted during Palaeoproterozoic orogenic events (e.g.
679 Skridlaite et al., 2003; cf. Bogdanova et al., 2006). Some, like the PANCAKE WARR profile
680 between Ukraine and Hungary not far north of RomUkrSeis (cf. Fig. 1), image crust within

the Osnitsk-Mikashevichi Igneous Belt (OMIB; according to the Fennoscandian basement map of Gorbatschev and Bogdanova, 1993) domain of the EEC. The OMIB was strongly affected by accretionary igneous processes in the middle Palaeoproterozoic and lies along the suture between the Fennoscandian segment of the EEC and the mainly Archaean-aged Sarmatian segment of the EEC, of which the Podolian Domain encountered by RomUkrSeis is a key part (e.g. Bogdanova et al., 2006). This suture, and the superimposed OMIB, are thought to have been themselves later mildly reactivated with the formation of a half-graben perpendicular to the synchronous Rodinia break-up axis (i.e., roughly coincident with the TTZ) in the late Precambrian (e.g. Bogdanova et al, 2008; Krzywiec et al., 2018; Poprawa et al., 2020). PANCAKE displays a thick lower crustal layer (up to 20-25 km) with $V_p$ 6.6-7.4 km/s (Starostenko et al., 2013), which contrasts with the absence of a high velocity lower crustal layer on the eastern, EEC domain, of RomUkrSeis. The velocity structure of the Podolian Domain as seen on RomUkrSeis is more comparable to other mainly Archaean domains found outside of Europe such as the Superior Province in Canada, the Pilbara and Yilgarn cratons in western Australia and the Kaapvaal and Zimbabwe cratons in southern Africa (e.g. Abbott et al., 2013), which mainly do not display high velocity lower crustal layers.

### *6.2 The western domain: southern Apuseni Mountains-Transylvanian Basin (km 0-300)*

In this domain the Transylvanian Basin overlies crust that is exposed in the Apuseni Mountains to its southwest. This crust was formed as a result of complex Mesozoic convergence and shortening processes, including crystalline basement-involved thrusting and nappe emplacement and the accretion of large ophiolitic bodies that led to the suturing of the Tisza and Dacia terranes (Săndulescu, 1988; Tari et al., 1995; Fodor et al., 1999; Csontos and Vörös, 2004; Bortolotti et al., 2004 and references therein; Hoeck et al, 2009, Robertson et. al., 2009). The inferred Tisza-Dacia suture lies not far north of the profile (Fig. 2) so that the RomUkrSeis seismic model illuminates the crust of the Dacia unit, presumably including fold and thrust shortening structures as well as possibly underlying older crystalline basement of uncertain affinity (e.g. Csontos and Vörös, 2004; Schmid et al., 2008).

#### *6.2.1 Transylvanian Basin and other sedimentary cover*

The Late Cretaceous and younger Transylvanian Basin is well-imaged in the velocity model (Figs. 5) as the body at km 130-270 with thickness up to 3-4 km and $V_p$ up to 3.60 km/s, typical of sedimentary rocks that have not been deeply buried and indurated. This unit overlies another sedimentary layer, though with slightly more consolidated sedimentary strata ($V_p$ up to 4.45 km/s) in the distance range km 120-300. This layer includes what looks like a narrow rift or pull-apart basin centred at about km 210-215 and as deep as ~6 km, a feature that is well constrained by the WARR data on the RomUkrSeis profile. These two sedimentary domains are shown together as a single sedimentary body (green colour) on the interpretive version of the velocity model in Figure 9. Though the Miocene sediments of the Transylvanian Basin are affected by salt tectonics and Neogene volcanism (Krézsek and Bally, 2006; Tiliţă et al., 2013), the WARR data do not resolve any evidence of these nor of

thrust deformation within the sedimentary package (e.g. Tiliţă et al., 2013). It is noted, however, that thrusting and strike-slip faulting are reported to cut pre-Miocene units (e.g. Ciulavu et al., 2000; Tiliţă et al., 2013), which may have relevance for the narrow rift-like structure at km 205.

A sedimentary unit with $V_p$ 4.18 km/s lies at the SW end of the RomUkrSeis profile (km 0-50) on the southern flank of the exposed southern Apuseni Mountains, where they consist mainly of Permian-Triassic sedimentary strata that were folded and thrusted during the Mesozoic tectonism. The model body at km 50-90 with velocity 5.40 km/s and inferred to a depth of ~4 km is interpreted as representing the Apuseni Mountains in the subsurface. Rocks of the southern Apuseni ophiolite complex also crop out in the southern Apuseni Mountains (e.g. Bortolotti et al., 2002, 2004; Reiser et al., 2016) and these contribute to raising the bulk velocity of this model unit. Neogene igneous intrusions also occur (cf. Seghedi et al., 2007) and heat flow in this area is locally elevated (up to 70-80 $mW/m^2$; Horvath et al., 2015). At km 90, velocities observed at the near surface decrease ($V_p$ 4.15 km/s), roughly at the location of a regional fault identified by Linzer et al. (1998), which, along with several others in this area, is associated with recent dextral strike-slip movements. This contrasts with the sinistral strike-slip Dragos Voda Fault (Linzer et al., 1998), crossed by RomUkrSeis at the northeastern limit of the Transylvanian Basin (DVF; Figs. 5 and 9).

*6.2.2 Crystalline crust*

The RomUkrSeis velocity model of the uppermost crystalline crust of the southern Apuseni Mountains-Transylvanian Basin domain is complex and, at the scale of the model, consists of four contiguous bodies. The shallowest, lying below the southern Apuseni Mountains between km 90 and 200 and in the depth range 2-7 km has $V_p$ 6.07-6.20 km/s ("Body 1" for purposes of further discussion in this section, as labelled in Fig. 5 and 9). To its southwest and deeper lies a body between the surface and km 90 in the depth range 4-10 km with quite uniform $V_p$ in the range 6.34-6.36 km/s ("Body 2"; cf. Figs. 5 and 9). Both these bodies overlie crustal units that display lower velocities. In the case of the former, the underlying unit is the southwestern part of the third uppermost crustal body ("Body 3"; cf. Figs. 5 and 9) that lies at depths up to ~12 km at km 220 and displays velocities in the range 5.95-6.0 km/s. To the northeast, "Body 3" directly underlies the sedimentary layers of the Transylvanian Basin described above and is bounded to the northeast by a SW-dipping velocity discontinuity, across which velocities are slightly higher. This is "Body 4" (cf. Figs. 5 and 9), lying between km 240 and km 320 at depths ~6-12 km and exhibiting poorly constrained velocities, highlighted by $V_p$ 6.10(?) km/s isovelocity line in Figure 5.

Body 1 has no obvious expression in the gravity and magnetic fields (Fig. 5) and, therefore, has no anomalous high magnetisation and density even though its velocity is higher than laterally contiguous units. It seems unlikely, therefore, that it is strongly associated with the ophiolite complex in this area and, similarly, an island arc fragment preserved in the Tisza-Dacia suture zone (e.g. Csontos and Vörös, 2004), even if its magmatic component (such as oceanic arc volcanics) were mixed with significant volumes of sedimentary strata. Body 1 is

confined by distinct seismic boundaries on both its top and its base, which could be indicative of an exotic origin, for example, as a felsic fragment of the crystalline basement of Tisza wedged into Dacia as a result of complex transpressional tectonics in the Tisza-Dacia suture zone as is suggested on Figure 9. Such a possibility is supported by its subsurface proximity to the extent of Tisza projected at the surface (vicinity of SP15302 on Fig. 2).

Body 2, in contrast to Body 1, corresponds to a gravity high (up to ~+20 mGal) and to a slightly elevated magnetic field (Fig. 5). Further, the RomUkrSeis seismic data permitted $V_s$ 3.80 km/s to be determined for this body (and, accordingly a $V_p/V_s$ of approximately 1.67; Fig. 5, lower panel). Rocks of the southern Apuseni ophiolitic complex are exposed at the surface above Body 2 (in the vicinity of SP15301) and its model velocities compare well with those of ophiolite complexes worldwide. An interpretation for Body 2, therefore, is that it consists of rocks of oceanic layer 2 (pillow lavas and sheeted dyke complex) and/or the upper part of oceanic layer 3 ($V_p$ 6.4-6.8 km/s and $V_s$ 3.6-3.8 km/s; Christensen and Salisbury, 1975; Christensen, 1978).

Body 3, in contrast to both bodies 1 and 2, corresponds, most likely, to the "normal" Dacian basement of the Transylvanian Basin consisting mainly of highly deformed late Palaeozoic and Mesozoic sediments transported in basement-involved thrusts and overlying nappes (Fig. 9). The base of Body 3 can be traced from 8 km depth at km 120 (Apuseni Mountains) to 12 km depth at km 220 (central part of the Transylvanian Basin) and, after a narrow deepening to 13-14 km at km 235-240 rises to about 5 km under the Carpathians. This deepening occurs some 30-35 km northeast of the narrow rift structure imaged at the base of the Transylvanian Basin.

The velocity of uppermost crustal Body 4 is poorly constrained. It could be characterised by a crystalline basement-like velocity of 6.1 km/s or could be similar to that of the near vertical prism with sedimentary-like velocities lying immediately to its northeast ($V_p$ 5.35 km/s and less) that characterises the upper part of the velocity model in its Eastern Carpathian-TTZ domain. Body 4 projects to the surface in an area of abundant Neogene magmatism (Fig. 2) associated with relatively high surface heat flow (Fig. 5). The Dragos Voda Fault (DVF; Fig. 2) also crosses the profile at the surface in this vicinity. Possible interpretations for Body 4 include intruded and highly tectonised crystalline basement or that it forms part of the Dacian basement of the Transylvanian Basin similar to Body 3. Given the velocity ambiguity of this body it cannot be precluded that it comprises Palaeozoic-Mesozoic sedimentary rocks with affinity to the adjacent Carpathian sedimentary prism.

Within the Apuseni Mountains-Transylvanian Basin domain of the RomUkrSeis profile, the middle and lower crust, from a depth of about 10 km to the Moho, is different between the Apuseni Mountains segment and the Transylvanian Basin segment. In the former, $V_p$ increases from 6.2 km/s to a bit higher than 6.4 km/s at the Moho, which lies in the range 30-35 km, dipping slightly to the northeast. In contrast, the 6.4 km/s velocity contour beneath the Transylvanian Basin is as shallow as 17-18 km at km 250. $V_p$ increases to as high as 6.56 km/s at the Moho in the Transylvanian Basin part of the lower crust. The spatial coincidence

of the higher velocity lower crust with the Transylvanian Basin depocentre suggests a genetic link between basin subsidence and isostasy-perturbing processes in the lower crust (and presumably underlying mantle lithosphere). It is, of course, not possible to preclude that these crustal features are inherited features (i.e., older than the Transylvanian Basin) or that they are actually younger (e.g., possibly linked to the formation of the adjacent Pannonian Basin).

*6.2.3 Moho and upper mantle*

The Moho in the western domain of RomUkrSeis is at roughly similar depths throughout (30-35 km) with the exception of a narrow structure almost as deep as ~40 km at km 220. This is 20 km laterally offset from the similar narrow deepening of the base of upper crustal Body 3 at km 235-240, which, in turn, is 25 km laterally offset from the narrow rift-like structure at the base of the Transylvanian Basin. It cannot be excluded that the slightly shallower Moho northeast of the narrow structure at km 200 is genetically linked to the higher velocity lower crust above it and processes forming the Transylvanian Basin, although it is offset from the main depocentre of the basin. It is further noted that there is no evidence of Moho deepening beneath the higher topography (and denser upper crust) of the Apuseni Mountains suggesting that the crust in this part of the western domain of RomUkrSeis is not in isostatic equilibrium. A reflector is observed in the upper mantle beneath the eastern Transylvanian Basin part of this segment of RomUkrSeis, shown at a depth of ~52 km in Figures 5 and 9 but the data do not permit determining whether it represents a velocity increase or a velocity decrease. Figure 5 shows $V_p$ 8.35(?) km/s but it could just as well be less than 8.15-8.2 km/s.

*6.2.4 Comparison with nearby WARR profiles*

The main characteristics of the sub-sedimentary uppermost crust along the Apuseni Mountains-Transylvanian Basin domain of RomUkrSeis are similar to those found along the VRANCEA-2001 WARR profile (see Fig. 1). The point of intersection of RomUkrSeis and VRANCEA-2001 at the surface is shown in Figs. 5 and 9). The intersection is very nearly at the terminus of VRANCEA-2001 and Hauser et al. (2007) did not utilise data recorded northwest of their final shot point so a direct comparison at the intersection point is not very meaningful. Hauser et al. (2007), nevertheless, also interpreted crustal velocity structure in this area in terms of thrust-and-nappe tectonics. The depth to Moho of both profiles is comparable although the VRANCEA-2001 model displays higher lower crustal velocities (6.8-7.0 km/s below 25 km depth) than RomUkrSeis and a lower uppermost mantle velocity of 7.9 km/s compared to ~8.2 km/s on RomUkrSeis. Correlation of the critical phases defining these velocities is possible over greater offset distances on RomUkrSeis suggesting that the RomUkrSeis model velocities may be more reliable.

***6.3 The central domain: Eastern Carpathians and the TTZ (km 300-430)***

This section deals with the part of the RomUkrSeis velocity model imaging the complex transition zone, called the Teisseyre-Tornquist Zone (TTZ), between the Tisza-Dacia lithosphere overprinted by Transylvanian Basin-Carpathian tectonics west of the TTZ and the

Precambrian lithosphere of the East European Craton (EEC) to its east. The TTZ is understood to have been a first-order tectonic boundary inherited from late Precambrian times when it was formed as the continental margin of Baltica after the break-up of the pre-existing proto-continent Rodinia. Thereafter it formed a "backstop" to the accretion to its southwest of allochthonous lithospheric terranes during the Palaeozoic Caledonian and Variscan orogenies (e.g. Pharaoh, 1999; Pharaoh et al., 2006; Narkiewicz et al., 2015) and was subsequently reactivated during the Late Palaeozoic and Mesozoic-Cenozoic (e.g. Winchester et al., 2006; Narkiewicz, 2007; Hippolyte, 2002). This culminated with the Eastern Carpathian orogeny, which overprinted the TTZ and masked its expression in the surface geology of the RomUkrSeis profile. Accordingly, the crustal features in this domain of the RomUkrSeis profile must strongly reflect the lithosphere-scale structures produced by the processes initially establishing the TTZ in the late Precambrian and Palaeozoic even though these may have been later overprinted. Overprinting will have been imposed not only by younger structures produced by the compressional tectonics of the Carpathian orogeny but also by extensional, back-arc (?) basin-forming processes that presaged the Carpathian orogeny.

*6.3.1 Sedimentary units*

The most profound feature within this RomUkrSeis domain is a narrow Carpathian prism (Outer Carpathians and Carpathian foredeep) at km 320-360 characterised by velocities implying that it is composed of sedimentary and metasedimentary rocks. This body, as seen in Figures 5 and 9, has a width of ~40 km and dips at about 40 degrees to the southwest. As mentioned earlier (section 5.2), however, modelling constraints cannot exclude that the "Carpathian prism" possibly encompasses some or all of Body 4 to its immediate southwest (the area marked by green and pink stripes in Figures 9 and 10). To the northeast, it merges with the Neoproterozoic and younger, platform and foredeep sedimentary cover of the Volyn-Podolsk Monocline (section 6.1).

There are five seismic reflection profiles in the Ukrainian sector of the Outer Carpathians and Carpathian foredeep (profiles P-1 to P-5 located in Fig. 10a). Of these profiles P-5 (Fig. 10c; Zayats, 2013), lies closest by (~50 km) and sub-parallel to the RomUkrSeis profile, and provides some calibration of the structure and composition of the Carpathian sedimentary prism. The uppermost ~6 km with velocities 4.7-4.9 km/s and possibly some of the underlying 5.35 km/s unit corresponds with the Cretaceous-Neogene flysch complex of the Outer Carpathians. The 5.35 km/s unit otherwise consists of the older, more compacted (meta) sediments of the pre-Neoproterozoic-early Palaeozoic platform, overlain by continental shelf and deeper water units and, in turn, overlain by sediments deposited in the Caledonian foredeep basin (e.g. Sliaupa et al., 2006) and during later Variscan age reactivations in the Palaeozoic. It is noted that the seismic reflection interpretation suggests that the sedimentary prism is not quite as deep as the velocity model. This is likely linked to velocities used for depth converting the reflection image but may also reflect the resolving capabilities of both datasets. Structural cross-sections based on mapping the surface geology of the Eastern Carpathian nappes are generally in keeping with the reflection and velocity models, suggesting a thickness of some 8-10 km of Cretaceous and younger strata in Ukraine (e.g.

Shlapinsky, 2015; Nakapelyukh et al., 2018) and in northern Romania (Stefánescu and Working Group, 1988, Schmid et al., 2008; Matenco et al., 2010).

Reflection profile P-5 (Fig. 10c) also shows that the sedimentary succession underlying the main flysch complex is cut by a normal fault, labelled the Fore-Carpathian Fault (FCF; Fig. 10). It is associated with a series of other nearby faults in Ukraine, including the Rava-Ruska Fault (RRF; Fig. 10), which generally affect older strata but not the youngest, Cenozoic, sediments of the Carpathian foredeep (e.g. Kruglov and Tsipko, 1988; Tectonic map of Ukraine, 2007; Zayats, 2013). The FCF, in its deeper expression, according to the interpretation of Zayats (2013; Fig. 10c), although there is a lack of direct age calibration in this complex region, displays extensional, or transtensional, tectonics older than Carpathian thrusting. This would include reactivation of the TTZ during the latest stages of Variscan tectonics or during post-Variscan Late Palaeozoic to Triassic transtensional instability affecting the European lithosphere (e.g. Ziegler et al., 2006; Mazur et al., 2020). It is possible that the FCF as seen in Figure 10c is reactivating an older, much deeper structure that formed originally during the Neoproterozoic-early Palaeozoic formation of the continental margin of Baltica and establishment of the TTZ in the first instance. In this regard, it is of interest that the velocity model has imaged a deeper, fairly steeply dipping velocity discontinuity (~km 360, depth range ~8-18 km; Figs. 5 and 9) that projects upwards to be roughly coincident with the FCF as seen in Figure 10c. This steeply dipping velocity discontinuity could accordingly be interpreted as part of a major, upper crustal scale (if not whole crust scale), fault (zone) inherited from the formation of the Baltic margin and thereafter a locus of TTZ reactivation.

*6.3.2 Crystalline crust*

From the vicinity of the steeply dipping velocity discontinuity mentioned above throughout the rest of the crystalline crustal layer, the central domain of the RomUkrSeis velocity profile exhibits reduced velocities compared to the adjacent crustal domains. At km 360, $V_p$ 6.3 km/s, occurs immediately above the Moho. This is some 30 km deeper than similar velocities elsewhere along the profile (Fig. 5). The 6.20 km/s velocity isoline also deepens significantly in the central (Eastern Carpathians and TTZ) domain. The strong negative gravity anomaly observed in this domain (values as low as -100 mGal compared to background values of ~-30-40 mGal and ~0 mGal in the Transylvanian Basin and Ukrainian Shield domains, respectively) is likely caused not only by the Carpathian sedimentary prism in the uppermost crust but from a reduced crustal density throughout the crust. It cannot be precluded that some of the material in this zone, below the Carpathian sedimentary prism and bounded by the inferred FCF to the northeast are meta-sedimentary and meta-volcanogenic rocks of a Mesoproterozoic-Neoproterozoic (e.g. Riphean) basin that pre-existed and possibly localised the break-up of Rodinia within the proto-TTZ.

There is limited coverage by the RomUkrSeis S-wave velocity model in the crustal part of this segment of the profile (Fig. 5; $V_s$ 3.67-3.78 km/s) indicating $V_p/V_s$ 1.64 at shallower depths and $V_p/V_s$ 1.73(?) at greater depths, just above the mantle. In general, there is too much uncertainty to shine much light on the assertion above that this part of the crust includes

significant volumes of meta-sedimentary and/or meta-volcanogenic rocks.

*6.3.3 Moho and upper mantle*

The geometry of the Moho within the central domain of the profile is profoundly variable, displaying a narrow keel (<40 km wide and as thick as ~12 km) dipping northeast on its southwestern side and almost vertical on its northeastern side. The maximum Moho depth at the apex of this keel is about 50 km and is the greatest Moho depth observed along the RomUkrSeis profile as a whole. Although the general trend of the Moho depth along the RomUkrSeis profile as a whole corresponds with the recently compiled Moho map of Bielik et al. (2018) for the Carpathian-Pannonian region, the 50 km deep keel inferred along RomUkrSeis was not resolved there. In this regard, the ray-tracing solution used in the modelling and described in section 5.3 as "a wedge of crustal material" in the mantle (km 340-350) seems to be well justified by the SP15303 and SP15304 record sections and, indeed, it cannot be excluded that crustal velocities occur at even greater depths than 50 km.

As elsewhere on the RomUkrSeis profile, upper mantle velocities are not atypical with $V_p$ 8.2 km/s. However, because crustal velocities immediately above the Moho are comparatively low in this segment of the profile, the velocity contrast at the Moho is higher than elsewhere. An upper mantle reflector is observed at 50-55 km depth straddling the boundary of the southwestern domain of the profile and this one (Figs. 5 and 9), mentioned here rather than in subsection 6.2.3 because it is subparallel to the overlying Moho boundary dipping northeast on the southwestern side of the TTZ crustal keel.

*6.3.4 Comparison with nearby WARR and other deep seismic profiles crossing the TTZ*

The deep structure of the TTZ north of the Carpathian belt, mainly in Poland, where it is covered by Permian and younger sediments of the Polish Trough (e.g. Dadlez et al., 1995), has been imaged on a number of WARR seismic profiles, including TTZ, POLONAISE'97 and CELEBRATION (e.g. Grad et al., 2003; Janik et al., 2005, 2009; Guterch et al., 2015). In southeastern Poland, the TTZ was crossed by deep reflection seismic profile POLCRUST-01 (Malinowski et al., 2013; Narkiewicz et al., 2015; Krzywiec et al., 2017), the location of which is shown on Figure 1.

With respect to basin architecture and crustal structure, the POLONAISE'97 profile P4 (Grad et al., 2003) is particularly comparable to the RomUkrSeis profile, with the sedimentary package of the Polish Trough, ~150 wide and ~10 km thick, is underlain by material with low P-wave velocity (5.8 km/s) down to 18 km, interpreted as deeply buried Neoproterozoic-Palaeozoic strata (Pharaoh et al., 2006). Like RomUkrSeis, relatively low velocity crust is also inferred below the basin to even greater depths (e.g. 28 km; Guterch et al., 2015). This is in contrast with the modelled velocity structure on CELEBRATION profile CEL05 (located on Fig. 1). Here, the TTZ is underlain by a domal uplift with $V_p$ 5.6-6.1 km/s to a depth of 22 km underlain by moderately high velocity lower crust with $V_p$ 6.65-6.85 km/s (Grad et al., 2006a; Janik et al., 2009a).

With respect to the structure of the Moho and upper mantle all profiles have their own peculiarities but one striking feature in common for all profiles is that the Moho across the TTZ deepens from 25-35 km within the accreted Phanerozoic terranes to the southwest to greater than 40 km within the EEC to the northeast. A distinct crustal keel as seen on RomUkrSeis has not generally been observed on other profiles crossing the TTZ north of the Carpathians. However, similar very abrupt Moho steps situated analogously to the Inner/Outer Carpathians contact were found along several profiles intersecting the western Carpathians (Środa, 2010; Hrubcová and Środa, 2015). North-northeast dipping seismic boundaries (reflectors) in the upper mantle comparable to the one observed on RomUkrSeis sub-parallel to the Moho forming the southwestern flank of the crustal keel are also observed below the western Carpathians (e.g. Grad et al., 2006b; Janik et al., 2009a, 2011; Guterch et al., 2015). These inclined seismic boundaries at 60-70 km depth were associated with collisional interactions (including underthrusting) of younger lithospheric terranes (ALCAPA and Tisza-Dacia) with the Caledonian-EEC lithosphere beyond the Carpathian arc (e.g. Grad et al., 2006b; Guterch et al., 2015; Verpakhovska et al., 2018).

The deep structure of the TTZ where it is obscured by the Eastern Carpathians is crossed by WARR profiles PANCAKE (Starostenko et al., 2013; Verpakhovska et al., 2018), from Ukraine into the Pannonian Basin in Hungary, and VRANCEA99 (Hauser et al., 2001) and VRANCEA-2001 (Hauser et al., 2007), which intersect in the foreland of the Carpathian belt at its southeasternmost tip, the former running SSW-NNE, subparallel to RomUkrSeis and the latter perpendicular to it, crossing the TTZ at a fairly oblique angle. VRANCEA-2001 is also, in part, imaged by deep reflection seismic profiling ("DACIA-PLAN"; Panea et al., 2005).

The PANCAKE crustal velocity structure is broadly comparable with RomUkrSeis, with a Carpathian sedimentary prism displaying similar velocities but broader and deeper (down to 25 km depth compared to 20 km) and, below this, generally reduced velocities in the underlying crust compared to either the cratonic or Phanerozoic segments of the profile, though not as marked as seen on RomUkrSeis. More obvious differences occur in the lowermost crust and in the disposition of the Moho. The Moho is shallower beneath the Pannonian Basin on PANCAKE than the Transylvanian Basin on RomUkrSeis (20-25 km versus 30-40 km) and deeper beneath the EEC on PANCAKE than on RomUkrSeis (45-50 km versus 35-40). The thicker EEC crust seen on PANCAKE is the consequence of a high velocity lower crustal layer ($V_p$ ~7-7.4 km/s) that is not imaged below RomUkrSeis and is most likely genetically linked to the existence of the Osnitsk-Mikashevichi Igneous Belt that formed in this part of the EEC in the Palaeoproterozoic and which is younger than the unmodified Podolian Domain crossed by RomUkrSeis.

VRANCEA-2001 crosses the Vrancea intermediate seismicity zonezone at the southeastern tip of the Carpathian arc, from an eastern terminus in the North Dobrogea "orogen", lying at the southern margin of the EEC, to a western terminus in the southern Transylvanian Basin (Fig. 1). Its velocity structure (Hauser et al., 2007) has similarities to RomUkrSeis, notably the Outer Carpathian-Carpathian foreland basin (Foscani Basin in this area) sedimentary

prism displaying $V_p$ less than 6 km/s down to about 20-22 km, comprising what are interpreted as sedimentary layers of Palaeozoic to Cenozoic age. The interpretation of these layers as sedimentary strata is quite robust given its layered appearance in the reflection seismic image of Panea et al. (2005), who refer to "a thick rift-like sedimentary basin underlying this transition area, in the depth range 10-25 km" (p. 307), underlying the younger sedimentary strata of the Focsani Basin and outermost Carpathian nappes. VRANCEA99 (Hauser et al., 2001) does not present a strong image of the Carpathian sedimentary prism as it runs tangentially to the bend of the orogen, essentially along strike rather than across it.

Hauser et al.'s (2001; 2007) interpretations of both the VRANCEA99 and VRANCEA-2001 profiles involve near vertical, crustal through-going structures such as the Capidava-Ovidiu, Peceneaga-Camena and Sfantu Gheorghe faults (COF, PCF and SGF on Fig. 2). These faults, in particular the first two, have been generally considered to be elements of the southeastern prolongation of the exposed TTZ southeast of the Carpathian deformation front in the Dobrogea domain of southeastern Romania (e.g. Seghedi et al., 1999; Mucuta et al., 2006; Starostenko et al., 2013b; Narkiewicz et al., 2015; Amashukeli et al., 2019). Bocin et al. (2013) found, from modelling of fairly high resolution gravity and magnetic data along a segment of the VRANCEA-2001 profile (and constrained by the WARR and reflection seismic images as well as shallow seismic profiles and surface geology), that there is an abrupt and marked change in crystalline crustal properties in the subsurface corresponding to the adjacent and overlying western limit of the sedimentary successions imaged by Panea et al. (2005) and adopted as such by Hauser et al. (2007). This near-vertical structure, extrapolated downwards, intersects the Moho in the zone where it deepens from about 35 km beneath the Transylvanian Basin to about 45 km beneath Dobrogea in VRANCEA-2001 and marks the boundary between crustal segments of different tectonic affinity. Its lateral abruptness suggests that it was displaced as a strike-slip fault prior to the development of the Carpathian orogenic belt that seals it.

## 7. Integrated interpretation: Precambrian to Cenozoic tectonic evolution of the RomUkrSeis lithosphere

### *7.1 Precambrian-early Palaeozoic*

The EEC segment of the crust and upper mantle lithosphere imaged by RomUkrSeis was accreted and assembled primarily in the Archaean with Palaeoproterozoic tectonic overprinting. By sometime in the late Mesoproterozoic or Neoproterozoic, after one or more earlier global cycles of proto-continental assembly and break-up, it formed part of the supercontinent Rodinia, which itself broke apart in the late Neoproterozoic, leaving behind proto-continent Baltica (the conjugate margin of which is generally thought to be part of what is now the Amazonian craton of present-day South America) that has formed the EEC. The velocity structure of much of this segment of RomUkrSeis (east of about km 430) is largely, if not exclusively, therefore, the consequence of pre-Neoproterozoic (primarily Archaean and Palaeoproterozoic) crustal accretionary and assembly processes. The possibility that the

antiformal structure of the upper crust-lower crust boundary (axis at km 490 and depth 15 km), and possibly the sub-parallel flexure of the Moho below it, is a Palaeozoic-aged modification is addressed below.

The western flank of the EEC segment of the crust and upper mantle lithosphere imaged by RomUkrSeis represents the Baltica continental margin of the oceanic domain that formed as a result of the break-up of Rodinia. As such, the crystalline crust of Baltica here will have been extended, thinned and overlain by a series of Neoproterozoic-early Palaeozoic sedimentary successions, including pre-rift platform strata, syn-rift strata and, perhaps especially, strata of a thick post-rift thermal sag passive continental margin basin. The low crustal velocities inferred in the RomUkrSeis velocity model accordingly are likely representative of thinned crystalline crust and Neoproterozoic-early Palaeozoic metasedimentary rocks. By the Ordovician the passive continental margin of Baltica became a collisional one and, eventually, the backstop of the German-Polish Caledonides (and their southeastern prolongation into the present-day Carpathian-Pannonian realm; e.g. Winchester et al., 2006), producing an adjacent syn-orogenic foreland basin of Ordovician to Devonian age on cratonic crust. The foreland basin strata are represented in the RomUkrSeis model by the deeper part of the “Carpathian” sedimentary wedge (light green units in the model) and possibly some of the lower velocity upper crustal material that it overlies.

The antiformal structure of the upper crust-lower crust boundary, and possibly the sub-parallel flexure of the Moho below it, to the east of the Baltica margin and mentioned earlier, is older than at least much of the overlying sedimentary succession since there is no comparable displacement of the base of the sedimentary units in the velocity model. However, there is a low amplitude antiform on the refracting horizon (axis at about km 430 and depth 5 km). Although the antiformal part of this horizon is not directly imaged in the nearby reflection profiling nor is its age constrained by RomUkrSeis, it very likely represents the base of Neoproterozoic sediments as seen immediately to the west in Figure 10. This suggests the possibility of a mild post-Neoproterozoic flexure of the crust as a whole in this part of the EEC segment of RomUkrSeis. Moreover, the abrupt truncation of the flexure in the lower crustal layer of the EEC crust on its western boundary and the correlative zone of complexity at the Moho almost immediately below it is suggestive of a zone of crustal-scale strike-slip motions (km 430-440). This may be related to the possible crustal flexure since it also coincides laterally with the axis of the basement antiform (km 440). Since Mesozoic and younger sedimentary horizons do not seem to be affected, such flexure of the EEC crust, if it exists, would most likely have been imposed by transpressional tectonics during oblique Caledonian collision and suturing in the Early Palaeozoic and not later.

### *7.2 Late Palaeozoic-Mesozoic*

The Variscan Orogeny succeeded the Caledonian Orogeny in central Europe in the late Palaeozoic and Variscan-derived tectonic units were accreted and sutured at this time to the earlier assembled Caledonian lithosphere that had been itself sutured to Baltica in the early Palaeozoic. The lithosphere emplaced and/or deformed during the Variscan Orogeny,

including overprinted Caledonian elements, became gravitationally destabilised at the close of the Variscan Orogeny (and onset of the break-up of Pangaea) with the formation of large Permo-Carboniferous sedimentary basins such as the Central European Permian Basin (e.g. Ziegler et al., 2006). In particular, the Polish Trough, coincident with the TTZ and lying north of the subsequently emplaced Carpathian deformation front, forms an important axis of Permo-Carboniferous subsidence related to this phase of tectonic destabilisation (e.g. van Wees et al., 2000). According to regional paleo-tectonic reconstructions (e.g. Barrier et al., 2018), the whole of the TTZ through to the convergent margin of the Paleotethys oceanic domain in the area of the present-day western Black Sea was extensionally or transtensionally reactivated at this time.

The crustal units forming the upper lithosphere imaged in the RomUkrSeis velocity model west of the Carpathians have similarly inherited the consequences of Variscan deformation and metamorphism and subsequent late Palaeozoic-Triassic wrench-faulting and basin formation. These are recorded in the rocks of the present-day Tisza-Dacia units, including nappes with Palaeozoic basement and Permian and Mesozoic sedimentary cover, identified as the upper crustal velocity bodies within the Apuseni Mountains and those underlying the Transylvanian Basin in the RomUkrSeis model. The Tisza-Dacia units are, however, generally not thought to have formed in situ, but rather may have been assembled behind the Variscan deformation front, possibly south and west of the present-day location of the RomUkrSeis profile, and then displaced into their current positions during the Cenozoic (during which time they were further deformed; e.g. Ustaszewski et al., 2008). The RomUkrSeis model does not provide any diagnostic evidence of whether the crustal units are allochthonous or autochthonous or to what degree; nevertheless, the complexity of the upper crust and the mosaic pattern of its constituent units are not inconsistent with such a tectonic history.

If these units are allochthonous then they have moved into place during the Cenozoic, when the Carpathians were formed and the present-day Carpathian deformation front established. As such, they would have trailed behind subducting oceanic (or ocean-like) lithosphere that formed during the Mesozoic in a back-arc setting linked to the Tethyan subducting plate boundary, which lay somewhere in the vicinity of the present-day Black Sea or just south of it. Just as the Black Sea formed as a back-arc basin associated with this convergent plate margin, so did a back-arc basin– the Carpathian Basin (or Embayment) – form in the region of the present-day Pannonian-Carpathian tectonic domain, also associated with the convergent Tethys margin. Regional geology and plate kinematic considerations (e.g. Barrier et al., 2018) suggest that rifting in the Carpathian back-arc basin was linked to the subducting Tethys margin by a transform plate boundary occupying the location of the TTZ (at the margin of the EEC) and involving the major fault zones now exposed in the Romanian foreland of the (future) Carpathians (cf. Fig. 1). According to Barrier et al. (2018), this was kinematically a transpressional plate boundary rather than a purely strike-slip one and it remained active until the Early Cretaceous when the formation of the Carpathian Basin was complete (thereafter to be closed during Carpathian orogenesis) and formation of the Black Sea began (e.g. Nikishin et al., 2015).

The pinch structures imaged at the base of nominally allochthonous Dacia-Tisza upper crustal units (km 240) and on the Moho (km 220) line-up vertically within a lateral zone of only 20 km suggesting the possibility of a common cause, such as a crustal throughgoing, mainly strike-slip fault, zone. No single continuous fault is necessarily implied but rather a zone of disseminated near vertical deformation structures such as a crustal-scale "flower structure" comprising a number of fault strands. The "narrow, rift-like" or pinch structure at the base of the Transylvanian Basin (~km 210), could be an expression of the same crustal-scale flower-structure possibly affecting the underlying crystalline crustal units and Moho. Displacements on such a structure, should it exist, cannot be younger than the earliest stages of formation of the Transylvanian Basin, since it is sealed by its sedimentary strata, which are Cenozoic in age, but could be the same age as sediments in the inferred narrow, rift structure that underlies it. These are late Early-Late Cretaceous in age if the RomUkrSeis imaged structure is analogous to similar rift-like structures seen in nearby seismic reflection profiling (e.g. de Broucker, 1998; Ciulavu and Bertotti, 1994; Krézsek and Bally, 2006).

The transpressional tectonic environment in the area implied by the regional geology in the reconstructions of Barrier et al. (2018) had dissipated by the earliest Cretaceous. The higher velocity lower crust (compared laterally with adjacent lower crust) could be the result of an early stage of late Early-Late Cretaceous rifting and lower crustal magmatic intrusion leading to the formation of the Transylvanian Basin. Certainly, the higher velocity lower crust has a strong correlation with the location of the Transylvanian Basin and magmatic intrusion of mantle material into the lower crust, elevating its velocity and density, during rifting is a very well-known and documented phenomenon (e.g., Mooney et al., 1983; Thybo et al., 2000; DOBREfraction'99 Working Group, 2003).

### *7.3 Cenozoic*

The emplacement of the Carpathian nappe units and the crustal units to their west and beneath them (ALCAPA-Tisza-Dacia composite terrane) in the Cenozoic is the final, and obviously highly complex, event forming the present-day architecture of the crust and upper mantle along the RomUkrSeis profile. The RomUkrSeis velocity model cannot resolve the regional complexity of this process, for example in the Transylvanian Basin behind the Carpathian deformation front, which also displays Cenozoic compressional shortening related to deformation taking place in the Carpathian nappe belt (e.g. Krézsek and Bally, 2006). Nevertheless, the most profound features of the RomUkrSeis velocity model are almost certainly the consequences of lithosphere shortening during the formation of the Carpathian Orogen. These are the Carpathian sedimentary prism, in the upper crust, and the crustal keel, which involves the lower crust and the upper mantle. Both these features are in keeping with the conventional view that the geodynamics forming the Carpathians involved subduction of the Carpathian Embayment (back-arc basin) lithosphere and its eventual closure with suturing of the ALCAPA-Tisza-Dacia lithosphere to the EEC lithosphere. There does remain some debate surrounding the subduction model in respect to the Eastern Carpathians. Fillerup et al. (2010), for example, favoured a lower crust (and underlying mantle lithosphere) delamination model based on seismic reflection profiling, including the DACIA-PLAN profile of Panea et

al. (2005), roughly coincident with the VRANCEA-2001 profile (located on Fig. 1).

The emplacement of the Carpathian sedimentary prism in the upper crust is not very sensitive to the choice of a subduction or delamination model; in either case upper crustal, mainly sedimentary units but also incorporating some crystalline basement rocks (e.g. Roure et al., 1993; Bocin et al., 2005; Verpakhovska et al., 2018), have been folded and stacked and this represents a concomitant shortening of upper crustal lithosphere. According to Burchfiel (1976) there is some 125 km of shortening recorded in the eastern Carpathian fold- and thrust-belt from the palinspastic restoration of a geological cross-section about 150 km south of the RomUkrSeis profile. Matenco and Bertotti (2000) estimated about 40 km shortening to be representative for the external nappes only of the Eastern Carpathians around the same location. To the north of RomUkrSeis (about 70 km), recent work by Nakapelyukh et al. (2018), in part calibrated with fission track data, suggests a much greater degree of shortening (340-390 km). In the RomUkrSeis velocity model the Carpathian nappes are stacked to a depth of about 8 km within the Carpathian sedimentary prism (overlying older sedimentary units within it) and, since this is calibrated by geological mapping and shallow reflection studies, it is consistent with the range of palinspastic estimates of Carpathian upper crustal and sedimentary layer shortening mentioned above.

The geometry of the mantle keel and surrounding units as expressed in the RomUkrSeis velocity model cannot be considered diagnostic in respect of discriminating subduction from delamination to "shorten" the lower crust and mantle lithosphere although it is more suggestive of the former (or, at least underthrusting of crustal units into the upper mantle if not actual complete lithosphere subduction). That the dipping upper mantle reflector (km 250-320) is sub-parallel to the dipping Moho above it may be significant in this regard. It is also noted that the "pinch" structure at km 230 in the strongly expressed seismic boundary interpreted as an intracrustal basal detachment beneath the Apuseni Mountains, discussed in sub-section 7.2, may alternatively be interpreted as revealing the incomplete image of an underthrusting geometry of Cenozoic age on this detachment surface.

The northeast-vergent thrusting mapped at the surface and exposed in the Outer Carpathians is accompanied by southwest-vergent underthrusting of Carpathian and older sedimentary units in the upper crust. In contrast, the lower crustal and upper mantle display northeast-vergent underthrusting, providing an overall structure similar to the "crocodile" structures caused by "interwedging" tectonics (Meissner et al., 2002; Snyder, 2002) with shortening at the TTZ and craton margin first at the base of the crust and upper mantle and, thereafter, in the upper crust and basement. A number of profiles crossing the TTZ, including BABEL (offshore), POLONAISE and CELEBRATION 2000 (Meissner et al., 2002; Guterch et al., 2015) have been interpreted in such a way. The RomUkrSeis WARR data do not resolve whether additional crocodiles may exist in the crystalline crust beneath the Carpathians and TTZ. It also cannot be ruled out that the lower crust-upper mantle "crocodile" was partly emplaced during the earlier Caledonian (transitioning to Variscan) accretionary phases at the craton margin/TTZ and only reactivated during subsequent tectonic events culminating in Carpathian orogenesis.

## 8. Summary and conclusions

WARR seismic profile RomUkrSeis is 675 km long and crosses from NE to SW three distinct lithospheric domains of different structure and tectonic evolution: the Archaean old cratonic domain of the East European Craton (EEC; southwestern part of the Ukrainian Shield and the cratonic margin), the Eastern Carpathians and the Teisseyre-Tornquist Zone (TTZ), and the younger composite Tisza-Dacia terrane with the Transylvanian Basin and Apuseni Mountains. The structure of the crust and upper mantle revealed along the RomUkrSeis profile echoes many disparate geodynamic processes involved in its formation and deformation from the Archaean through to the present-day, almost the whole of Earth history. It is characterised by significant lateral heterogeneity, as well as by complex Moho topography. The main results are summarised as follows.

(1) The eastern domain of RomUkrSeis, crossing the predominantly Archaean, Sarmatian segment of the EEC, is characterised by a crust of 38-40 km thickness and displays generally reduced velocities in the middle and lower crust compared to the predominantly Palaeoproterozoic cratonic crust to the north, where a higher velocity lower crustal layer is more typical.

(2) The central domain of RomUkrSeis incorporates the TTZ, the transition zone between the cratonic domain of the EEC to the northeast and the younger Tisza-Dacia terrane to the southwest. The crust in this area is usually considered as having been affected by rifting and associated magmatic activity during the break-up of Rodinia in Neoproterozoic-Early Palaeozoic times although there is no direct evidence of this from the RomUkrSeis profile.

(3) The central domain also encompasses the Eastern Carpathian fold-and-thrust belt (accretionary prism), formed in the Miocene on the already existing TTZ structure, which had further evolved during the Palaeozoic accretion of terranes to the EEC after its initial formation in Neoproterozoic-Early Palaeozoic times. There are decreased crustal velocities beneath the sedimentary succession in this area. A keel structure on the Moho boundary (to 50 km depth) in the zone between the Inner and Outer Carpathians separates crust of different thicknesses, 32-35 km under the younger domain to the southwest and up to 42 km under the cratonic domain to the northeast.

(4) Under the Eastern Carpathians, in the central domain of the profile, there is a thick sedimentary unit, from the surface to a depth of 15 km, interpreted to consist of two sedimentary successions, nested into each other. A Carpathian basin consists of a Cretaceous and younger-flysch complex with $V_p$ 4.9 km/s down to 6 km depth, underlain by more compacted, older (Mesozoic and Palaeozoic) sediments with $V_p$ 5.4 km/s. The crustal unit resolved below these sedimentary successions and above ~20 km is interpreted to represent metasedimentary rocks, mainly of Neoproterozoic age deposited on the Archaean-Palaeoproterozoic crystalline basement of the EEC and its margin.

(5) The TTZ imaged on the RomUkrSeis profile compared to other profiles crossing it where it lies beneath the Carpathian Mountains (e.g. PANCAKE and VRANCEA-2001) reveals that it has a variable structure, width and evolution along its strike in this area. Concurrently, there are a number of common features such as the inheritance and nesting of sedimentary basins and/or accretionary prisms of different ages, generally low velocity crust and significant changes in Moho depth beneath the TTZ.

(6) The Tisza-Dacia terrane crust of the Transylvanian Basin and Apuseni Mountains is relatively thin (~32 km). A high-velocity body is identified at 4-12 km depth, which is interpreted as a rootless fragment of the ophiolite complexes associated with the Mesozoic accretion of Tisza and Dacia into a single terrane and partly exposed in the Apuseni Mountains. The lower crust displays slightly higher velocities beneath the Transylvanian Basin and there is some suggestion in the velocity model of crustal-scale strike-slip tectonics in this area.

(7) Moho depth varies significantly along the RomUkrSeis profile, from 32 to 50 km, in particular but not exclusively at the boundaries of the three constituent domains. There is no detected strong velocity differentiation among the uppermost mantle domains ($V_p$ 8.15-8.21 km/s) that could imply strong compositional variations in the upper mantle along the profile. Moho shape, especially in the area between the Inner and Outer Carpathians, suggests an apparent dip to the NE, interpretable as thrusting of Tisza-Dacia upper mantle beneath the TTZ domain, which, in turn, could be thrusted under the cratonic (EEC) domain. In the upper mantle, seismic boundaries with velocities in the range 8.3-8.35 km/s are observed in the central and northeast domains, sub-parallel to the shape of the overlying Moho.

## Acknowledgements

RomUkrSeis was carried out by a consortium of organisations, the Faculty of Geology and Geophysics and the Doctoral School of Geology of the University of Bucharest (Romania), the Subbotin Institute of Geophysics of the National Academy of Sciences of Ukraine (Kiev), the Institute of Geophysics of the Polish Academy of Sciences (Warsaw), the Deutsches GeoForschungsZentrum (Potsdam) and the School of Geosciences of the University of Aberdeen (Scotland). Financial support for drilling/shooting works on the territory of Romania came from S.C Prospectiuni S.A. (with a special mention to former CEO Gehrig Stannard Schultz, currently at EPI Group, United Kingdom), Hunt Oil of Romania, Repsol Romania and on the territory of Ukraine from Ukrgeofizika. Participation of the Polish group in this work was supported within statutory activities No 3841/E-41/S/2014-2020 of the Ministry of Science and Higher Education of Poland. The authors express their sincere appreciation of the activities of many people who took part in field work and data acquisition. A large part of the instrumentation was provided by the Geophysical Instrument Pool of the Deutsches GeoForschungsZentrum (GFZ), Potsdam, Germany. Christian Haberland is thanked for his support and kindness facilitating the loan of this equipment to the

RomUkrSeis consortium. The public domain packages GMT (Wessel and Smith, 1995) and Seismic Unix (Cohen and Stockwell, 1997) were used in the preparation of maps and for seismic data processing. The authors with to thank Professor Richard England (University of Leicester) and an anonymous reviewer for their constructive comments on an earlier version of this manuscript. This version is mch improved as a result.

## References

Abbott, Dallas H., Mooney, Walter D., VanTongeren, Jill A., 2013. The character of the Moho and lower crust within Archean cratons and the tectonic implications. Tectonophysics, 609, 690-705. https://doi.org/10.1016/j.tecto.2013.09.014

Amashukeli, T., Murovskaya, A., Yegorov,a T., Alekhin V., 2019. The deep structure of the Dobrogea and Fore-Dobrogea trough as a reflection of the development of the Trans-European suture zone. Geofizicheskiy Zhurnal, 41(1), 153-171.

Bala, A., Raileanu, 2017. Assessing of the crustal models and active faults systems in western part of Romania with applications in seismic hazard. Romanian Reports in Physics, 69, article 704.

Barrier, E., Vrielynck, B., Brouillet, J.F., Brunet, M.F. (Contributors: Angiolini, L., Kaveh, F., Plunder, A., Poisson, A., Pourteau, A., Robertson, A., Shekawat, R., Sosson, M. and Zanchi, A.), 2018. Paleotectonic Reconstruction of the Central Tethyan Realm. Tectono-Sedimentary-Palinspastic maps from Late Permian to Pliocene. CCGM/CGMW, Paris, http://www.ccgm.org. Atlas of 20 maps (scale: 1/15 000 000).

Bielik, M., Makarenko, I., Csicsay, K., Legostaeva, O., Starostenko, V., Savchenko, A., Šimonová, B., Dérerová, J., Fojtíková, L., Pašteka, R., Vozár, J., 2018. The refined Moho depth map in the Carpathian-Pannonian region. Contributions to Geophysics and Geodesy, 48 (2), 179-190.

Bocin, A., Stephenson, R., Matenco, L., Mocanu, V., 2013. Local gravity and magnetic modelling in the Vrancea Zone, south-eastern Carpathians: redefinition of the edge of the East European Craton beneath the south-eastern Carpathians. Journal of Geodynamics, 71, 52-64, doi: 10.1016/j.jog.2013.08.003

Bogdanova, S.V., Bingen, B., Gorbatschev, R., Kheraskova, T.N., Kozlov, V.I., Puchkov, V.N., Volozh, Yu.A., 2008. The East European Craton (Baltica) before and during the assembly of Rodinia. Precambrian Research, 160, 23-45. https://doi.org/10.1016/j.precamres.2007.04.024

Bogdanova, S.V., Gintov, O.B., Kurlovich, D.M., Lubnina, N.V., Nilsson, M.K.M., Orlyuk, M.I., Pashkevich, I.K., Shumlyanskyy, L.V., Starostenko, V.I., 2013. Late Palaeoproterozoic

mafic dyking in the Ukrainian Shield of Volgo-Sarmatia caused by rotation during the assembly of supercontinent Columbia (Nuna). Lithos, 174, 196-216. https://doi.org/10.1016/j.lithos.2012.11.002

Bogdanova, S., Gorbatschev, R., Grad, M., Janik, T., Guterch, A., Kozlovskaya, E., Motuza, G., Skridlaite, G., Starostenko, V., Taran, L., EUROBRIDGE and POLONAISE Working Groups, 2006. EUROBRIDGE: new insight into the geodynamic evolution of the East European Craton, in: D.G. Gee and R.A. Stephenson (Eds.), European Lithosphere Dynamics, Geological Society of London Memoir, 32, 599-625.

Bortolotti, V., Marroni, M., Nicolae, I., Pandolfi, L., Principi, G., Saccani, E., 2002. Geodynamic implications of Jurassic ophiolites associated with island-arc volcanics, South Apuseni Mountains, western Romania. Int. Geol. Rev., 44(10), 938-955.

Bortolotti, V., Marroni, M., Nicolae, I., Pandolfi, L., Principi, G., Saccani, E., 2004. An update of the Jurassic ophiolites and associated calcalkaline rocks in the South Apuseni Mountains (western Romania). Ofioliti, 29, 5-18.

Bourgeois, O., Ford, M., Diraison, M., Le Carlier de Veslud, C., Gerbault, M., Pik, R., Ruby, N. & Bonnet, S., 2007. Separation of rifting and lithospheric folding signatures in the NW-Alpine foreland, Int. J. Earth Sci., 96, 1003-1031.

Boyko, G.Yu., Loznyak, P.Yu., Zayats, Kh.B., Anikeev, S.G., Petrashkevich, M.I., Kolodiy, V.V., Gayvanovich, O.P., 2003. The deep geological structure of the Carpathian region. Geology and Geochemistry of Combustible Fossils, 2, 52-62 (in Ukrainian).

Burchfiel, B.C., 1976. Geology of Romania. Geological Society of America, Special Paper 158, 82 pp.

Červený, V., Pšenčík, I., 1984. SEIS83 – numerical modelling of seismic wave fields in 2-D laterally varying layered structures by the ray method, in Engdahl., R. (Ed.), Documentation of Earthquake Algorithms, 36-40.

Chekunov, A.V. (Ed.), 1989. Lithosphere of the Central and Eastern Europe. East European platform. Naukova Dumka, Kiev, p. 180 (in Russian).

Christensen, N.I., 1978. Ophiolites, seismic velocities and oceanic crustal structure. Tectonophysics, 47, 131-157.

Christensen, N.I., 1996. Poisson's ratio and crustal seismology, J. Geophys. Res., 101, 3139-3156.

Christensen, N.I., Salisbury, M.H., 1975. Structure and constitution of the lower ocean crust. Rev. Geophys. Space Phys., 13, 57-86.

Ciulavu, D., Bertotti, G., 1994. The Transylvanian Basin and its Upper Cretaceous substratum. Romanian Journal of Tectonics 75, 59-64.

Ciulavu, D., Dinu, C., Szakacs, A., Dordea, D., 2000. Neogene kinematics of the Transylvanian basin (Romania). AAPG Bulletin, 10 (84), 1589-1615.

Claesson, S., Bibikova, E., Bogdanova, S., Skobelev, V., 2006. Archaean terranes, Palaeoproterozoic reworking and accretion in the Ukrainian Shield, East European Craton, in: D.G. Gee and R.A. Stephenson (Eds.), European Lithosphere Dynamics, Geological Society of London Memoir, 32, 645-654.

Cohen, J.K., Stockwell, J.W., Jr., 1997. CWP/SU: Seismic Unix Release 30: a free package for seismic research and processing. Golden: Center for Wave Phenomena, Colorado School of Mines.

Csontos, L., Vörös, A., 2004. Mesozoic plate tectonic reconstruction of the Carpathian Region. Palaeogeography,Palaeoclimatology. Palaeoecology 210 (1), 1-56. https://doi.org/10.1016/j.palaeo.2004.02.033

Csontos, L., Nagymarosy, A., 1998. The Mid-Hungarian line: a zone of repeated tectonic inversions. Tectonophysics 297, 51-71. https://doi.org/10.1016/S0040-1951(98)00163-2

Csontos, L., Nagymarosy, A., Horváth, F., Kovác, M., 1992. Tertiary evolution of the Intra-Carpathian area: A model. Tectonophysics, 208(1-3), 221-241. https://doi.org/10.1016/0040-1951(92)90346-8

Dadlez, R., 1993. Teisseyre-Tornquist tectonic zone in Poland. Publ. Inst. Geophys. Pol. Acad. Sci. A-20 (255), 49-51.

Dadlez, R., Grad, M., Guterch, A., 2005. Crustal structure below the Polish Basin: Is it composed of proximal terranes derived from Baltica? Tectonophysics, 411, 111-128.

Dadlez, R., Narkiewicz, M., Stephenson, R.A., Visser, M., van Wees, J-D., 1995. Tectonic evolution of the Polish Trough: modelling implications and significance for central European geology. Tectonophysics, 252, 179-195.

De Broucker, G., Mellin, A., Duindam, P., 1998. Tectono-Stratigraphic evolution of the Transylvanian Basin, pre-salt sequence, Romania. In: Dinu, C., Mocanu, V. (Eds.), Geological and Hydrocarbon Potential of the Romanian area. Bucharest Geosciences Forum 1, 36-70.

DOBREfraction'99 Working Group, 2003. "DOBREfraction'99"–velocity model of the crust and upper mantle beneath the Donbas Foldbelt (east Ukraine). Tectonophysics 371, 81-110.

https://doi.org/10.1016/S0040-1951(03)00211-7

Fillerup, Melvin A., Knapp, James H., Knapp, Camelia C., Raileanu, Victor, 2010. Mantle earthquakes in the absence of subduction? Continental delamination in the Romanian Carpathians. Lithosphere, 5; 333-340. https://doi.org/10.1130/L102.1

Fodor, L., Csontos, L., Bada, G., István Györfi, I., Benkovics, L., 1999. Tertiary tectonic evolution of the Pannonian Basin system and neighbouring orogens: a new synthesis of palaeostress data. Geological Society, London, Special Publications, 156, 295-334. https://doi.org/10.1144/GSL.SP.1999.156.01.15

Gągała, Ł., Vergés, J., Saura, E., Malata, T., Ringenbach, J.-C., Werner, Ph., Krzywiec, P., 2012. Architecture and orogenic evolution of the northeastern Outer Carpathians from cross-section balancing and forward modeling. Tectonophysics, 532-535, 223-241. https://doi.org/10.1016/j.tecto.2012.02.014

Geological Map of Main Structure Levels in Ukrainian SSR and Moldavian SSR. Scale 1:1000000. Zaritsky, A.I. (Ed.), 1987. Kiev: Ministry of Geology of the USSR.

Gintov, O.B., 2004. Zones of faults of the Ukrainian shield. Influence of the processes of fault formation on the formation of the structure of the earth's crust. Geofizicheskiy Zhurnal, 26, 3-24 (in Russian).

Gintov, O.B., 2005. Field Tectonophysics and Its Applications in Studies of Deformations of the Earth’s Crust in the Territory of Ukraine. Feniks, Kiev, 2005 (in Russian)

Golonka, J., Gahagan, L., Krobicki, M., Marko, F., Oszczypko, N., Ślączka, A. 2006. Plate-tectonic Evolution and Paleogeography of the Circum-Carpathian Region. In: The Carpathians and their Foreland: Geology and Hydrocarbon Resources: AAPG Memoir 84, 11-46. https://doi.org/10.1306/985606M843066

Gorbatschev, R., Bogdanova, S., 1993. Frontiers in the Baltic Shield. Precambrian Research, 64, 3-21.

Gordienko, V.V., Gordienko, I.V., Zavgorodnyaya, O.V., Logvinov, I.M., Tarasov, V.N., 2011. Evolution of the tectonosphere of the Volyn-Podolsk plate. Geofizicheskiy Zhurnal, 33, 30-49 (in Russian).

Grad, M., 2019. Podolian, Saxonian and Baltic plates – Teisseyre-Tornquist Line and the edge of the East European Craton, Geochemistry, 79, 422-433, https://doi.org/10.1016/j.chemer.2019.03.002

Grad, M., Guterch, A., Keller, G.R., Janik, T., Hegedűs, E., Vozár, J., Ślączka, A., Tiira, T., & Yliniemi, J., 2006a. Lithospheric structure beneath trans-Carpathian transect from

Precambrian platform to Pannonian basin CELEBRATION 2000 seismic profile CEL05, J. Geophys. Res. 111, B03301, https://doi.org/10.1029/2005JB003647

Grad, M., Guterch, A., Mazur, S., Keller, G.R., Špičák, A., Hrubcová, P., Geissler, W.H., 2008. Lithospheric structure of the Bohemian Massif and adjacent Variscan belt in central Europe based on profile S01 from the SUDETES 2003 experiment. Journal of Geophysical Research, 113, B10304, https://doi.org/10.1029/2007JB005497

Grad, M., Janik T., Guterch, A., Środa, P., Czuba, W. and EUROBRIDGE'94-97, POLONAISE'97 & CELEBRATION 2000 Seismic Working Groups, 2006b. Lithospheric structure of the western part of the East European Craton investigated by deep seismic profiles, Geological Quarterly 50, 9-22.

Grad, M., Jensen, S.L., Keller, G.R., Guterch, A., Thybo, H., Janik, T., Tiira, T., Yliniemi, J., Luosto, U., Motuza, G., Nasedkin, V., Czuba, W., Gaczyński, E., Sroda, P., Miller, K.C., Wilde-Piórko, M., Komminaho, K., Jacyna, J., Korabliova, L., 2003. Crustal structure of the Trans-European suture zone region along POLONAISE'97 seismic profile P4. J. Geophys. Res. 108 (B11), 2541. https://doi.org/10.1029/2003JB002426

Grad, M., Tripolsky, A.A., 1995. Crustal structure from P and S seismic waves and petrological models of the Ukrainian Shield, Tectonophysics, 250, 89-112. https://doi.org/10.1016/0040-1951(95)00045-X

Guterch, A., Grad, M., Keller, G.R., Brück, E., 2015. 1.17. Crust and Lithosphere Structure – Long Range Controlled Source Seismic Experiments in Europe. In: Schubert G. (Ed.), Treatise on Geophysics (Second Edition). Volume 1: Deep Earth Seismology. Elsevier.

Haas, J., Péró, C., 2004. Mesozoic evolution of the Tisza Mega-unit. Int. J. Earth Sci., 93, 297-313.

Hauser, F., Raileanu, V., Fielitz, W., Bala, A., Prodehl, C., Polonic, G., Schulze, A., 2001. VRANCEA99 – the crustal structure beneath the southeastern Carpathians and the Moesian Platform from a seismic refraction profile in Romania. Tectonophysics, 340, 233-256.

Hauser, F., Raileanu, V., Fielitz, W., Dinu, C., Landes, M., Bala, A., Prodehl, C., 2007. Seismic crustal structure between the Transylvanian Basin and the Black Sea, Romania. Tectonophysics, 430, 1-25. https://doi.org/10.1016/j.tecto.2006.10.005

Hippolyte, J.-C., 2002. Geodynamics of Dobrogea (Romania): new constraints on the evolution of the Tornquist-Teisseyre Line, the Black Sea and the Carpathians. Tectonophysics, 357, 33-53. https://doi.org/10.1016/S0040-1951(02)00361-X

Hoeck, V., Ionescu, C., Balintoni, I., Koller, F., 2009. The Eastern Carpathians "ophiolites" (Romania): Remnants of a Triassic ocean. Lithos, 108, 151-171.

https://doi.org/10.1016/j.lithos.2008.08.001

Holbrook, W.S., Mooney, W.D., Christensen, N.I., 1992. The seismic velocity structure of the deep continental crust, in Continental Lower Crust, edited by D.M. Fountain, R. Arculus, and R. Kay, 21-43, Elsevier, New York.

Horváth, F., Musitz, B., Balázs, A., Véghd, A., Uhrine, A., Nádorc, A., Koroknaia, B., Papd, N., Tótha, T., Wórum, G., 2015. Evolution of the Pannonian Basin and its geothermal resources. Geothermics, 53, 328-352. https://doi.org/10.1016/j.geothermics.2014.07.009

Hrubcová, P., Środa, P., 2015. Complex local Moho topography in the Western Carpathians: Indication of the ALCAPA and the European Plate contact, Tectonophysics, 638, 63-81. https://doi.org/10.1016/j.tecto.2014.10.013

Hurtig E., Cermak V., Haenel R., Zui V.I., 1991. Geothermal Atlas of Europe. Hermann Haack Verlagsgesellscaft mbH, Geographisch-Kartographische Anstalt, Gotha, set of 36 maps and Explanatory Notes, 156 p.

Janik, T., Grad, M., Guterch, A., CELEBRATION 2000 Working Group, 2009a. Seismic structure of the lithosphere between the East European Craton and the Carpathians from the net of CELEBRATION 2000 profiles in SE Poland. Geol. Quart. 53, 141-158.

Janik, T., Grad, M., Guterch, A., Dadlez, R., Yliniemi, J., Tiira, T., Keller, G.R., Gaczyński, E., CELEBRATION 2000 Working Group, 2005. Lithospheric structure of the Trans-European Suture Zone along the TTZ & CEL03 seismic profiles (from NW to SE Poland). Tectonophysics, 411, 129-156. https://doi.org/10.1016/j.tecto.2005.09.005

Janik, T., Grad, M., Guterch, A., Vozár, J., Bielik, M., Vozárova, A., Hegedűs, E., Kovács, C.S., Kovács, I., Keller, G.R., and CELEBRATION 2000 Working Group, 2011. Crustal structure of the Western Carpathians and Pannonian Basin: seismic models from CELEBRATION 2000 data and geological implications, Journal of Geodynamics, 52, 97-113. https://doi.org/10.1016/j.jog.2010.12.002

Janik T., Kozlovskaya E., Heikkinen P., Yliniemi Ju., Silvennoinen H., 2009b. Evidence for preservation of crustal root beneath the Proterozoic Lapland-Kola orogen (northern Fennoscandian shield) derived from P and S wave velocity models of POLAR and HUKKA wide-angle reflection and refraction profiles and FIRE4 reflection transect. J. Geophys. Res., 114, B06308, 1-34. https://doi.org/10.1029/2008JB005689

Kolomiyets, A.V., Kharchenko, A.V., 2008. Tuning parallel computations for low-bandwidth network. Computer Mathematics 1, 63-69 (in Russian).

Komminaho, K., 1998. Software manual for programs MODEL and XRAYS: A graphical interface for SEIS83 program package, University of Oulu, Dep. of Geophys., Rep. 20, 31

pp.

Kostyukevich, A.S., Starostenko, V.I., Stephenson, R.A., 2000. The full-wave images of the models of the deep lithosphere structures constructed according to DSS and CDP data interpretation. Geofizicheskiy Zhurnal 22 (4), 96-98.

Kravchenko, S.L., 2007. The age of the final phase of magmatism in the Late Precambrian in Volyn area according to new geochronological and paleomagnetic data. Reports of the National Academy of Sciences of Ukraine, 2, 116-119 (in Russian).

Krézsek, C., Filipescu S., 2005. Middle to late Miocene sequence stratigraphy of the Transylvanian Basin (Romania). Tectonophysics, 410, 437-463. https://doi.org/10.1016/j.tecto.2005.02.018

Krézsek, C., Bally, A., 2006. The Transylvanian Basin (Romania) and its relation to the Carpathian fold and thrust belt: Insights in gravitational salt tectonics. Mar. Petrol. Geol., 23, 405-442. https://doi.org/10.1016/j.marpetgeo.2006.03.003

Kruglov, S.S., Tsipko, A.K. (Eds), 1988. Tectonics of Ukraine. Nedra: Moscow. 254 p. (in Russian).

Krzywiec, P., Gągała, Ł., Mazur, S., Słonka, Ł., Kufrasa, M., Malinowski, M., Pietsch K., Golonka, J., 2017. Variscan deformation along the Teisseyre-Tornquist Zone in SE Poland: Thick-skinned structural inheritance or thin-skinned thrusting? Tectonophysics, 718, 83-91. https://doi.org/10.1016/j.tecto.2017.06.008

Krzywiec, P., P. Poprawa, M. Mikołajczak, S. Mazur, M. Malinowski, 2018. Deeply concealed half-graben at the SW margin of the East European Craton (SE Poland) – Evidence for Neoproterozoic rifting prior to the break-up of Rodinia. Journal of Palaeogeography, 7(1), 88-97. https://doi.org/10.1016/j.jop.2017.11.003

Kutas, R.I., 2013. Geothermal model of the earth's crust across the eastern Carpathians along the seismic profile DOBRE-3 (PANCAKE). Geodynamics, 15, 192-194. (in Ukrainian)

Kutas, R.I., 2015. Geothermal conditions and crustal structure of the Northwestern Carpathians. Geoinformatika, 56, 96-12.

Linzer, H.-G., Frisch, W., Zweigel, P., Girbacea, R., Hann, H.-P., Moser, F., 1998. Kinematic evolution of the Romanian Carpathains. Tectonophysics 297, 133-156. https://doi.org/10.1016/S0040-1951(98)00166-8

Majorowicz, J., Wybraniec, S., 2011. New terrestrial heat flow map of Europe after regional paleoclimatic correction application. Int. J. Earth Sci., 100, 881-887

Malinowski, M., Guterch, A., Narkiewicz, M., Probulski, J., Maksym, A., Majdanski, M., Środa, P., Czuba, W., Gaczyński, E., Grad, M., Janik, T., Jankowski, L., Adamczyk, A., 2013. Deep seismic reflection profile in Central Europe reveals complex pattern of Paleozoic and Alpine accretion at the East European Craton margin. Geophysical Research Letters, 40, 3841-3846. https://doi.org/10.1002/grl.50746

Matenco, L., Bertotti, G., 2000. Tertiary tectonic evolution of the external East Carpathians (Romania). Tectonophysics, 316, 255-286.

Matenco, L., Krezsek, C., Merten, S., Schmid, S., Cloetingh, S., Andriessen, P., 2010. Characteristics of collisional orogens with low topographic build-up: an example from the Carpathians. Terra Nova, 22, 155-165. https://doi.org/10.1111/j.1365-3121.2010.00931.x

Mazur, S., Aleksandrowski, P., Gągała, Ł., Krzywiec, P., Żaba, J., Gaidzik, K., Sikora, R., 2020. Late Palaeozoic strike- slip tectonics versus oroclinal bending at the SW outskirts of Baltica: case of the Variscan belt's eastern end in Poland. International Journal of Earth Sciences (Geol Rundsch). https://doi.org/10.1007/s00531-019-01814-7

Meissner, R., Thybo, H., Abramovitz, T.J., 2002. Interwedging and inversion structures around the Trans European Suture Zone in the Baltic Sea, a manifestation of compressive tectonic phases. Tectonophysics 360, 265-280. https://doi.org/10.1016/S0040-1951(02)00356-6

Merten, S., Matenco, L., Foecken, J.P.T., Stuart, F.M., Andriessen, P.A.M., 2010. From nappe stacking to out-of sequence postcollisional deformations: Cretaceous to Quaternary exhumation history of the SE Carpathians assessed by low-temperature thermochronology. Tectonics, 29 (3). https://doi.org/10.1029/2009TC002550

Mooney, W.D., Andrews, M.C., Ginzburg, A., Peters, D.A., Hamilton, R.M., 1983. Crustal structure of the northern Mississippi Embayment and a comparison with other continental rift zones. Tectonophysics, 94, 327-348.

Mucuta, D.M., Knapp, C.C., Knapp, J.H., 2006. Constraints from Moho geometry and crustal thickness on the geodynamic origin of the Vrancea Seismogenic Zone (Romania). Tectonophysics, 420, 23-36. https://doi.org/10.1016/j.tecto.2006.01.018

Nakapelyukh, M., Bubniak, I., Bubniak, A., Jonckheere, R., Ratschbacher, L., 2018. Cenozoic structural evolution, thermal history, and erosion of the Ukrainian Carpathians fold-thrust belt. Tectonophysics 722, 197-209. https://doi.org/10.1016/j.tecto.2017.11.009

Narkiewicz, M., Maksym, A., Malinowski, M., Grad, M., Guterch, A., Petecki, Z., Probulski, J., Janik, T., Majdański, M., Środa, P., Czuba, W., Gaczyński, E., Jankowski, L., 2015. Transcurrent nature of the Teisseyre–Tornquist Zone in Central Europe: results of the POLCRUST-01 deep reflection seismic profile. Int. J. Earth Sci. 104, 775-796.

Narkiewicz, M., 2007. Development and inversion of Devonian and Carboniferous basins in the eastern part of the Variscan foreland (Poland). Geological Quarterly 51, 231-56.

Nikishin, A.M., Okay, A.I., Tüysüz, O., Demirer, A., Wannier, M., Amelin, N., Petrov, E. 2015. The Black Sea basins structure and history: new model based new deep penetration regional seismic data. Part 2: tectonic history and paleogeography. Marine and Petroleum Geology, 59, 656-670.

Panea, I., Stephenson, R., Knapp, C., Mocanu, V., Drijkoningen, G., Matenco, L., Knapp, J., Prodehl, K., 2005. Near-vertical seismic reflection image using a novel acquisition technique across the Vrancea Zone and Foscani Basin, south-eastern Carpathians (Romania). Tectonophysics, 410, 293-309.

Pavlenkova, N.I., 1996. Crust and upper mantle structure in northern Eurasia from seismic data. Adv. Geophys. 37, 1-133.

Pease, V., Daly, J.S., Elming, S.-Å., Kumpulainen, R., Moczydlowska, M., Puchkov, V., Roberts, D., Saintot, A., Stephenson, R., 2008. Baltica in the Cryogenian, 850-630 Ma. Precambrian Research, 160, 46-65.

Pharaoh, T.C., 1999. Palaeozoic terranes and their lithospheric boundaries within the Trans-European Suture Zone (TESZ): a review. Tectonophysics, 314, 17-41. https://doi.org/10.1016/S0040-1951(99)00235-8

Pharaoh, T.C., Winchester, J.A, Verniers, J., Lassen, A., Seghedi, A., 2006. The western accretionary margin of the East European Craton: an overview. In: Gee, D.G., Stephenson, R.A. (eds.) European Lithosphere Dynamics. Geol Soc London Memoir 32, pp. 291-311.

Plašienka, D., Grecula, P., Prutiš, M., Kováč, M., Hovorka, D., 1997. Evolution and structure of the Western Carpathians: an overview. In: Grecula, P., Hovorka, D., Prutiš, M. (Eds.), Geological Evolution of the Western Carpathians. Mineralna Slov., 1-24.

Poprawa, P., Krzemińska, E., Pacześna, J., Armstrong, R., 2020. Geochronology of the Volyn volcanic complex at the western slope of the East European Craton – Relevance to the Neoproterozoic rifting and the break-up of Rodinia/Pannotia. Precambrian Research, 346, 105817. https://doi.org/10.1016/j.precamres.2020.105817

Powell, C.M., Li, Z.X., Meert, J.G., Park, J.K., 1993. Paleomagnetic constraints on timing of the Neoproterozoic breakup of Rodinia and the Cambrian formation of Gondwana. Geology, 21, 889-892.

Reiser, M.K., Schuster, R., Spikings, R., Tropper, P., Fügenschuh, B., 2016. From nappe stacking to exhumation: Cretaceous tectonics in the Apuseni Mountains (Romania). Int. J. Earth Sci. (Geol Rundsch). https://doi.org/10.1007/s00531-016-1335-y

Robertson, A.H.F., Karamata, S., Šarić, K., 2009. Ophiolites and related geology of the Balkan region. Lithos, 108, vii-x. https://doi.org/10.1016/j.lithos.2008.10.013

Roure, F., Bessereau, G., Kotarba, M., Kusmierek, J., Strzetelski, W., 1993. Structure and hydrocarbon habitats of the Polish Carpathian Province. AAPG Bulletin, 77, 1660.

Rudnick, R.L., Fountain, D.M., 1995. Nature and Composition of the continental crust: a lower crustal perspective, Rev. Geophys., 33, 267-309.

Săndulescu, M., 1975. Essai de synthese structurale des Carpathes. Bulletin de la Société Géologique de France. S7-XVII (3): 299-358. https://doi.org/10.2113/gssgfbull.S7-XVII.3.299

Săndulescu, M., 1984. Geotectonica României (translated title: Geotectonics of Romania). Ed. Tehnica, Bucharest, 450 pp.

Săndulescu, M. 1988. Cenozoic tectonic history of the Carpathians. In: Royden, L., Horváth, F. (Eds.), The Pannonian Basin: a study in basin evolution. AAPG Memoir 45, pp. 17-25.

Săndulescu, M., Kräutner, H., Borcos, M., Nastaseanu, S., Patrulius, D., Stefanescu, M., Ghenea, C., Lupu, M., Savu, H., Bercia, I., Marinescu F., 1978. Geological map of Romania. Scale 1:1.000.000. Bucharest: Institute of Geology and Geophysics.

Schmid, S.M., Bernoulli, D., Fugenschuh, B., Matenco, L., Schaefer, S., Schuster, R., Tischler, M., Ustaszewski, K., 2008. The Alpine-Carpathian-Dinaridic orogenic system: correlation and evolution of tectonic units. Swiss Journal of Geosciences, 101, 139-183. https://doi.org/10.1007/s00015-008-1247-3

Seghedi, A., Oaie, G., Iordan, M., Avram, E., Tatu, M., Ciulavu, D., Vaida, M., Rădan, S., Nicolae, I., Seghedi, I., Szakács, A., Drăgănescu, A., 1999. Geology and structure of the Precambrian and Paleozoic basement of North and Central Dobrogea. Mesozoic history of North and Central Dobrogea. Romanian Journal of Tectonics and Regional Geology, 77, supplement 2, p. 72.

Seghedi, I., Bojar A.-V., Downes, H., Roşu E., Tonarini S., Mason P., 2007. Generation of normal and adakite-like calc-alkaline magmas in a non-subductional environment: An Sr–O–H isotopic study of the Apuseni Mountains Neogene magmatic province, Romania. Chemical Geology 245, 70-88. https://doi.org/10.1016/j.chemgeo.2007.07.027

Seghedi, Ioan, Downes, Hilary, Szakács, Alexandru, Mason, Paul R.D., Thirlwall, Matthew F., Roşu, Emilian, Pécskay, Zoltán, Márton, Emö, Panaiotu, Cristian, 2004. Neogene–Quaternary magmatism and geodynamics in the Carpathian-Pannonian region: a synthesis. Lithos 72, 117-146. https://doi.org/10.1016/j.lithos.2003.08.006

Shcherbak, N., Artemenko, G., Lesnaya, I., Ponomarenko, A., 2005. Geochronology of the Precambrian of the Ukrainian Shield. The Archaean. Naukova Dumka, Kiev (in Russian).

Shcherbak, N., Artemenko, G., Lesnaya, I., Ponomarenko, A., 2008. Geochronology of the Precambrian of the Ukrainian Shield. The Proterozoic. Naukova Dumka, Kiev (in Russian).

Shlapinskyi, V., 2015. The Geological Architecture of the Skyba, Krosno, Duklya-Chornogora Nappes of the Ukrainian Carpathians and Prospects of Oil and Gas (unpublished Doctoral Thesis). Institute of Geology and Geochemistry of Combustible Minerals, Lviv (in Ukrainian).

Shumlyansky, L., Hawkesworth, C., Dhuime, B., Billström, K., Claesson, S., Storey, C., 2015. 207Pb/206Pb ages and Hf isotope composition of zircons from sedimentary rocks of the Ukrainian Shield: Crustal growth of the south-western part of East European craton from Archean to Neoproterozoic. Precambrian Research, 260, 39-54. https://dx.doi.org/10.1016/j.precamres.2015.01.007

Skridlaitė, G., Willingshofer, E., Stephenson, R.A., 2003. P-T-t modelling of Proterozoic terranes in Lithuania: geodynamic implications for accretion of southwestern Fennoscandia, 2003. GFF (Swedish Geological Journal), 125, 201-211.

Sliaupa, S., Fokin, P., Lazauskiene, J., Stephenson, R.A., 2006. The Vendian-Early Palaeozoic sedimentary basins of the East European Craton, in: D.G. Gee and R.A. Stephenson (Eds.), European Lithosphere Dynamics, Geological Society of London Memoir, 32, 449-462.

Snyder, D.B., 2002. Lithospheric growth at margins of cratons. Tectonophysics, 355, 7-22. https://doi.org/10.1016/S0040-1951(02)00131-2

Środa, P., Czuba, W., Grad, M., Guterch, A., Tokarski, A., Janik, T., Rauch, M. Keller, G.R., Hegedűs, E., Vozár, J. & CELEBRATION 2000 Working Group, 2006. Crustal and upper mantle structure of the Western Carpathians from CELEBRATION 2000 profiles CEL01 and CEL04: Seismic models and geological implications. Geophysical Journal International, 167, 737-760. https://doi.org/10.1111/j.1365-246X.2006.03104.x

Środa, P., 2010. The bright spot in the West Carpathian upper mantle: a trace of the Tertiary plate collision and a caveat for a seismologist. Geophysical Journal International, 182, 1-10. https://doi.org/10.1111/j.1365-246X.2010.04595.x

Starostenko, V., Janik, T., Stephenson, R., Gryn, D., Rusakov, O., Czuba, W., Środa, P., Grad, M., Guterch, A., Flűh, E., Thybo, H., Artemieva, I., Tolkunov, A., Sydorenko, G., Lysynchuk, D., Omelchenko, V. Kolomiyets, K., Legostaeva, O., Dannowski, A., Shulgin, A., 2017. DOBRE-2 WARR profile: the Earth's crust across Crimea between the Azov Massif and the

northeastern Black Sea Basin, [In]: Sosson, M., Stephenson, R.A., Adamia, S. A. (eds), Tectonic Evolution of the Eastern Black Sea and Caucasus. Geological Society, London, Special Publications, 428, 199-220. http://dx.doi.org/10.1144/SP428.11

Starostenko, V., Janik, T., Kolomiyets K., Czuba W., Środa P., Grad M., Kovács I., Stephenson R., Lysynchuk D., Thybo H., Artemieva I.M., Omelchenko V., Gintov O., Kutas R., Gryn D., Guterch A., Hegedűs E., Komminaho K., Legostaeva O., Tiira T., Tolkunov A., 2013a. Seismic velocity model of the crust and upper mantle along profile PANCAKE across the Carpathians between the Pannonian Basin and the East European Craton, Tectonophysics, 608, 1049-1072. https://doi.org/10.1016/j.tecto.2013.07.008

Starostenko, V., Janik, T., Lysynchuk, D., Środa, P., Czuba, W., Kolomiyets, K., Aleksandrowski, P., Gintov, O., Omelchenko, V., Komminaho, K., Guterch, A., Tiira, T., Gryn, D., Legostaeva, O., Thybo, H., Tolkunov A., 2013b. Mesozoic(?) lithosphere-scale buckling of the East European Craton in southern Ukraine: DOBRE-4 deep seismic profile, Geophysical Journal International, 195, 740-766. https://doi.org/10.1093/gji/ggt292

Starostenko, V., Janik, T., Yegorova, T., Farfuliak, L., Czuba, W., Środa, P., Thybo, H., Artiemieva, I., Sosson, M., Volfman Y., Kolomiyets, K., Lysynchuk, D., Omelchenko, V., Gryn, D., Guterch, A., Komminaho, K., Legostaeva, O., Tiira, T., Tolkunov, A., 2015. Seismic model of the crust and upper mantle in the Scythian Platform: the DOBRE-5 profile across the Northwestern Black Sea and the Crimean Peninsula, Geophysical Journal International, 201, 406-428. https://doi.org/10.1093/gji/ggv018

Starostenko, V., Janik, T., Yegorova, T., Czuba, W., Środa, P., Lysynchuk, D., Aizberg, R., Garetsky, R., Karataev, G., Gribik, Y., Farfuliak, L., Kolomiyets, K., Omelchenko, V., Komminaho, K., Tiira, T., Gryn, D., Guterch, A., Legostaeva, O., Thybo, H., Tolkunov, A., 2018. Lithospheric structure along wide-angle seismic profile GEORIFT 2013 in Pripyat-Dnieper-Donets Basin (Belarus and Ukraine), Geophysical Journal International, 212, 1932-1962, https://doi.org/10.1093/gji/ggx509

Stefanescu, M. and Working Group, 1988. Geological cross sections 1:200.000, Nr. 5-B, Section Biharia – Malu Mare Institutului Geologie si Geofizica, Bucharest.

Tari, G.C., Horvath, F., 1995. Middle Miocene extensional collapse in the Alpine–Pannonian transition zone. In: Horva´th, F., Tari, G., Bokor, Cs (Eds.), Hungary: Extensional Collapse of the Alpine Orogen and Hydrocarbon Prospects in the Basement and Basin Fill of the Western Pannonian Basin. AAPG International Conference and Exhibition 10-13 September Nice, Sixth Field Trip Notes, Hungary, pp. 75-105.

Tectonic map of Socialist Republic of Romania. Scale 1:1.000.000. Dumitrescu, I., Sandulescu, M. (Eds.), 1970. Bucharest: Institute of Geology (Romania).

Tectonic map of Ukraine. Scale.1: 1000000. Kruglov, S., Gursky, D. (Eds.), 2007. State

Geological Survey of Ukraine, Kiev (in Russian).

Tectonic Map of Ukraine: Explanatory note. Part 1., 2007. (Eds., Kruglov S.S., Arsiriy Yu. O., Velikanov V. Ya et al.). Kiev: UkrDGRI, 96 p. (in Ukrainian).

Thybo, H., Janik, T., Omelchenko, V.D., Grad, M., Garetsky, R.G., Belinsky, A.A., Karataev, G.I., Zlotski, G., Knudsen, U.E., Sand, R., Yliniemi, J., Tiira, T., Luosto, U., Komminaho, K., Giese, R., Guterch, A., Lund, C.-E., Kharitonov, O.M., Ilchenko, T., Lysynchuk, D.V., Skobelev, V.M., Doody, J.J., 2003. Upper lithosperic seismic velocity structure across the Pripyat Trough and Ukrainian Shield along the EUROBRIDGE '97 profile. Tectonophysics 371, 41-79. https://doi.org/10.1016/S0040-1951(03)00200-2

Thybo, H., Maguire, P., Birt, C., Perchuc, E., 2000. Seismic reflectivity of the lower crust and magmatic underplating beneath the Kenya rift. Geophysical Research Letters, 27, 2745-2749.

Tiliţa, M., Matenco, L., Dinu, C., Ionescu, L., Cloetingh, S., 2013. Understanding the kinematic evolution and genesis of a back-arc continental "sag" basin: the Neogene evolution of the Transylvanian Basin. Tectonophysics, 602, 237-258. https://doi.org/10.1016/j.tecto.2012.12.029

Uhlig, V., 1907. Uber die Tektonik der Karpathen. Sitzber. Kaiserl. Acad.Wiss. Wien, Math. Naturw. Kl. 116 (2), 871-981.

Usenko, O.V., 2010. Deep processes and magmatism of the Volyn-Podolsk plate. Geophysical Journal, 32(2), 66-77 (in Russian).

Ustaszewski, Kamil, Schmid, Stefan M., Fügenschuh, Bernhard, Tischler, Matthias, Kissling, Eduard, Spakman, Wim, 2008. A map-view restoration of the Alpine-Carpathian-Dinaridic system for the Early Miocene. Swiss Journal of Geosciences, 101, Supplement 1, S273-S294. https://doi.org/10.1007/s00015-008-1288-7

Ustaszewski, K., Schmid, S.M., Lugovic, B., Schuster, R., Schaltegger, U., Bernoulli, D., Hottinger, L., Kounov, A., Fugenschuh, B., Schefer, S., 2009. Late Cretaceous intra-oceanic magmatism in the internal Dinarides (northern Bosnia and Herzegovina): Implications for the collision of the Adriatic and European plates. Lithos, 108, 106-125. https://doi.org/10.1016/j.lithos.2008.09.010

van Wees, J-D., Stephenson, R.A., Ziegler, P.A., Bayer, U., McCann, T., Dadlez, R., Gaupp, R., Narkiewicz, M., Bitzer, F., Scheck, M., 2000. On the origin of the southern Permian Basin, Central Europe. Marine and Petroleum Geology, 17, 43-59.

Verpakhovska, A., Pylypenko, V., Yegorova, T., Murovskaya, A., 2018. Seismic image of the crust on the PANCAKE profile across the Ukrainian Carpathians from the migration method. Journal of Geodynamics, 121, 76-87. https://doi.org/10.1016/j.jog.2018.07.006

Wessel, P., Smith, W.H.F., 1995. New version of the Generic Mapping Tools released. EOS, 76, 329.

Winchester, J.A., Pharaoh, T.C., Verniers, J., Ioane, D., Seghedi, A. 2006. Palaeozoic accretion of Gondwana-derived terranes to the East European Craton: recognition of detached terrane fragments dispersed after collision with promontories. In: Gee, D.G. & Stephenson, R.A. (eds) European Lithosphere Dynamics. Geological Society, London, Memoir 32, 323-332.

Wybraniec, S, Zhou, S, Thybo, H., Forsberg, R., Perchuc, E., Lee, M., Demianov, G.D., Strakhov, V.N., 1998. New map compiled of Europe's gravity field. EOS, 79, 437-442.

Yegorova, T.P., Starostenko, V.I., Kozlenko, V.G., Yliniemi, J., 2004. Lithosphere structure of the Ukrainian Shield and Pripyat Trough in the region of EUROBRIDGE-97 (Ukraine and Belarus) from gravity modelling. Tectonophysics 381, 29-59. https://doi.org/10.1016/j.tecto.2002.06.003

Zayats, Kh., 2013. The Structure of Minerals of the Western Region of Ukraine on the Basis of Seismic Studies and the Directions for Oil and Gas Exploration Study. USGEI, Lviv 136 p. (in Ukrainian).

Zelt, C.A., 1994. Software Package ZPLOT. Bullard Laboratories, University of Cambridge.

Zelt, C.A., Smith, R.B., 1992. Seismic traveltime inversion for 2-D crustal velocity structure, Geophys. J. Int. 108, 16-34. https://doi.org/10.1111/j.1365-246X.1992.tb00836.x

Ziegler, P.A., Schumacher, M.E., Dèzes, P., van Wees, J.-D., Cloetingh, S., 2006. Post-Variscan evolution of the lithosphere in the area of the European Cenozoic Rift System. In European Lithosphere Dynamics ed. D.G. Gee and R.A. Stephenson. Geological Society, London, Memoirs, 32, 97-112.

Table 1. Locations and other parameters of explosive sources used along the RomUkrSeis profile

| Shot Point number | Distance (km) | Latitude N $\varphi$ (deg) | Longitude E $\lambda$ (deg) | Altitude h (m) | Time UTC (y:d:h:m:s) | Charge TNT (kg) | Borehole depth (m) | No. of boreholes |
|---|---|---|---|---|---|---|---|---|
| SP15301 | 47.385 | 46.01962 | 22.44078 | 269 | 2014:241:03:00:56.11 | 1200 | 28.0 | 24 |
| SP15302 | 112.505 | 46.31472 | 23.16945 | 931 | 2014:242:02:59:48.86 | 1000 | 25.0 | 20 |
| SP15303 | 175.060 | 46.71592 | 23.76762 | 450 | 2014:241:02:13:14.25 | 800 | 24.5 | 16 |
| SP15304 | 242.772 | 47.08298 | 24.47790 | 356 | 2014:241:03:20:32.67 | 800 | 25.2 | 16 |
| SP15305 | 303.347 | 47.43347 | 25.09458 | 1011 | 2014:243:03:00:20.45 | 450 | 15.5 | 16 |
| SP15306 | 373.114 | 47.78702 | 25.86125 | 469 | 2014:242:02:10:01.09 | 800 | 22.5 | 16 |
| SP15307 | 392.069 | 47.93912 | 26.01222 | 424 | 2014:242:02:21:25.58 | 800 | 24.5 | 16 |
| SP15308 | 449.674 | 48.29805 | 26.57945 | 183 | 2014:240:21:00:01.85 | 700 | 30.0 | 14 |
| SP15309 | 497.053 | 48.58333 | 27.05917 | 242 | 2014:241:21:30:00.33 | 700 | 30.0 | 14 |
| SP15310 | 547.505 | 48.88083 | 27.57972 | 293 | 2014:241:21:00:38.31 | 700 | 30.0 | 14 |
| SP15311 | 599.387 | 49.18222 | 28.12333 | 301 | 2014:240:21:33:00.25 | 900 | 30.0 | 18 |

**Figure captions**

Figure 1. Location of the RomUkrSeis profile and previous WARR (stars representing shot points and tightly compacted dots recording stations, names in red) and deep reflection (solid black lines, names in black) seismic profiles in the study area.

Figure 2. Tectonic setting of the RomUkrSeis profile area (from Tectonic map of Ukraine, 2007; Tectonic Map of the Socialist Republic of Romania, 1970; Geological Map of Main Structure Levels in the Ukrainian SSR and the Moldavian SSR, 1987; Sandulescu et al., 1978, Bogdanova et al., 2013) with inset map showing the location of RomUkrSeis within the basic tectonic architecture of Europe (see text). The RomUkrSeis seismic line crosses from NE to SW the southwestern part of the East European Craton (EEC), the Teisseyre-Tornquist Zone (TTZ) overlain by the Carpathian Foredeep, the Outer and the Inner Eastern Carpathians, the Transylvanian Basin and Apuseni Mountains. Blue stars are RomUkrSeis shot points and tightly compacted red dots are recorder locations. The study area is mapped in terms of litho-tectonic basement complexes represented by the Precambrian crustal domains of the EEC and the Phanerozoic crustal domains of ALCAPA, Tisza and Dacia. The Tisza-Dacia composite terrane is largely overlain by sediments of the Transylvanian Basin along RomUkrSeis. Abbreviations: BD – Bug Domain (Ukrainian Shield), COF – Capidava-Ovidiu Fault, DVF – Dragos Voda Fault, KP – Korosten Pluton (Ukrainian Shield), MHFZ – Mid-Hungarian Fault Zone, PCF – Peceneaga-Camena Fault, PD – Podolian Domain (Ukrainian Shield), SGF – Sfantu Gheorghe Fault, VD – Volyn Domain (Ukrainian Shield).

Figure 3. Geophysical data in the area of RomUkrSeis profile. From top to bottom: magnetic anomalies (EMAG2: Earth Magnetic Anomaly Grid, 2-arc-minute resolution; https://www.ngdc.noaa.gov/geomag/emag2.html); Bouguer gravity anomalies (Wybraniec et al., 1998); surface heat flow (Hurtig et al., 1991, Kutas, 2013; 2015). Seismic sources along RomUkrSeis are marked by black stars and recorder stations by tightly compacted red dots. Black dotted lines outline the main tectonic units crossed by RomUkrSeis (AM – Apuseni Mountains, EEC – East European Craton, IC – Inner Carpathians, OC – Outer Carpathians, TB – Transylvanian Basin).

Figure 4a and 4b. Trace-normalised, vertical-component P-wave seismic record sections for (a) shot points SP15301-SP15305 and (b) shot points SP15306-SP15311. The reduction velocity is 8.0 km/s. Blue ellipses (labelled LVZ) indicate evidence of low velocity zones; red ellipses indicate evidence of strong increases in apparent velocity. Other abbreviations: $P_{sed}$ – seismic refractions from sedimentary layers; $P_g$ and $S_g$ – P and S refractions from the upper and middle crystalline crust; $P_{ov}$ and $S_{ov}$ – P and S overcritical crustal phases; $P_cP$ – reflections from mid-crustal discontinuities, $P_MP$ and $S_MS$ – P- and S-waves reflected from the Moho boundary; $P_n$ – refractions from the uppermost mantle, immediately below the Moho; $P_2P$ and $P_{mantle}$ – P-wave phases from the upper mantle.

Figure 4c. Examples of trace-normalised, vertical-component, common seismic record sections for P- and S-waves for shot points SP15303, SP15306 and SP15310 with band-pass

filter (1-8 Hz). The reduction velocity is 8.0 km/s. Phases are labelled as in Figures 4a,b.

Figure 5. Two-dimensional models of P- and S-wave seismic velocities in the crust and upper mantle along the RomUkrSeis profile derived by forward ray-trace modelling using SEIS83 (Červený & Pšenčík 1984). Model $V_p/V_s$ ratios are shown where available for the EEC and in the shallow crust at the southwestern end of the model (lowermost panel). Thick, black solid and dashed lines represent major velocity discontinuities (boundaries). Only those parts of the discontinuities that have been constrained by reflected or refracted arrivals of P-waves are shown: solid line – refraction only; dashed line – refraction and reflection; dotted line – reflection only. Thinner lines represent inferred velocity isolines with values in km/s shown in white boxes. The positions of tectonic units at the surface, including the approximate extent of the TTZ along the profile, are indicated. Inverted triangles show positions of shot points. Blue arrows show intersections with other WARR profiles (as labelled, EB'97 and VRANCEA-2001; cf. Fig. 1). Wells considered when constructing an initial geological model prior to the velocity modelling are also shown. Vertical exaggeration is ~11:1 for upper part of the model and ~2.4:1 for the whole model. "Bodies 1-4" discussed in the text are identified by numbers in grey circles in the first of these. Gravity and magnetic anomalies as well as surface heat flow along the profile are as in Figure 3 and topography along the profile is also shown.

Figure 6. Examples of seismic modelling along the RomUkrSeis profile, for the model presented in Figure 5: (a) SP15301, (b) SP15303, (c) SP15304, (d) SP15306, (e) SP15307, (f) SP15310 and (g) SP15311. Middle panel in each: seismic record sections (amplitude-normalised vertical component) of P-waves with theoretical travel-times calculated using SEIS83; 2-15 Hz band-pass filter reduction velocity of 8.0 km/s. Lower panels: selected rays from SEIS83 defining the common model interfaces. Upper panels: full-wave synthetic seismograms derived from the SEIS83 velocity model using TESSERAL (Kostyukevich et al. 2000). Abbreviations are as in Figures 4a,b.

Figure 7. Examples of seismic modelling of S-waves (SP15306, SP15307, SP15310 and SP15311) with bandpass filter (1–8 Hz) and reduction velocity of 4.62 km/s. Abbreviations as in Figures 4a,b.

Figure 8. (a) Theoretical (black circles) and observed (green points) travel-times for the P-wave velocity model presented in Figure 5, with reduction velocity of 8 km/s; (b) travel-time residuals for travel-times shown in (a); (c) ray coverage for the P-wave velocity model presented in Figure 5; DWS is derivative weight sum. Density of refracted rays is mapped to intensity of white colour. Yellow lines show fragments of discontinuities constrained by reflected phases and red points mark the "bottoming points" of modelled reflections (every third point is plotted) with their densities as a measure of the positioning accuracy of the reflectors.

Figure 9. Interpreted upper lithospheric structure along the RomUkrSeis profile from the velocity model in Figure 5. Shot point locations are shown by inverted triangles above the

profile; numbers indicate P-wave velocity in km/s. Solid black lines indicate seismic boundaries (refractions and/or reflections), short black lines in the lower crust below the Transylvanian Basin indicate reflecting boundaries. Label DVF indicates the approximate surface projection of the inferred Dragos Voda Fault mentioned in the text and seen in Figure 2. Blue arrows show intersections with other WARR profiles (as labelled, EB'97 and VRANCEA-2001; cf. Fig. 1). "Bodies 1-4" discussed in the text are identified by numbers in grey circles. Geophysical anomalies and topography along the profile are as in Figure 5.

Fig. 10. Comparison of the RomUkrSeis velocity model with upper crustal seismic reflection imaging in the vicinity of the TTZ: (a) tectonic setting (fragment of Figure 2; see Figure 2 for legend), additionally showing locations of Ukrainian Outer Carpathian-Carpathian foredeep seismic reflection profiles (black lines P-1 to P-5), surface traces of the Fore-Carpathian and Rava Ruska faults (red lines) and the Ukrainian border (dotted-dashed line); (b) fragment of the interpreted RomUkrSeis velocity model (Fig. 9) showing the coverage of the seismic profile P-5 and approximate surface projections of the subsurface Dragos Voda (DVF), Fore-Carpathian (FCF) and Rava Ruska (RRF) faults; (c) depth converted geological interpretation of profile P-5, located in (a) and modified after Zayats (2013). The geological legend pertains to (c) only. Vertical exaggeration for both (b) and (c) sections is 2.5:1.

**Figure 1**

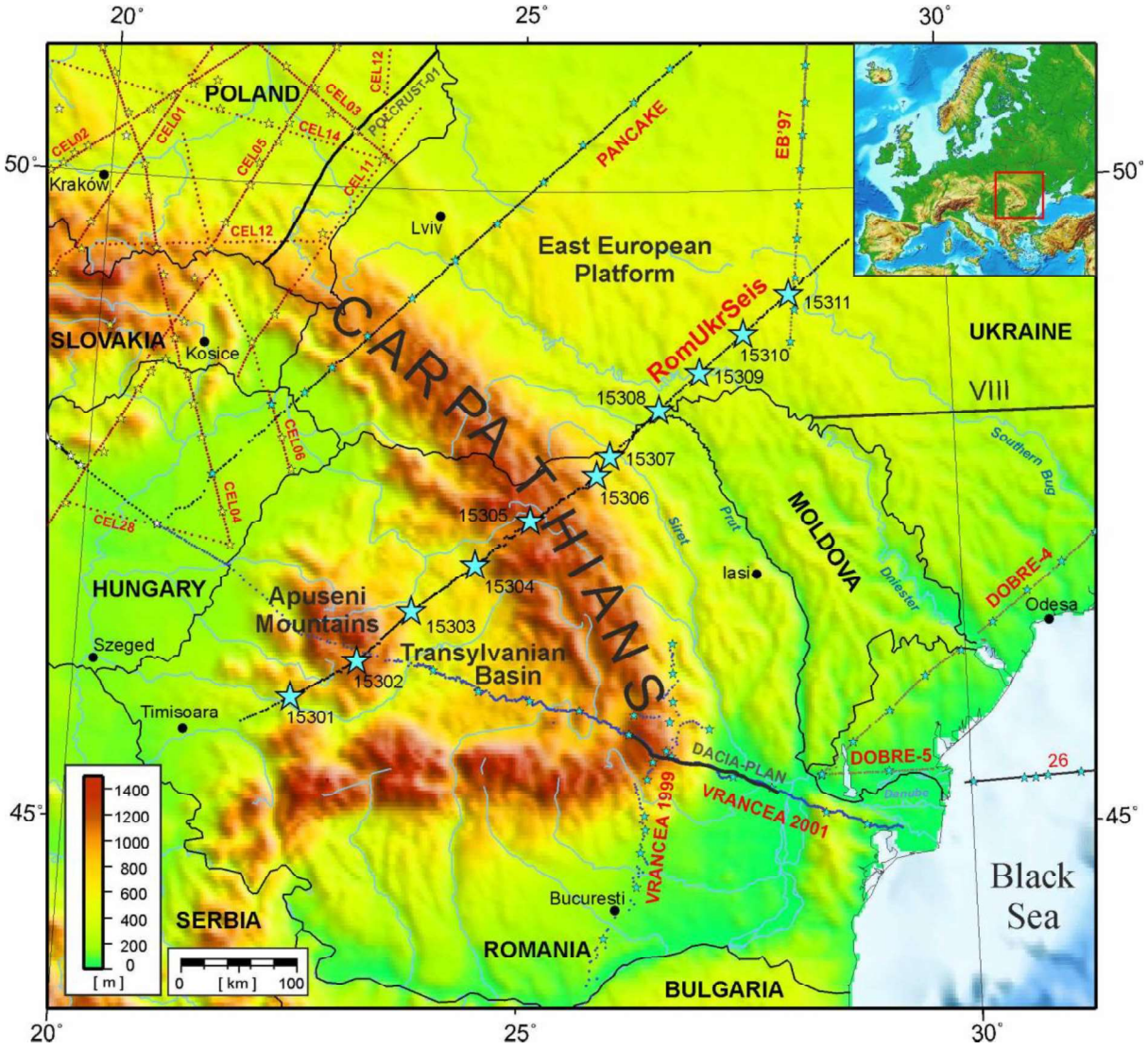


Figure 1. Location of the RomUkrSeis profile and previous WARR (stars representing shot points and tightly compacted dots recording stations, names in red) and deep reflection (solid black lines, names in black) seismic profiles in the study area.

**Figure 2**

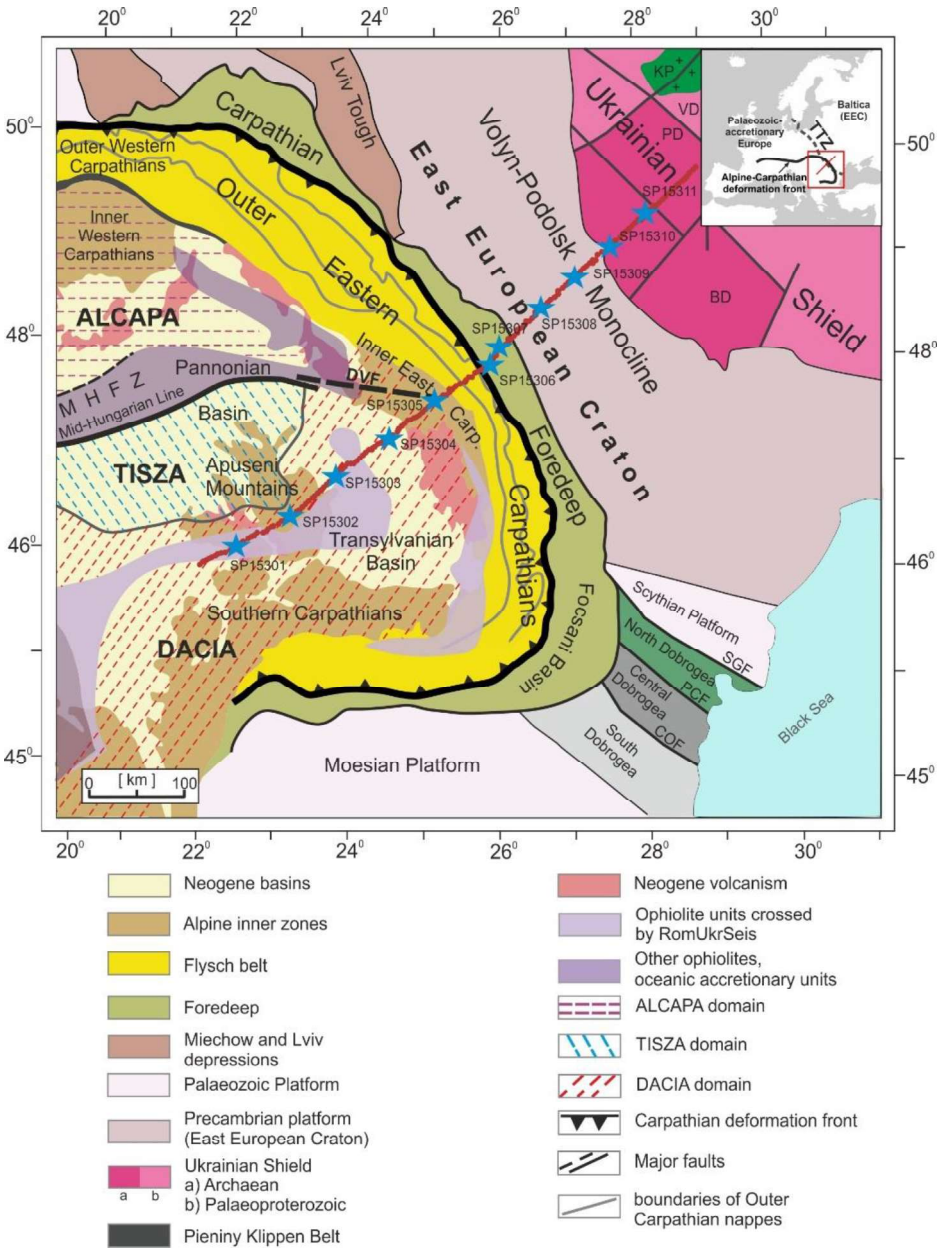


Figure 2. Tectonic setting of the RomUkrSeis profile area (from Tectonic map of Ukraine, 2007; Tectonic Map of the Socialist Republic of Romania, 1970; Geological Map of Main Structure Levels in the Ukrainian SSR and the Moldavian SSR, 1987; Sandulescu et al., 1978, Bogdanova et al., 2013) with inset map showing the location of RomUkrSeis within the basic tectonic architecture of Europe (see text). The RomUkrSeis seismic line crosses from NE to SW the southwestern part of the East European Craton (EEC), the Teisseyre-Tornquist Zone (TTZ) overlain by the Carpathian Foredeep, the Outer and the Inner Eastern Carpathians, the Transylvanian Basin and Apuseni Mountains. Blue stars are RomUkrSeis shot points and tightly compacted red dots are recorder locations. The study area is mapped in terms of litho-tectonic basement complexes represented by the Precambrian crustal domains of the EEC and the Phanerozoic crustal domains of ALCAPA, Tisza and Dacia. The Tisza-Dacia composite terrane is largely overlain by sediments of the Transylvanian Basin along RomUkrSeis. Abbreviations: BD – Bug Domain (Ukrainian Shield), COF – Capidava-Ovidiu Fault, DVF – Dragos Voda Fault, KP – Korosten Pluton (Ukrainian Shield), MHFZ – Mid-Hungarian Fault Zone, PCF – Peceneaga-Camena Fault, PD – Podolian Domain (Ukrainian Shield), SGF – Sfantu Gheorghe Fault, VD – Volyn Domain (Ukrainian Shield).

**Figure 3**

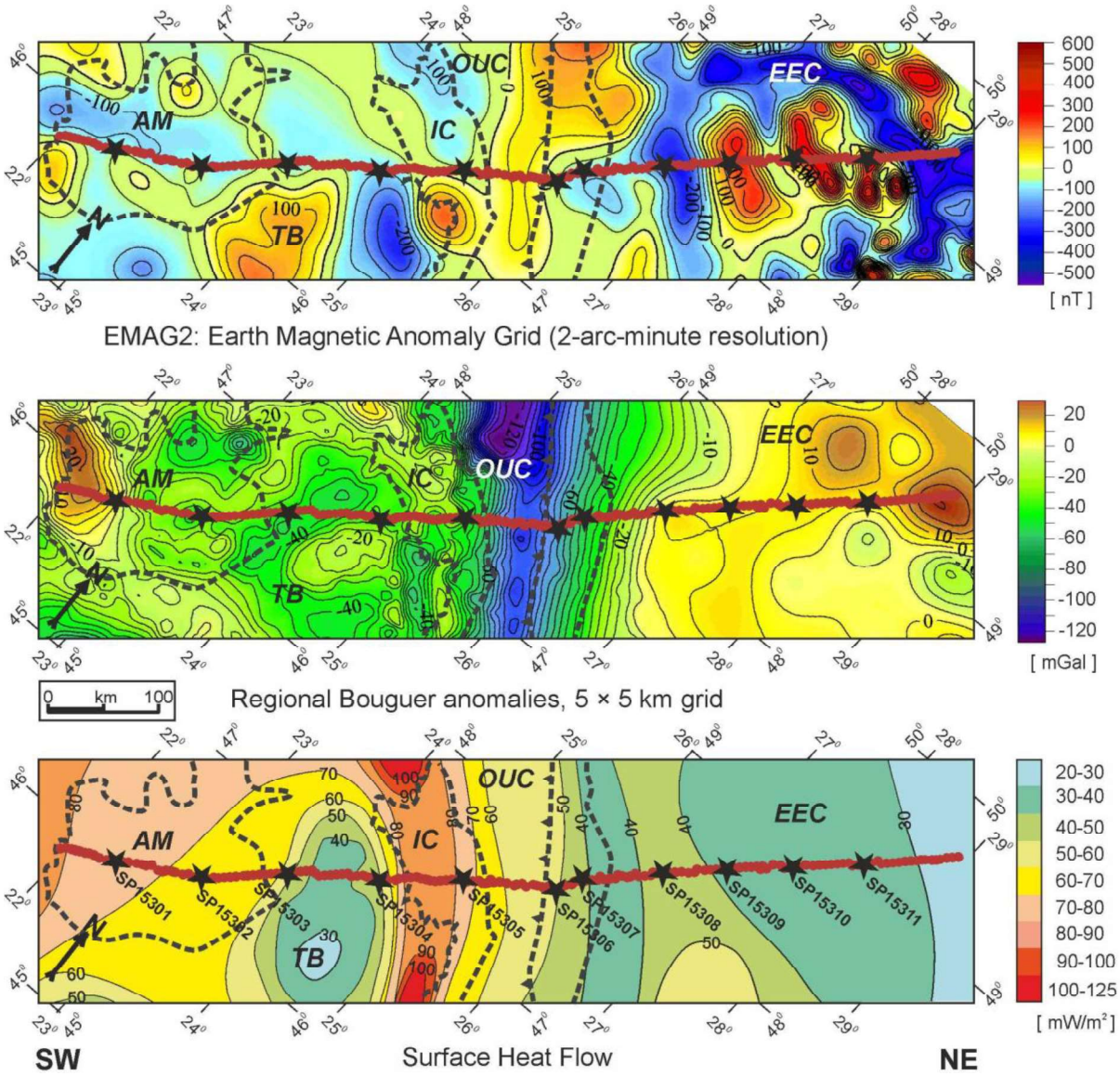


Figure 3. Geophysical data in the area of RomUkrSeis profile. From top to bottom: magnetic anomalies (EMAG2: Earth Magnetic Anomaly Grid, 2-arc-minute resolution; https://www.ngdc.noaa.gov/geomag/emag2.html); Bouguer gravity anomalies (Wybraniec et al., 1998); surface heat flow (Hurtig et al., 1991, Kutas, 2013; 2015). Seismic sources along RomUkrSeis are marked by black stars and recorder stations by tightly compacted red dots. Black dotted lines outline the main tectonic units crossed by RomUkrSeis (AM – Apuseni Mountains, EEC – East European Craton, IC – Inner Carpathians, OC – Outer Carpathians, TB – Transylvanian Basin).

**Figure 4a**

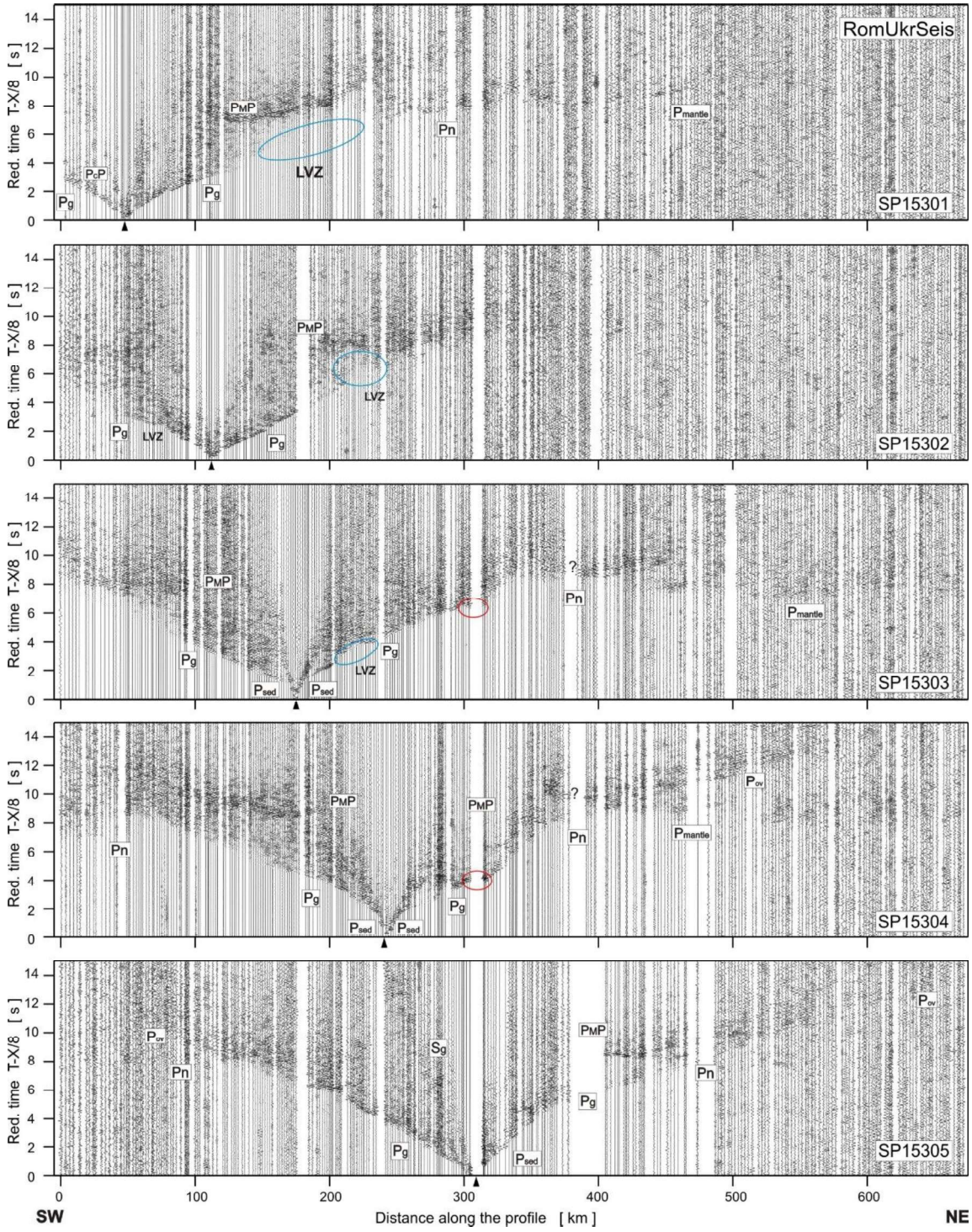


Figure 4a. Trace-normalised, vertical-component P-wave seismic record sections for (a) shot points SP15301-SP15305 and (b) shot points SP15306-SP15311. The reduction velocity is 8.0 km/s. Blue ellipses (labelled LVZ) indicate evidence of low velocity zones; red ellipses indicate evidence of strong increases in apparent velocity. Other abbreviations: $P_{sed}$ – seismic refractions from sedimentary layers; $P_g$ and $S_g$ – P and S refractions from the upper and middle crystalline crust; $P_{ov}$ and $S_{ov}$ – P and S overcritical crustal phases; $P_cP$ – reflections from mid-crustal discontinuities, $P_MP$ and $S_MS$ – P and S waves reflected from the Moho boundary; $P_n$ – refractions from the uppermost mantle, immediately below the Moho; $P_2P$ and $P_{mantle}$ – P-wave phases from the upper mantle.

**Figure 4b**

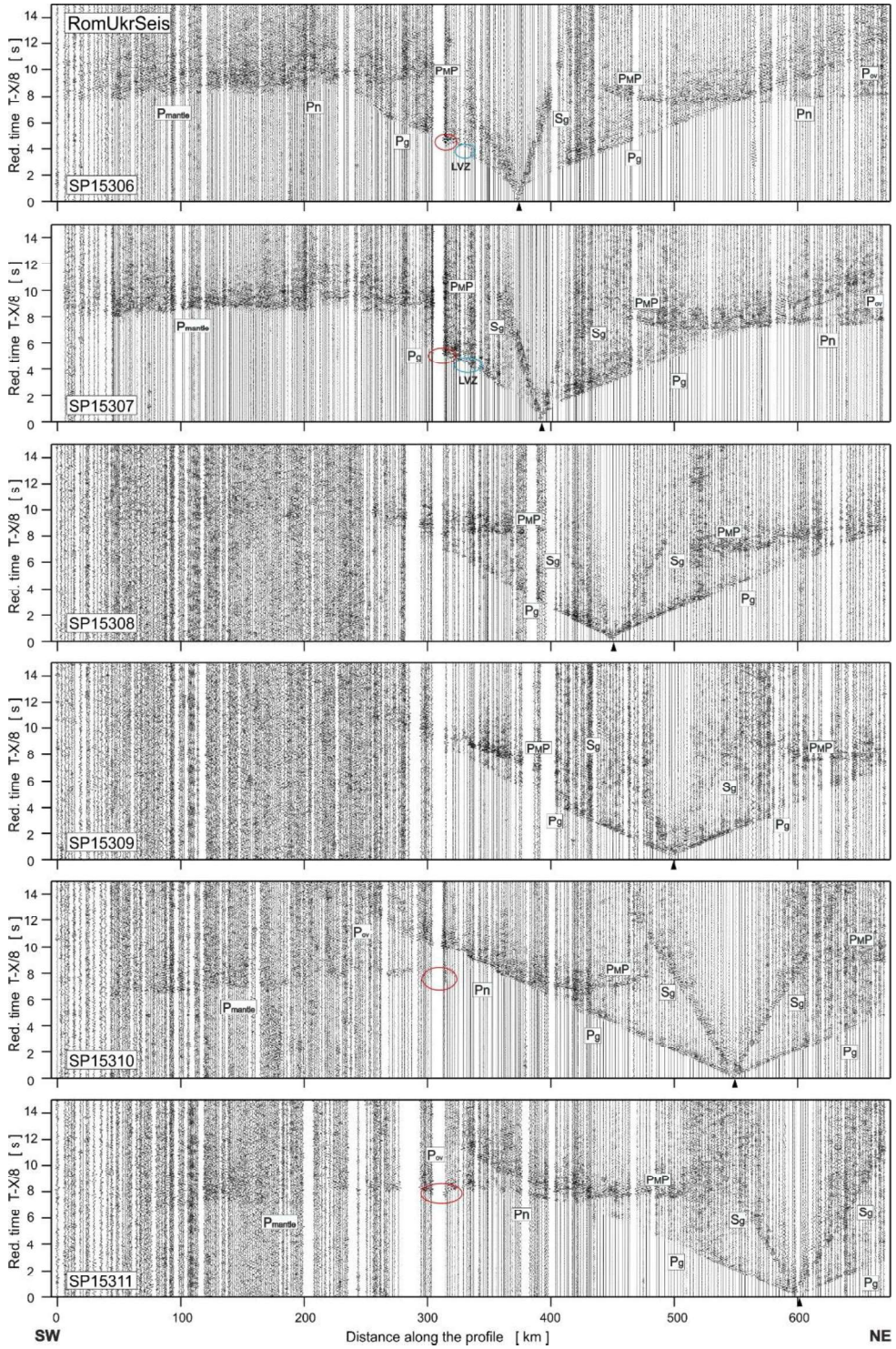


Figure 4b. Trace-normalised, vertical-component P-wave seismic record sections for (a) shot points SP15301-SP15305 and (b) shot points SP15306-SP15311. The reduction velocity is 8.0 km/s. Blue ellipses (labelled LVZ) indicate evidence of low velocity zones; red ellipses indicate evidence of strong increases in apparent velocity. Other abbreviations: $P_{sed}$ – seismic refractions from sedimentary layers; $P_g$ and $S_g$ – P and S refractions from the upper and middle crystalline crust; $P_{ov}$ and $S_{ov}$ – P and S overcritical crustal phases; $P_cP$ – reflections from mid-crustal discontinuities, $P_MP$ and $S_MS$ – P and S waves reflected from the Moho boundary; $P_n$ – refractions from the uppermost mantle, immediately below the Moho; $P_2P$ and $P_{mantle}$ – P-wave phases from the upper mantle.

**Figure 4c**

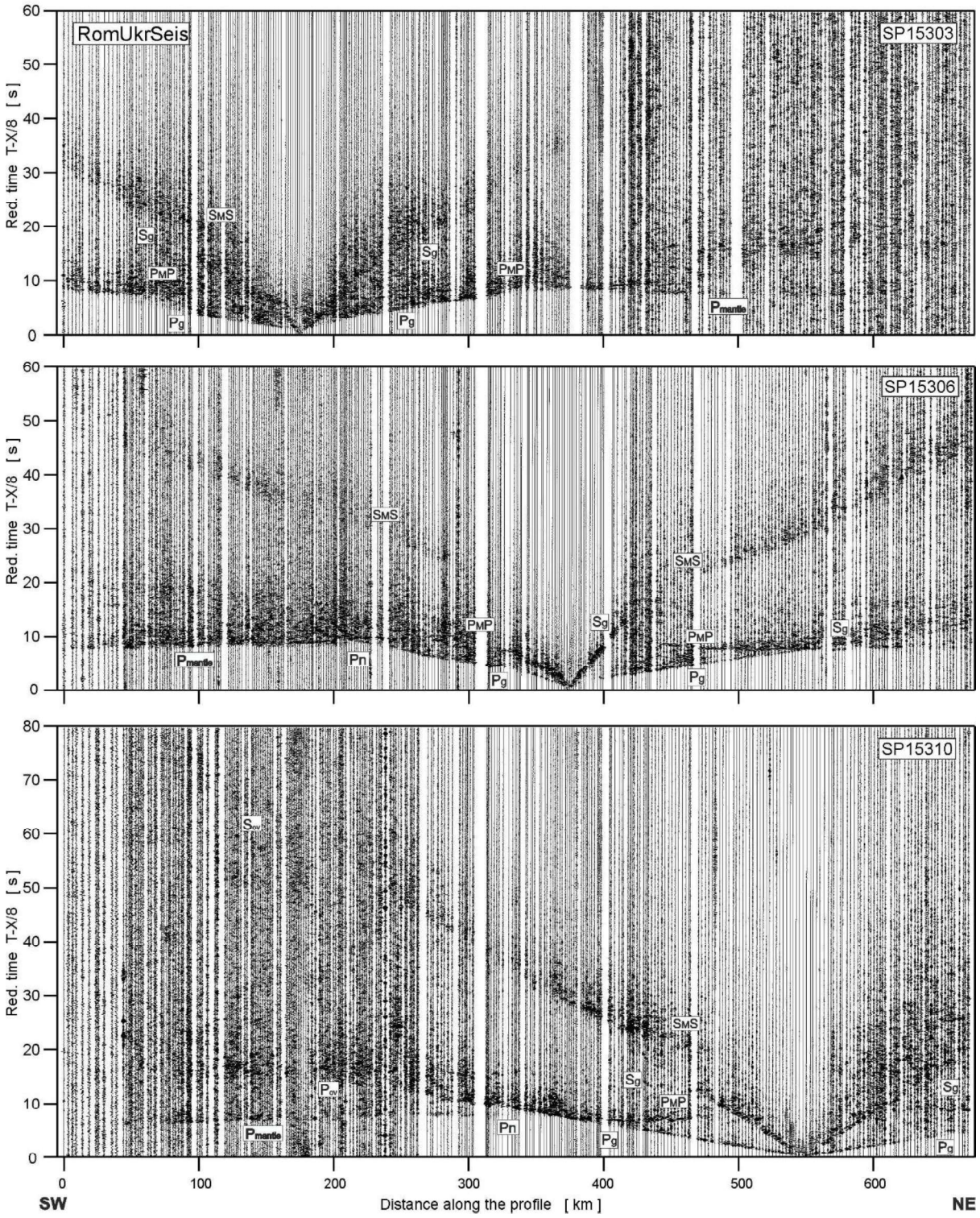


Figure 4c. Examples of trace-normalised, vertical-component, common seismic record sections for P- and S-waves for shot points SP15303, SP15306 and SP15310 with band-pass filter (1-8 Hz). The reduction velocity is 8.0 km/s. Phases are labelled as in Figures 4ab.

**Figure 5**

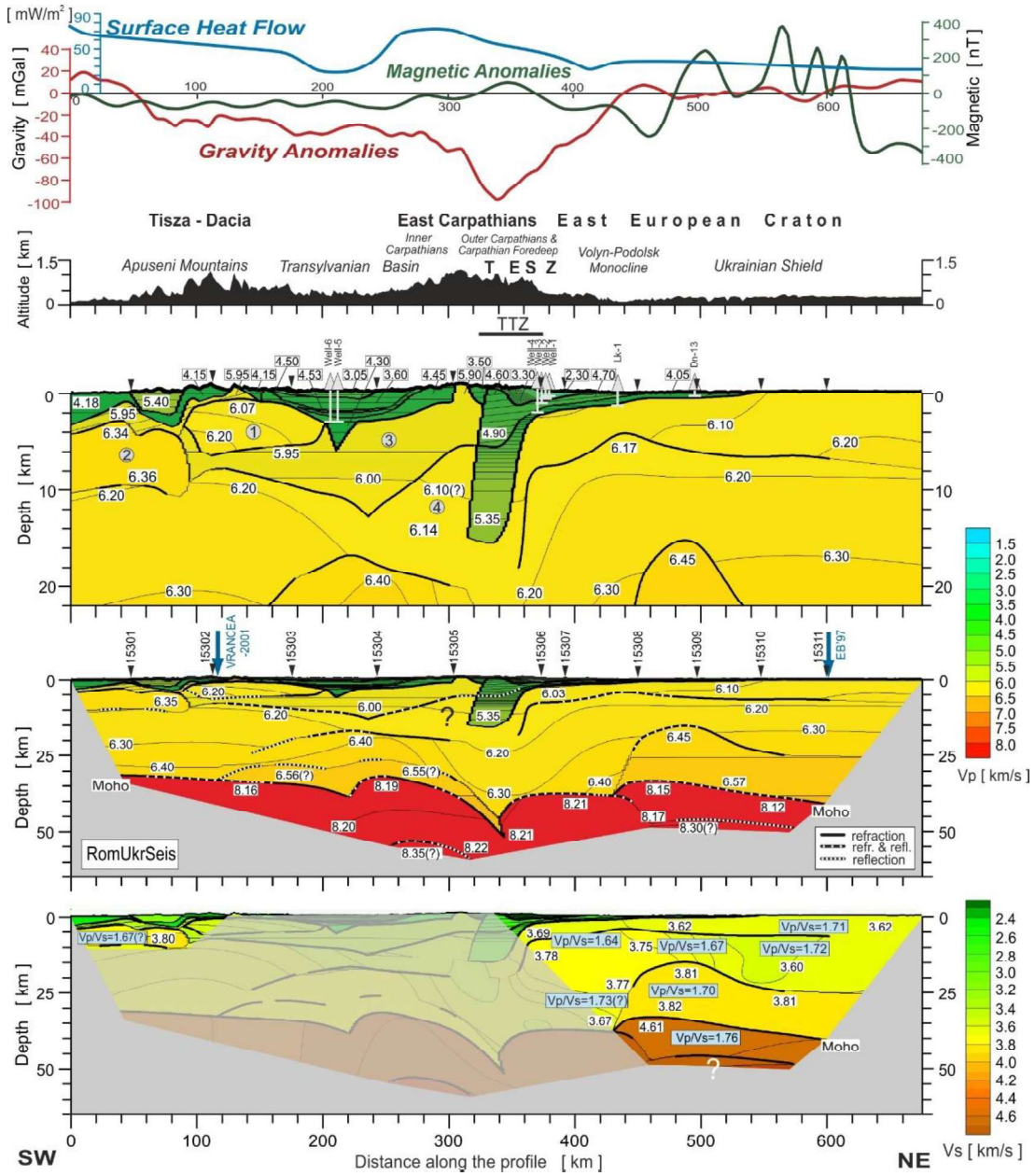


Figure 5. Two-dimensional models of P- and S-wave seismic velocities in the crust and upper mantle along the RomUkrSeis profile derived by forward ray-trace modelling using SEIS83 (Červený & Pšenčík 1984). Model Vp/Vs ratios are shown where available for the EEC and in the shallow crust at the southwestern end of the model (lowermost panel). Thick, black solid and dashed lines represent major velocity discontinuities (boundaries). Only those parts of the discontinuities that have been constrained by reflected or refracted arrivals of P-waves are shown: solid line – refraction only; dashed line – refraction and reflection; dotted line – reflection only. Thinner lines represent inferred velocity isolines with values in km/s shown in white boxes. The positions of tectonic units at the surface, including the approximate extent of the TTZ along the profile, are indicated. Inverted triangles show positions of shot points. Blue arrows show intersections with other WARR profiles (as labelled, EB'97 and VRANCEA-2001; cf. Fig. 1). Wells considered when constructing an initial geological model prior to the velocity modelling are also shown. Vertical exaggeration is ~11:1 for upper part of the model and ~2.4:1 for the whole model. "Bodies 1-4" discussed in the text are identified by numbers in grey circles in the first of these. Gravity and magnetic anomalies as well as surface heat flow along the profile are as in Figure 3 and topography along the profile is also shown.

**Figure 6a**

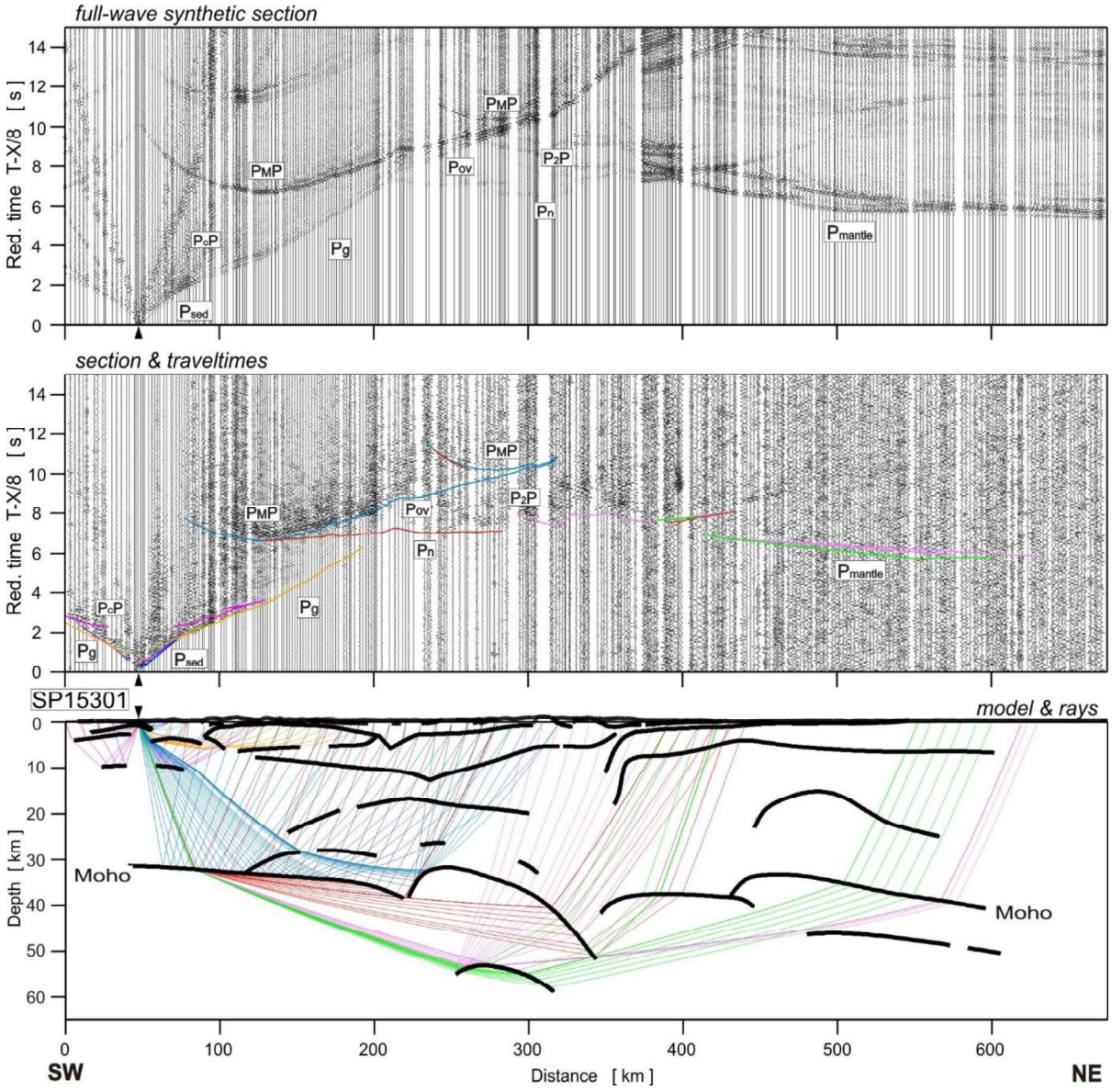


Figure 6a. Examples of seismic modelling along the RomUkrSeis profile, for the model presented in Figure 5: (a) SP15301, (b) SP15303, (c) SP15304, (d) SP15306, (e) SP15307, (f) SP15310 and (g) SP15311. Middle panel in each: seismic record sections (amplitude-normalised vertical component) of P-waves with theoretical travel-times calculated using SEIS83; 2-15 Hz band-pass filter reduction velocity of 8.0 km/s. Lower panels: selected rays from SEIS83 defining the common model interfaces. Upper panels: full-wave synthetic seismograms derived from the SEIS83 velocity model using TESSERAL (Kostyukevich et al. 2000). Abbreviations are as in Figures 4ab.

**Figure 6b**

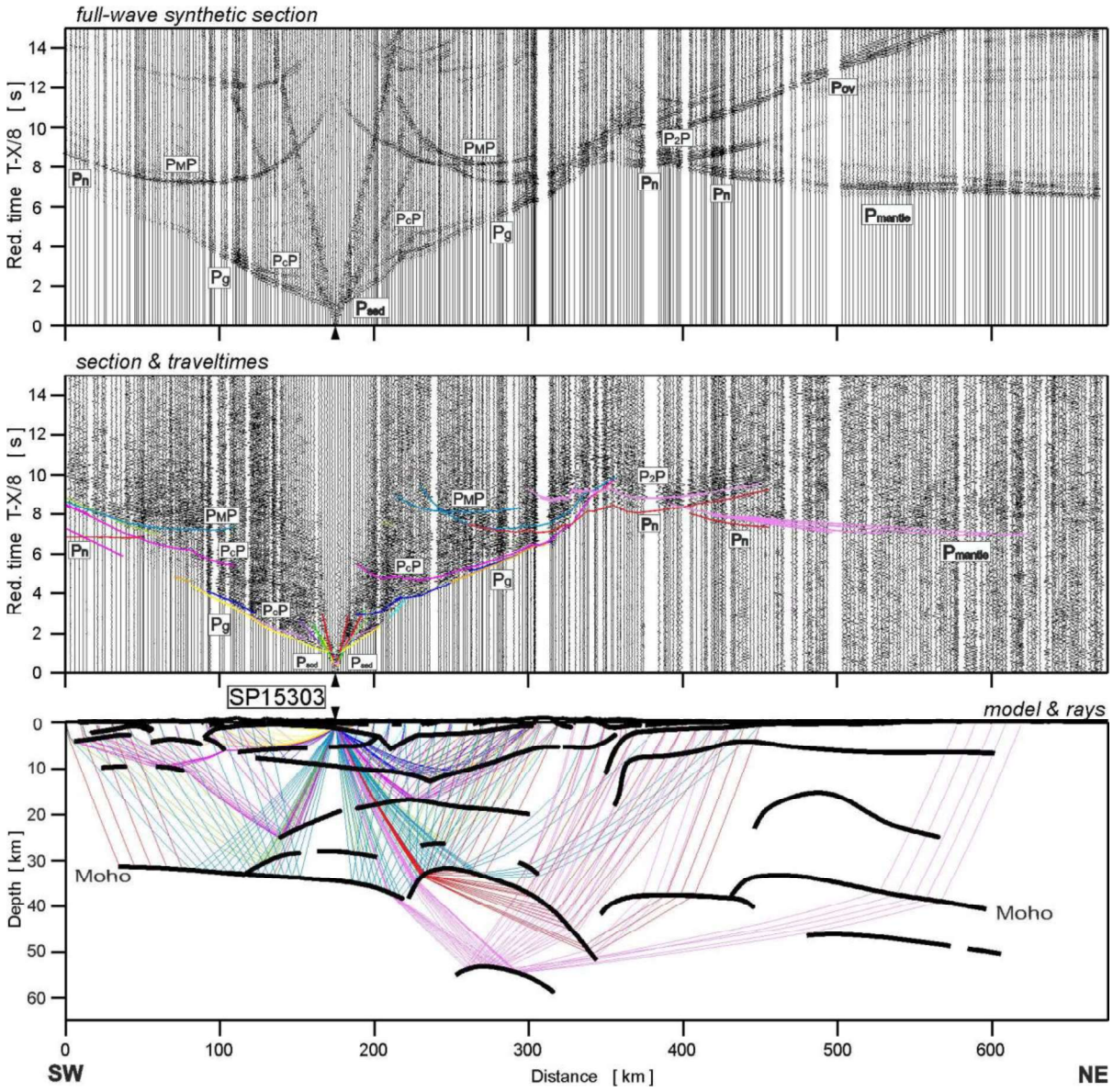


Figure 6b. Examples of seismic modelling along the RomUkrSeis profile, for the model presented in Figure 5: (a) SP15301, (b) SP15303, (c) SP15304, (d) SP15306, (e) SP15307, (f) SP15310 and (g) SP15311. Middle panel in each: seismic record sections (amplitude-normalised vertical component) of P-waves with theoretical travel times calculated using SEIS83; 2-15 Hz band-pass filter reduction velocity of 8.0 km/s. Lower panels: selected rays from SEIS83 defining the common model interfaces. Upper panels: full-wave synthetic seismograms derived from the SEIS83 velocity model using TESSERAL (Kostyukevich et al. 2000). Abbreviations are as in Figures 4ab.

**Figure 6c**

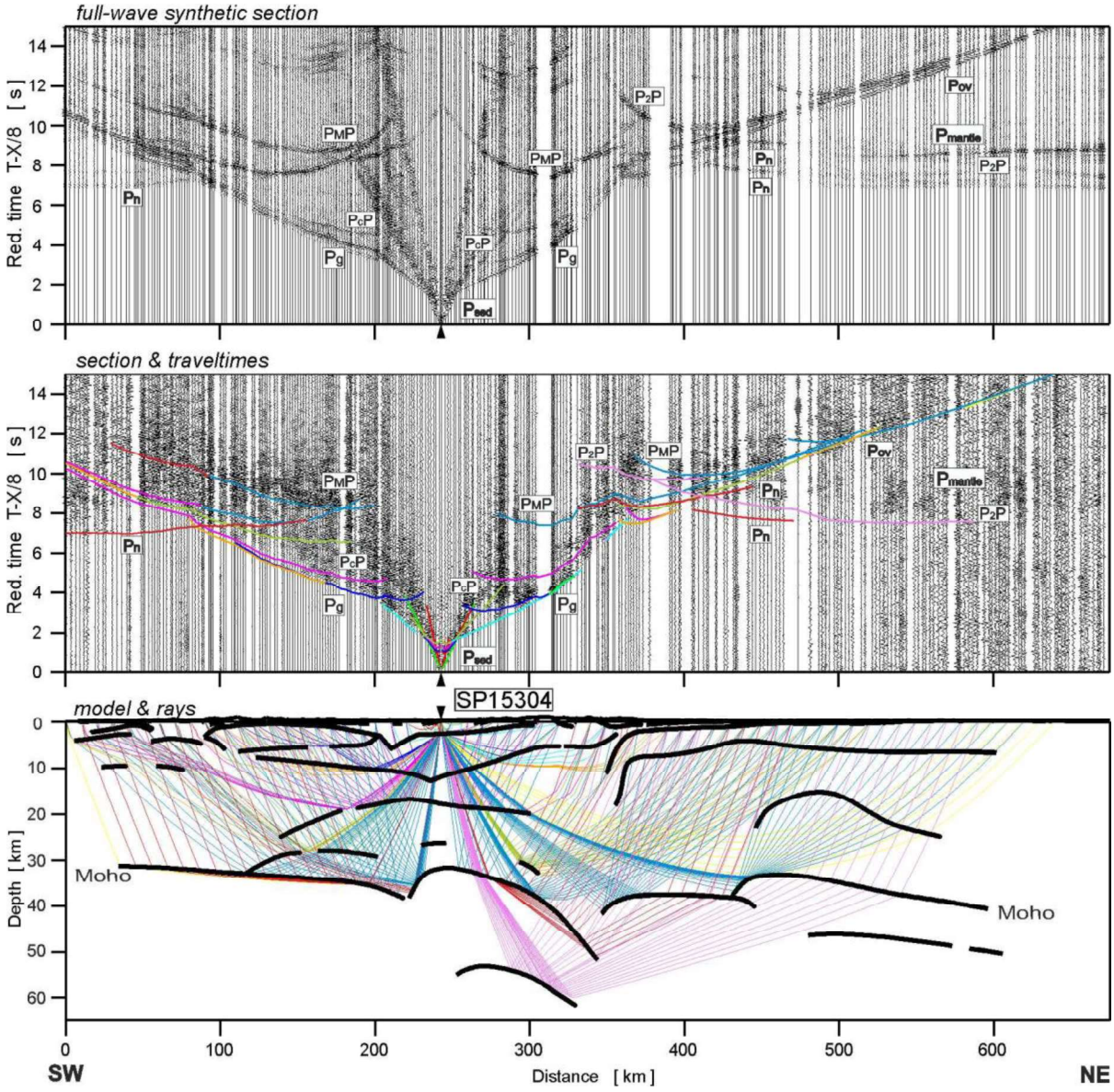


Figure 6c. Examples of seismic modelling along the RomUkrSeis profile, for the model presented in Figure 5: (a) SP15301, (b) SP15303, (c) SP15304, (d) SP15306, (e) SP15307, (f) SP15310 and (g) SP15311. Middle panel in each: seismic record sections (amplitude-normalised vertical component) of P-waves with theoretical travel times calculated using SEIS83; 2-15 Hz band-pass filter reduction velocity of 8.0 km/s. Lower panels: selected rays from SEIS83 defining the common model interfaces. Upper panels: full-wave synthetic seismograms derived from the SEIS83 velocity model using TESSERAL (Kostyukevich et al. 2000). Abbreviations are as in Figures 4ab.

**Figure 6d**

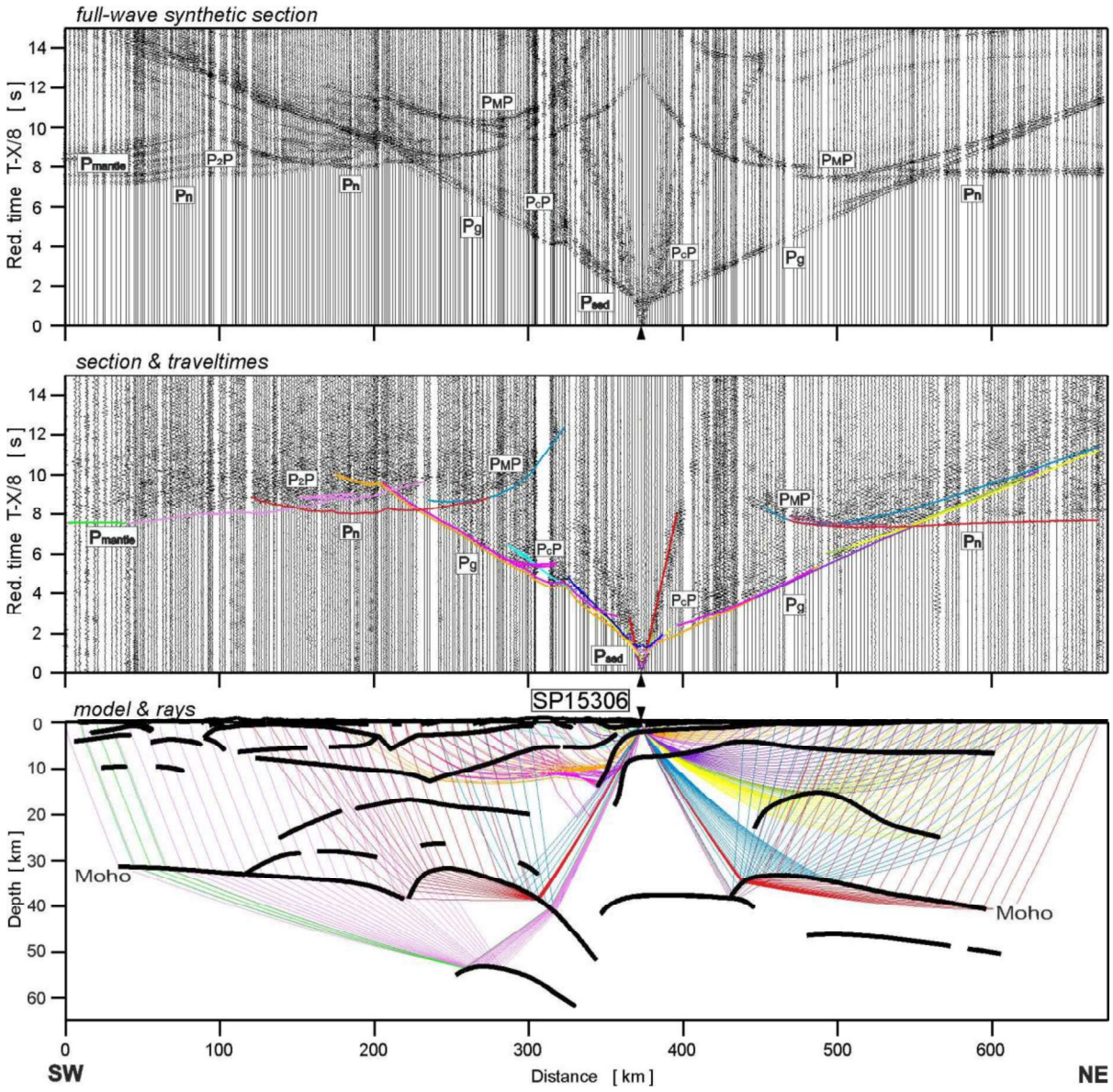


Figure 6d. Examples of seismic modelling along the RomUkrSeis profile, for the model presented in Figure 5: (a) SP15301, (b) SP15303, (c) SP15304, (d) SP15306, (e) SP15307, (f) SP15310 and (g) SP15311. Middle panel in each: seismic record sections (amplitude-normalised vertical component) of P-waves with theoretical travel times calculated using SEIS83; 2-15 Hz band-pass filter reduction velocity of 8.0 km/s. Lower panels: selected rays from SEIS83 defining the common model interfaces. Upper panels: full-wave synthetic seismograms derived from the SEIS83 velocity model using TESSERAL (Kostyukevich et al. 2000). Abbreviations are as in Figures 4ab.

**Figure 6e**

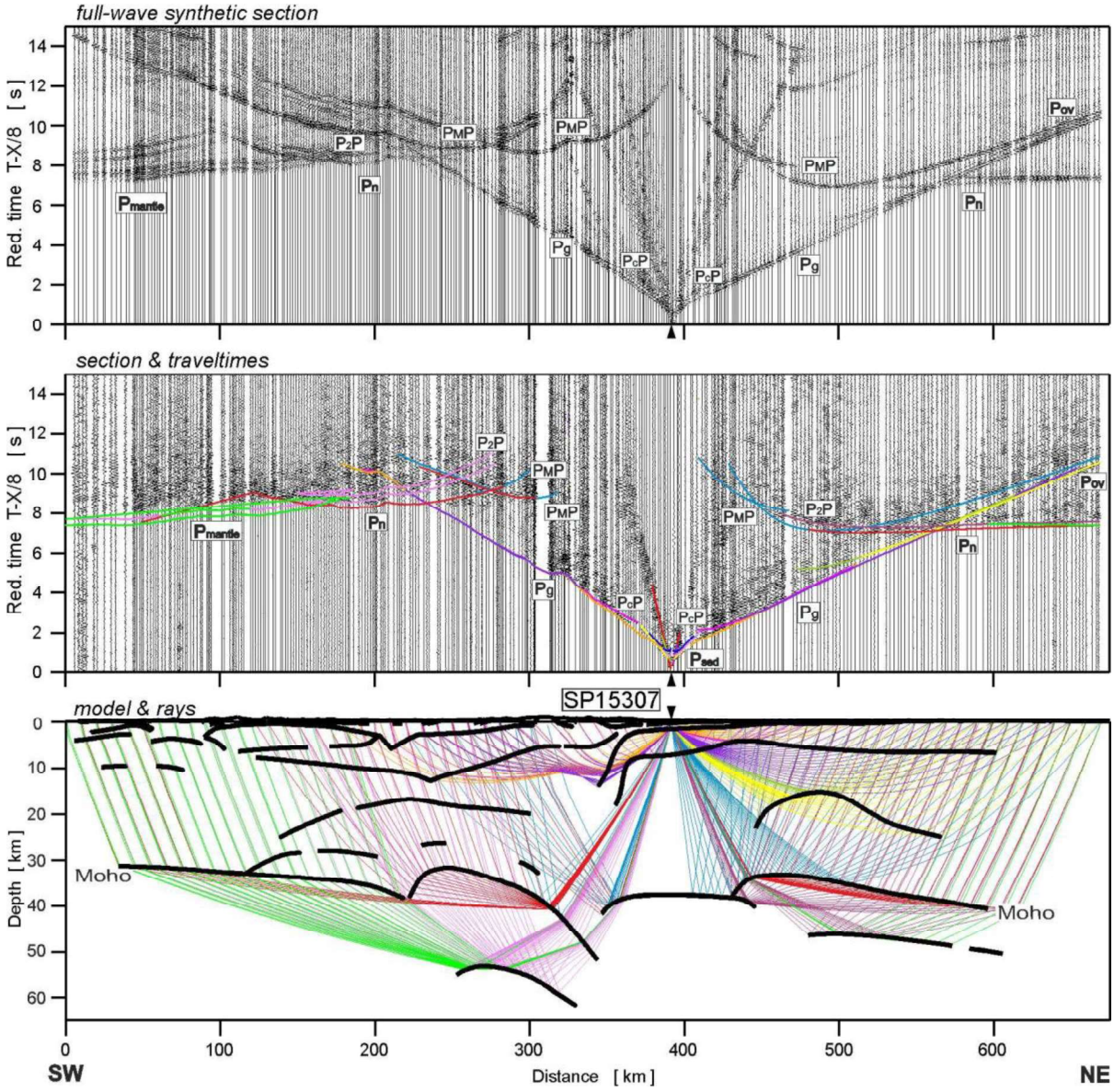


Figure 6e. Examples of seismic modelling along the RomUkrSeis profile, for the model presented in Figure 5: (a) SP15301, (b) SP15303, (c) SP15304, (d) SP15306, (e) SP15307, (f) SP15310 and (g) SP15311. Middle panel in each: seismic record sections (amplitude-normalised vertical component) of P-waves with theoretical travel times calculated using SEIS83; 2-15 Hz band-pass filter reduction velocity of 8.0 km/s. Lower panels: selected rays from SEIS83 defining the common model interfaces. Upper panels: full-wave synthetic seismograms derived from the SEIS83 velocity model using TESSERAL (Kostyukevich et al. 2000). Abbreviations are as in Figures 4ab.

**Figure 6f**

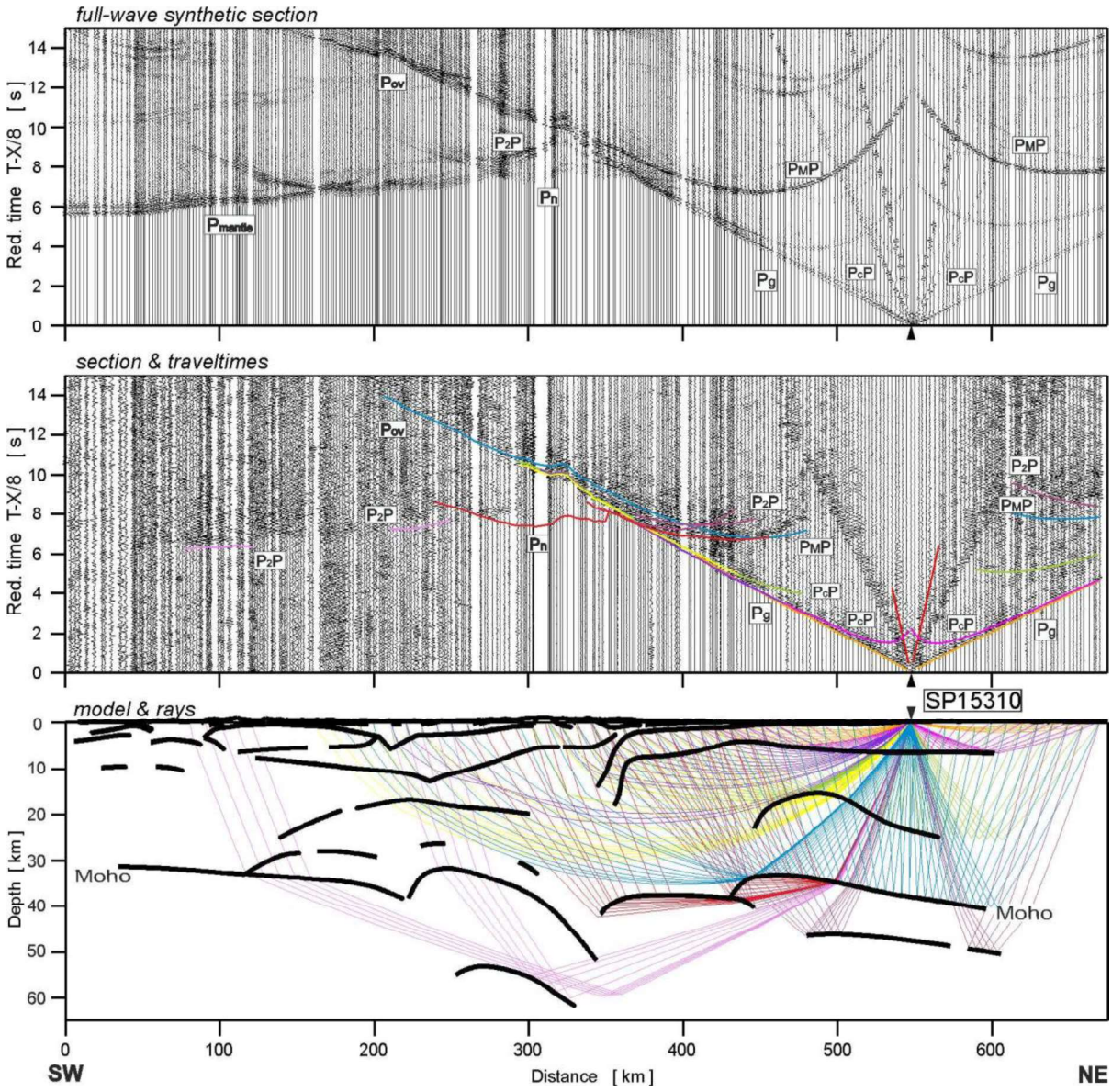


Figure 6f. Examples of seismic modelling along the RomUkrSeis profile, for the model presented in Figure 5: (a) SP15301, (b) SP15303, (c) SP15304, (d) SP15306, (e) SP15307, (f) SP15310 and (g) SP15311. Middle panel in each: seismic record sections (amplitude-normalised vertical component) of P-waves with theoretical travel times calculated using SEIS83; 2-15 Hz band-pass filter reduction velocity of 8.0 km/s. Lower panels: selected rays from SEIS83 defining the common model interfaces. Upper panels: full-wave synthetic seismograms derived from the SEIS83 velocity model using TESSERAL (Kostyukevich et al. 2000). Abbreviations are as in Figures 4ab.

**Figure 6g**

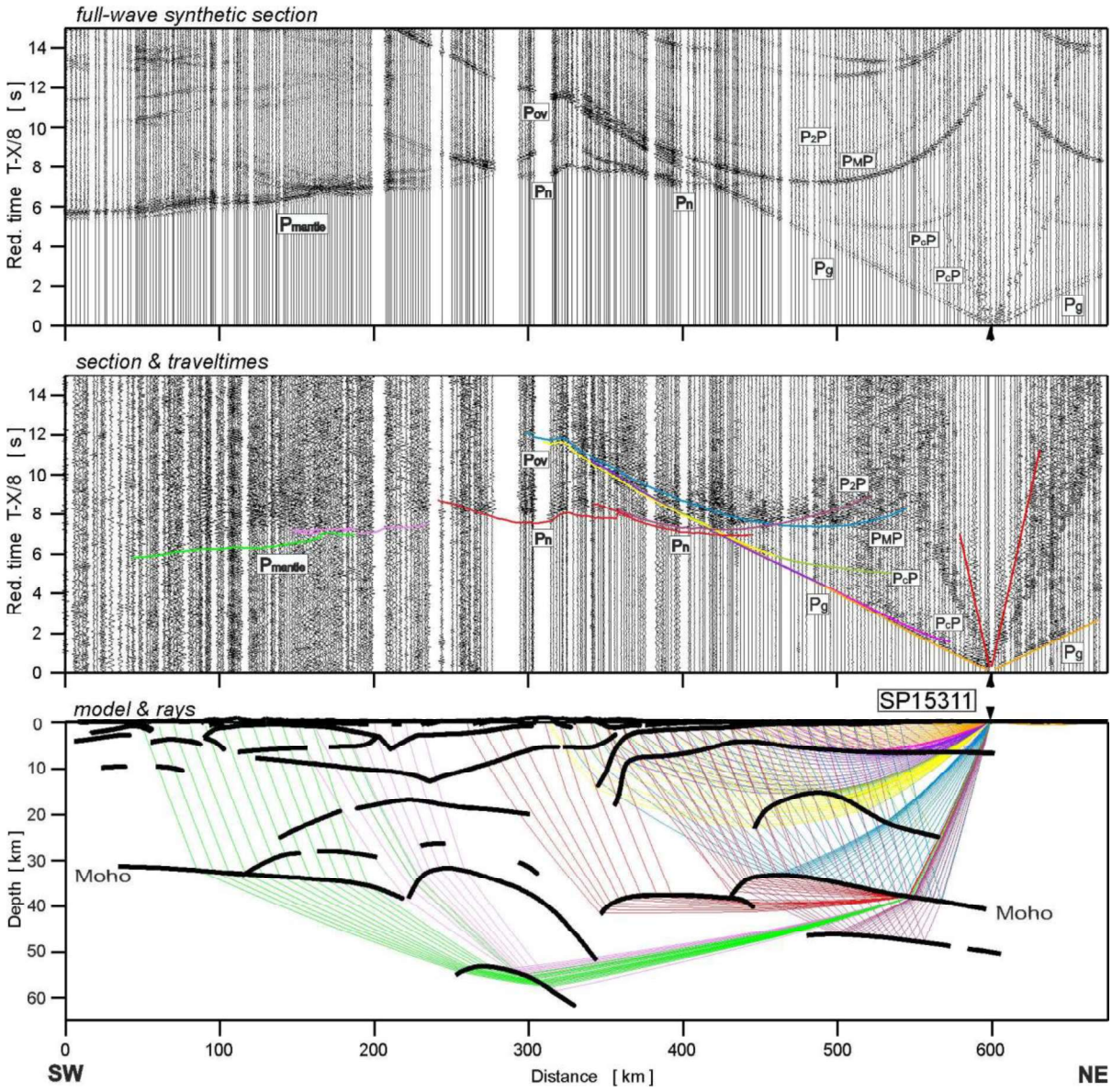


Figure 6g. Examples of seismic modelling along the RomUkrSeis profile, for the model presented in Figure 5: (a) SP15301, (b) SP15303, (c) SP15304, (d) SP15306, (e) SP15307, (f) SP15310 and (g) SP15311. Middle panel in each: seismic record sections (amplitude-normalised vertical component) of P-waves with theoretical travel times calculated using SEIS83; 2-15 Hz band-pass filter reduction velocity of 8.0 km/s. Lower panels: selected rays from SEIS83 defining the common model interfaces. Upper panels: full-wave synthetic seismograms derived from the SEIS83 velocity model using TESSERAL (Kostyukevich et al. 2000). Abbreviations are as in Figures 4ab.

**Figure 7**

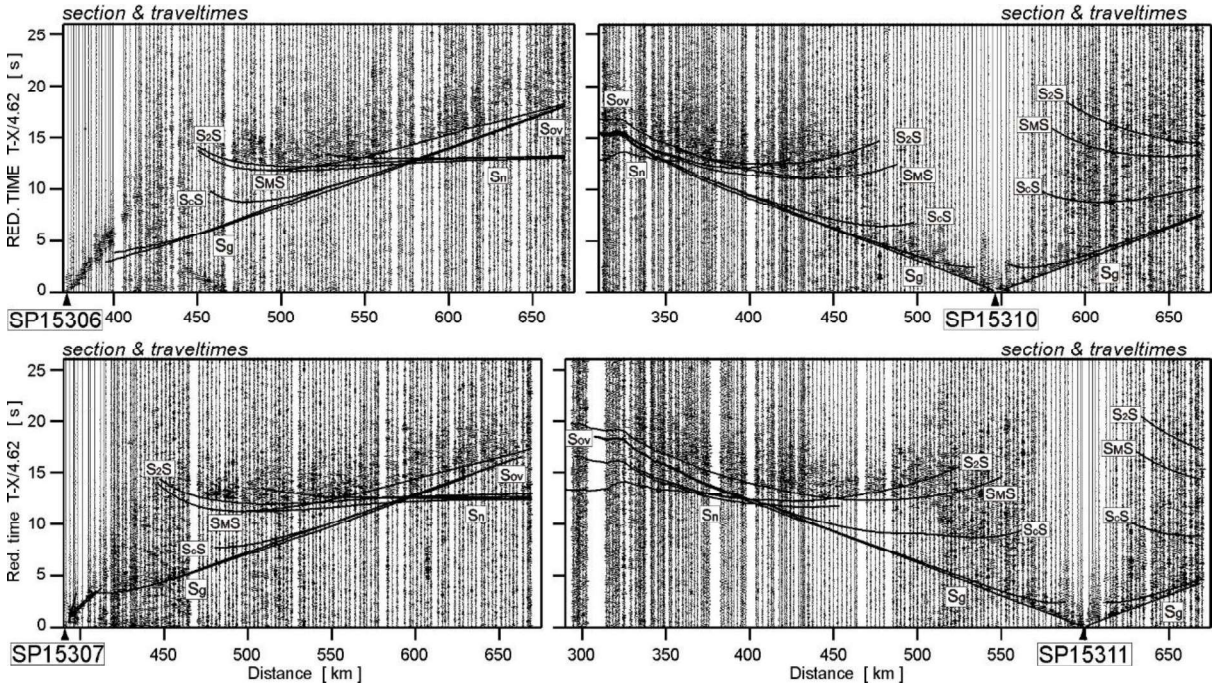


Figure 7. Examples of seismic modelling of S-waves (SP15306, SP15307, SP15310 and SP15311) with bandpass filter (1–8 Hz) and reduction velocity of 4.62 km/s. Abbreviations as in Figures 4ab.

**Figure 8**

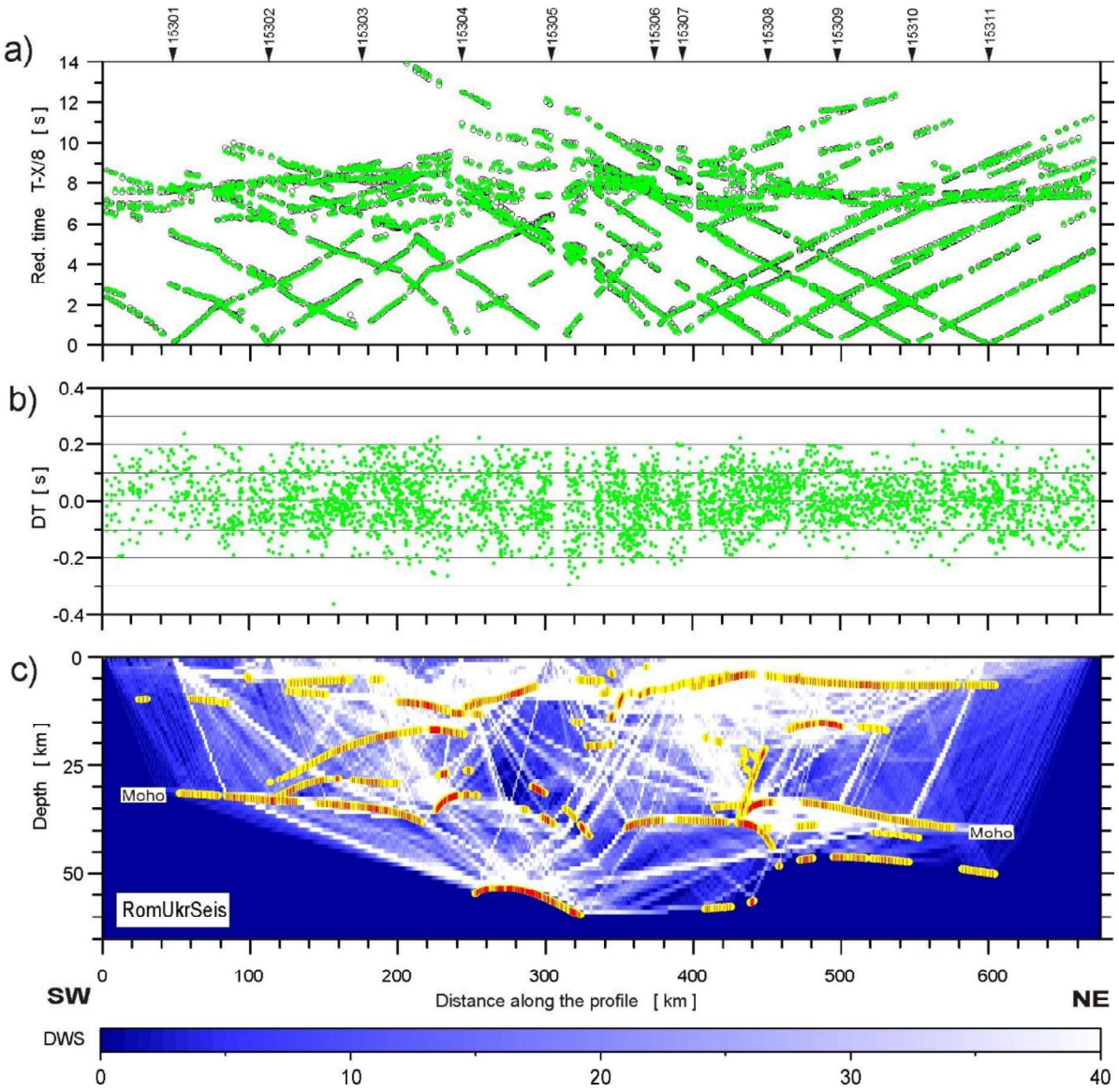


Figure 8. (a) Theoretical (black circles) and observed (green points) travel-times for the P-wave velocity model presented in Figure 5, with reduction velocity of 8 km/s; (b) travel-time residuals for travel-times shown in (a); (c) ray coverage for the P-wave velocity model presented in Figure 5; DWS is derivative weight sum. Density of refracted rays is mapped to intensity of white colour. Yellow lines show fragments of discontinuities constrained by reflected phases and red points mark the "bottoming points" of modelled reflections (every third point is plotted) with their densities as a measure of the positioning accuracy of the reflectors.

Figure 9

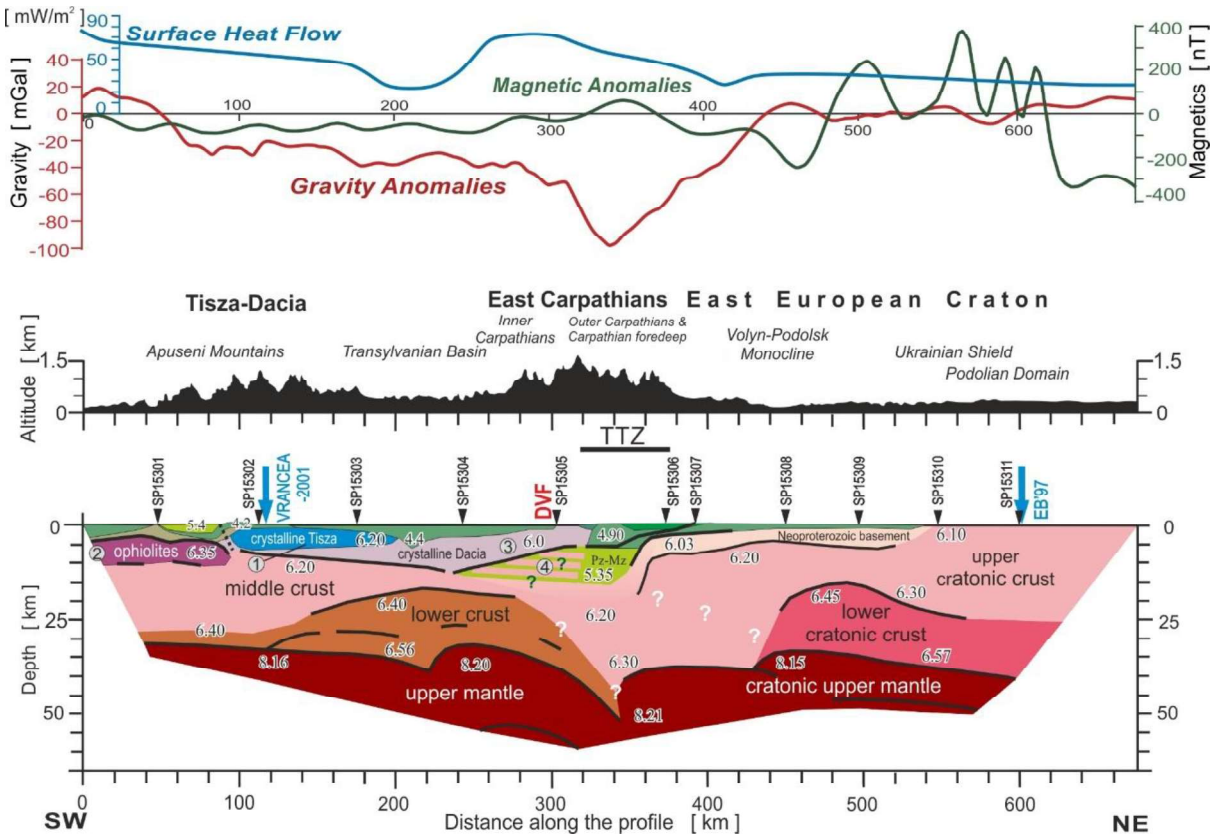


Figure 9. Interpreted upper lithospheric structure along the RomUkrSeis profile from the velocity model in Figure 5. Shot point locations are shown by inverted triangles above the profile; numbers indicate P-wave velocity in km/s. Solid black lines indicate seismic boundaries (refractions and/or reflections), short black lines in the lower crust below the Transylvanian Basin indicate reflecting boundaries. Label DVF indicates the approximate surface projection of the inferred Dragos Voda Fault mentioned in the text and seen in Figure 2. Blue arrows show intersections with other WARR profiles (as labelled, EB'97 and VRANCEA-2001; cf. Fig. 1). "Bodies 1-4" discussed in the text are identified by numbers in grey circles. Geophysical anomalies and topography along the profile are as in Figure 5.

**Figure 10**

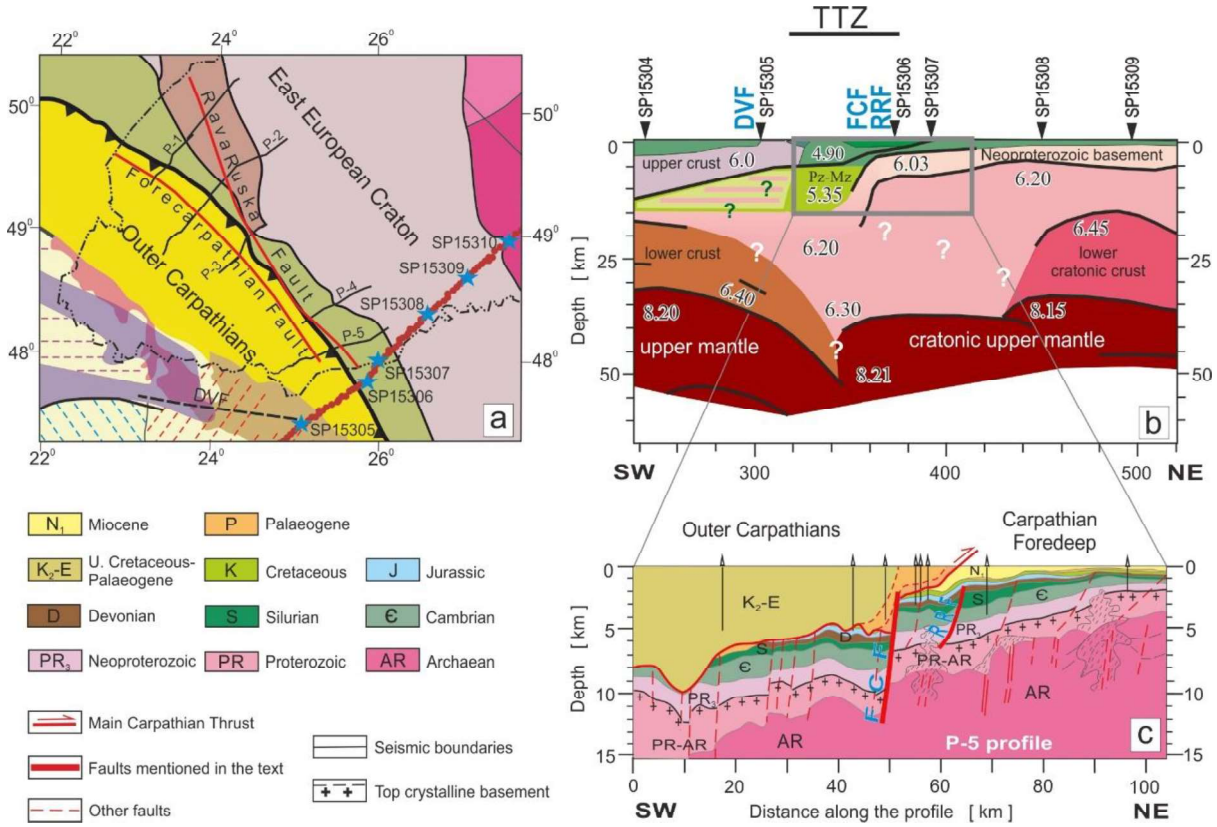


Fig. 10. Comparison of the RomUkrSeis velocity model with upper crustal seismic reflection imaging in the vicinity of the TTZ: (a) tectonic setting (fragment of Figure 2; see Figure 2 for legend), additionally showing locations of Ukrainian Outer Carpathian-Carpathian foredeep seismic reflection profiles (black lines P-1 to P-5), surface traces of the Fore-Carpathian and Rava Ruska faults (red lines) and the Ukrainian border (dotted-dashed line); (b) fragment of the interpreted RomUkrSeis velocity model (Fig. 9) showing the coverage of the seismic profile P-5 and approximate surface projections of the subsurface Dragos Voda (DVF), Fore-Carpathian (FCF) and Rava Ruska (RRF) faults; (c) depth converted geological interpretation of profile P-5, located in (a) and modified after Zayats (2013). The geological legend pertains to (c) only. Vertical exaggeration for both (b) and (c) sections is 2.5:1.